



universität
wien

MASTERARBEIT / MASTER THESIS

Titel der Masterarbeit / Title of the Master Thesis

„Investigating the Interface and Stability of the Human
Cannabinoid Receptor 1 - Oxytocin Receptor Heterodi-
meric Complex in Membrane“

verfasst von / submitted by

Michaela Eisenhuber BSc

angestrebter akademischer Grad / in partial fulfilment of the requirements for the degree of
Magistra pharmaciae (Mag.pharm.)

Wien, 2022 / Vienna, 2022

Studienkennzahl lt. Studienblatt /
degree program code as it appears on
the student record sheet:

UA 066 605

Studienrichtung lt. Studienblatt /
degree program as it appears on
the student record sheet:

Masterstudium Pharmazie

Betreut von / Supervisor:

Univ.-Prof. Mag. Dr. Thierry Langer

Mitbetreut von / Co-Supervisor:

Dr. Marcus Wieder, MSc MSc

Table of Contents

1	Introduction.....	1
1.1	G-protein coupled receptors.....	1
1.1.1	Common structural features.....	1
1.1.2	Diversity of GPCR.....	1
1.1.3	Signalling pathways of GPCR.....	2
1.1.4	Modes of GPCR activation.....	3
1.1.4.1	Biased activation.....	3
1.1.4.2	Intracellular activation.....	3
1.1.4.3	Transactivation.....	3
1.1.4.4	Biphasic activation.....	4
1.1.4.5	Dimerization activation.....	4
1.2	Cannabinoid receptors.....	4
1.2.1	Classification of cannabinoid receptors.....	5
1.2.2	Signalling pathways.....	5
1.2.3	Tissue distribution.....	5
1.2.4	Endogenous and exogenous cannabinoids.....	6
1.2.5	Structure of cannabinoid receptors.....	8
1.2.5.1	Available structure of inactive cannabinoid receptor 1.....	9
1.2.5.2	Available structure of active cannabinoid receptor 1.....	9
1.3	Oxytocin receptor.....	10
1.3.1	Signalling pathways.....	10
1.3.2	Tissue distribution.....	10
1.3.3	Oxytocin and exogenous ligands.....	10
1.3.4	Relationship to vasopressin.....	11
1.3.5	Structure of oxytocin receptor.....	12
1.3.5.1	Available structure of inactive oxytocin receptor.....	12
1.3.5.2	Available structure of active oxytocin receptor.....	13
1.4	GPCR dimerization.....	13
1.4.1	Methods to study dimerization.....	13
1.4.2	Cannabinoid receptor 1 and Oxytocin receptor dimerization.....	14
1.4.2.1	Cannabinoid receptor 1 dimerization.....	14
1.4.2.2	Oxytocin receptor dimerization.....	14
1.5	Bivalent ligands.....	15
1.6	Molecular docking and ranking methods in the theory.....	16
1.6.1	Protein-protein docking.....	16
1.6.1.1	Docking stage.....	16
1.6.1.2	Ranking stage.....	18
1.6.1.3	Benchmarks of protein-protein docking methods.....	18
1.6.2	Protein-ligand docking.....	18
1.6.2.1	Conformational search and docking.....	19

1.6.2.2	Evolution of binding energies and ranking	19
1.6.2.3	Benchmarks of protein-ligand docking methods	20
1.6.3	Ranking	20
1.6.3.1	Force field-based scoring functions	20
1.6.3.2	Knowledge-based scoring functions	20
1.6.3.3	Empirical scoring functions	21
1.6.3.4	Machine learning-based scoring functions	21
2	Aims and significance	22
3	Methods: Databases Software and Programs	23
3.1	RCSB-Protein Data Bank	23
3.2	CHARMM-GUI	23
3.3	PPM Server	24
3.4	Memdock Server	24
3.4.1	Docking	24
3.4.2	Ranking	25
3.5	Pymol	25
3.6	ChemDraw	25
3.7	Protein-ligand docking with LigandScout <i>via</i> AutoDock Vina	25
3.8	Maestro	26
3.9	OpenMM molecular dynamics toolkit	26
3.10	Visual molecular dynamics (VMD)	27
3.11	PyRosetta - Alanine scan	27
4	Results and discussion	28
4.1	Protein preparation and protein-protein docking <i>via</i> Memdock	28
4.1.1	Structures of the receptors	28
4.1.2	Selection and restoring missing amino acids of the receptor	28
4.1.3	PPM Server	29
4.1.4	Memdock Server	30
4.1.5	Pymol visualization of the Memdock results	31
4.2	Protein-ligand docking and design of bivalent ligands	32
4.2.1	Ligand selection	32
4.2.3	Protein-ligand docking <i>via</i> LigandScout and AutoDock Vina	34
4.2.4	Linker design	36
4.3	Membrane building <i>via</i> CHARMM-GUI	37
4.4	Molecular dynamics simulation	40
4.4.1	Root mean square deviation	41
4.4.2	Surface area assessment	56
4.4.3	PyRosetta Alanine scan	58
4.4.3.1	Pymol visual inspection	58
4.4.3.2	Energy scores	101
5	Conclusion and outlook	114
6	References	116

Abstract

Cannabinoid receptor 1 (CB1R) and oxytocin receptor (OTR) are class A G-protein coupled receptors that play an important role in a wide range of physiological and pathological processes. Since they are essential for numerous overlapping functions in the brain, they are considered attractive drug targets.

The structures of the receptors are available individually, each of the receptors is known to form both homodimers and heterodimers, however little is known about interaction, interface, and stability of the OTR-CB1 complex. Therefore, this work aims to gain knowledge about the CB1R-OTR complex by creating and examining a model of the receptor dimer using different computational tools.

First, the heterodimeric protein complex was generated by protein-protein docking. Afterwards, twelve heterobivalent ligands were created and docked to the protein complex and these protein complexes with their related heterobivalent ligands were then solvated and inserted in a membrane bilayer. Molecular dynamics simulations were performed for each complex and the results were analyzed regarding their stability and behaviour in the membrane. Analysis of key residues involved in the complex formation was performed through site-specific mutations. We were able to show high stability for nine out of the twelve receptor complexes with their related heterobivalent ligands. The core domain is located between TMH4 of the CB1R and TMH7 of the OTR and further interactions at the interfaces were shown between TMH2 and TMH1 of the CB1R and TMH1 of the OTR, TMH3 of the CB1R, and TMH7 of the OTR as well as TMH4 of the CB1R and TMH6/7 of the OTR. Outside the interface at the TMHs, interactions of residues at ECL1, ECL2, ICL1, ICL2, ICL3, and H8 of the CB1R and residues at the N-terminus, ICL3, ECL3, H8, and C-terminus of the OTR were identified. The number of involved amino acids varied among the twelve investigated interfaces. Moreover, hydrogen bonds were found to be located mainly at the extracellular and intracellular sides of the receptor complexes, and only a few hydrogen bonds are located at the transmembrane region of the receptor complexes.

Kurzfassung

Cannabinoid Rezeptor 1 (CB1R) und Oxytocin Rezeptor (OTR) sind G-Protein gekoppelte Rezeptoren der Klasse A, welche eine wichtige Rolle bei einer Vielzahl an physiologischen und pathophysiologischen Prozessen spielen. Da sie für verschiedenste Funktionen im Gehirn essenziell sind, gelten sie als wertvolle Zielstrukturen für Arzneimittel.

Die Strukturen der einzelnen Rezeptoren sind zwar vorhanden und es konnte nachgewiesen werden, dass sowohl CB1R als auch OTR hetero- und homodimere bilden können, jedoch ist nur sehr wenig über deren Interaktionen, das Interface zwischen den Rezeptoren und die Stabilität der dimeren Komplexe bekannt. Aus diesem Grund ist es das Ziel dieser Arbeit, mittels verschiedener computerbasierter Techniken, mehr Wissen über den CB1R-OTR-Komplex zu gewinnen, indem das Modell des Rezeptordimers erstellt und erforscht wird.

Zuerst wurde das Modell des heterodimeren Proteinkomplexes durch Protein-Protein-Docking erstellt. Weiters, wurden zwölf heterobivalente Liganden kreiert, durch molekulares Docking an den Proteinkomplex gebunden und danach wurden diese Proteinkomplexe mit ihren zugehörigen heterobivalenten Liganden in eine Lipidmembran integriert. Im nächsten Schritt wurde für jeden Komplex eine Moleküldynamik-Simulation durchgeführt und die Ergebnisse wurden hinsichtlich ihrer Stabilität und des Verhaltens in der Membran untersucht und Mutationsanalysen unterzogen. Für neun der zwölf Rezeptorkomplexe mit ihren zugehörigen heterobivalenten Liganden konnte eine hohe Stabilität nachgewiesen werden und drei Rezeptorkomplexen erwiesen sich als instabil. Es konnte ein asymmetrisches Interface des Rezeptorkomplexes nachgewiesen werden, dessen Core-Domäne zwischen TMH4 des CB1R und TMH7 des OTR lokalisiert ist. Weiters wurden am Interface Interaktionen zwischen TMH2 und TMH1 des CB1R und TMH1 des OTR, TMH3 des CB1R und TMH7 des OTR sowie zwischen TMH4 des CB1R und TMH6/7 des OTR festgestellt. Außerhalb des Interfaces zwischen den TMHs wurden Interaktionen zwischen Aminosäuren an ECL1, ECL2, ICL1, ICL2, ICL3 und H8 des CB1R und Aminosäuren am N-terminus, ECL3, ICL3, H8 und C-terminus des OTR entdeckt. Die Anzahl der involvierten Aminosäuren variierte zwischen den zwölf untersuchten Interfaces. Bei der Untersuchung der Rezeptorkomplexe bezüglich Wasserstoffbrückenbindungen, wurden diese hauptsächlich am extrazellulären und intrazellulären Bereich des Rezeptorkomplexes gefunden und nur sehr wenige waren in der transmembranären Region des Rezeptorkomplexes lokalisiert.

1 Introduction

In this master's thesis, the G-protein coupled receptors oxytocin (OTR) and cannabinoid receptor 1 (CB1R) and the dimers that they potentially form are investigated. In the following chapters, they are introduced in detail. Further molecular docking and ranking methods are presented in the theory.

1.1 G-protein coupled receptors

G-protein coupled receptors (GPCR) make up the largest families of transmembrane proteins and regulate a wide range of intracellular signalling by transducing signals from the extracellular to the intracellular side (Kooistra et al., 2021). They regulate different physiological and pathological processes in the body and therefore, they play an important role as therapeutic targets, as they affect a variety of disease-related signalling processes (Venkatakrisnan et al., 2013).

1.1.1 Common structural features

Specific structural features are shared for almost every representative throughout the class of GPCRs (Hilger et al., 2018; Oldham and Hamm, 2008). There is a central transmembrane region comprising seven α -helices (TMH1-7), an extracellular region consisting of three extracellular loops (ECL), the N-terminus, and an intracellular region consisting of three intracellular loops (ICL), an intracellular amphiphilic helix (H8), and the C-terminus (Jacoby et al., 2006). Driven by conformational changes, an extracellular bound ligand transduces its information to the intracellular region of the receptor where interaction with intracellular proteins takes place, which leads to the modulation of different intracellular signalling pathways (Venkatakrisnan et al., 2013).

To visualize the structure of GPCRs the most common methods are X-ray crystallography and cryogenic electron microscopy (cryo-EM) (Liang et al., 2017; Salon et al., 2011).

1.1.2 Diversity of GPCR

Different classification systems are used to categorise G-protein coupled receptors (GPCR). The most common one is the classification in six classes A-F depending according to their structural relation, despite classes D and E are not found in humans. The largest class A is also called "rhodopsin-like" and the oxytocin receptor (OTR), as well as the cannabinoid 1 receptor (CB1R), are allocated to this receptor class. Class B consists of two subfamilies, the secretin receptors and the adhesion receptors and class C are the metabotropic glutamate receptors. Class F receptors are also divided into two subclasses, the frizzled and smoothed receptors (Congreve et al., 2020; Horn et al., 2003).

1.1.3 Signalling pathways of GPCR

The GPCR-signalling can be mediated through the activation of different intracellular proteins. The most important signalling pathways are the G-proteins dependent pathways. Thereby, GPCRs interact with heterotrimeric guanine nucleotide-binding proteins (G-proteins) which leads to activation or inactivation of signalling pathways (Oldham and Hamm, 2008). G-proteins consist of $G\alpha$ -subunit, $G\beta$ -subunit and $G\gamma$ -subunit (McCudden et al., 2005; Smrcka, 2008). When an extracellular signal is transduced to the intracellular side of the receptor by conformational changes of the receptor, the $G\alpha$ undergoes conformational changes, dissociates from the $G\beta\gamma$ heterodimer and signalling pathways are triggered (**Figure 1**) (McCudden et al., 2005; Smrcka, 2008; Neves et al., 2002).

G-proteins are generally classified into four families: G_s , $G_{i/o}$, $G_{q/11}$ and $G_{12/13}$ depending on differences in their $G\alpha$ -subunit. (McCudden et al., 2005; Neves et al., 2002)

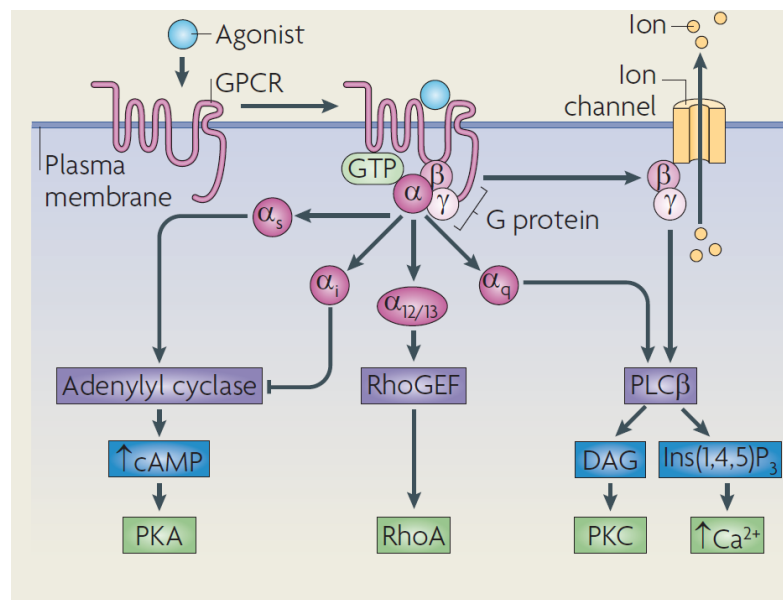


Figure 1. G-protein mediated pathways upon agonist binding to the GPCR. Adapted from Ritter and Hall, 2009.

$G\alpha_s$ -proteins stimulate the adenylyl cyclase (AC) which modulates the conversion of adenosine triphosphate (ATP) to 3',5'-cyclic adenosine monophosphate (cAMP) and pyrophosphate. The second messenger cAMP is responsible for different intracellular effects such as the activation of protein kinases and cyclic nucleotide-gated channels (Hurley 1999; Neves et al., 2002; Ritter and Hall, 2009). The $G\alpha_i$ -proteins are responsible for the inhibition of the AC and some representatives are known to activate the phosphodiesterase (PDE) (Hurley 1999; Margolskee, 2002). The $G\alpha_q$ -proteins activate the phosphoinositide phospholipase C-

β (PI-PLC), which hydrolyses the phosphatidylinositol-4,5-bisphosphate (PIP₂) into the second messenger inositol-1,4,5-trisphosphate (IP₃) and diacylglycerol (DAG). IP₃ regulates the level of calcium, whereas DAG activates protein kinase C (McCudden et al., 2005; Neves et al., 2002). The G $\alpha_{12/13}$ -proteins activate RhoGEFs which regulate small GTPases in the Rho-family. Cell functions such as embryonic development and immune response are regulated by this pathway (Ritter and Hall, 2009; Suzuki et al., 2009; Terrillon and Bouvier, 2004).

The G $\beta\gamma$ -heterodimer leads to a large number of signalling processes such as an increase of IP₃, activation of K⁺-channels and inhibition of N- and P/Q-type calcium currents (Canti, 1999; Cooper, 2003; Hurley 1999; Margolskee, 2002).

1.1.4 Modes of GPCR activation

Lately, five novel modes of GPCR activation were established: biased activation, intracellular activation, dimerization activation, transactivation, biphasic activation. These modes can either occur individually or simultaneously (Wang et al., 2018).

1.1.4.1 Biased activation

Biased activation describes a phenomenon, where certain substance classes lead to signalling pathway selectivity at the receptor (Smith et al., 2018). Thus, only certain intracellular signalling pathways related to this receptor are activated by these specific ligands and others, are not affected (Basith et al., 2018; Wacker et al., 2017). Therefore, it is possible to activate either the G-protein or β -arrestin pathway. The advantage of signalling pathway selectivity can be the prevention of drug-induced side effects, while a certain desired action of the drug is preserved (Wouters et al., 2019).

1.1.4.2 Intracellular activation

Since GPCRs are transmembrane proteins, they span across the membrane from the extracellular space to the intracellular space. However, intracellular activation is observed, which can be explained by two concepts. First, the GPCR in its complex with the ligand is internalized and continues signalling from the intracellular side and the second reason is the localization of GPCR at the membrane of different cell organelles, such as mitochondria, and are therefore intracellular ligand binding leads to intracellular signalling (Wang et al., 2018).

1.1.4.3 Transactivation

Since 1996 it is known that not only do GPCRs interact with each other, but also that they can interact with other membrane receptors, such as the epidermal growth factor receptor (EGFR). This leads to a wide range of receptor activation, mediated by different ligands binding to the same GPCR (Daub et al., 1996; Wang et al., 2018).

1.1.4.4 Biphasic activation

Biphasic activation describes the activation of the GPCR at different times, so the receptor is activated shortly after ligand binding and again a short time later when the ligand is still binding. The exact mechanism of this biphasic activation remains unclear till now (Katsidoni et al., 2013; Wang et al., 2018).

The biphasic activation is divided into three different modes. The first mode describes a G-protein mediated down streaming effect in the first phase and a β -arrestin mediated down streaming effect in the second phase (Gesty-Palmer et al., 2006; Wang et al., 2018). The second mode is defined as the exact opposite and the third mode mentions an activation of different G-protein mediated down streaming effects in the first phase and second phase (Gong et al., 2008; Hadi et al., 2013; Wang et al., 2018).

1.1.4.5 Dimerization activation

There are three categories of dimerization activation to differ. The first category comprises receptors that can mediate signalling only if they dimerize as homodimeric or heterodimeric complexes but not as monomers (Wang et al., 2018).

The second category is characterized by different receptor signalling, depending on whether they exist as dimers or monomers. So is receptor A responsible for signalling pathway A and receptor B responsible for signalling pathway B but the receptor dimer AB results in signalling pathway C (Marc Parmentier, 2015).

The third category describes receptors that can change from signalling *via* G-protein to signalling *via* β -arrestin and *vice versa*, depending on whether they exist in their monomeric or dimeric conformation (Wang et al., 2018).

1.2 Cannabinoid receptors

There is a long history behind the therapeutic use of cannabinoids addressing the cannabinoid receptors since the cultivated plant *Cannabis sativa*, which contains cannabinoids as active ingredients is used for therapeutical and spiritual issues for several millennia (Sarfraz et al., 2005, Al-Zoubi et al., 2019). Cannabinoid receptors are known to play an important role in neuronal development and neuromodulatory processes and in the recent past, cannabinoid receptors have drawn great attention, due to their extensive potential in therapeutic value. More and more pathophysiological conditions involving cannabinoid receptors have been found, such as cancer, neurodegenerative disorders, and metabolic syndromes (Al-Zoubi et al., 2019; Bosier et al., 2010). A negative aspect of cannabinoids in clinical usage and therefore still a huge challenge to be overcome is the psychoactive effect, which is responsible for the limited therapeutic use (Zou and Kumar, 2018).

1.2.1 Classification of cannabinoid receptors

The endocannabinoid system comprises of two cannabinoid receptors, cannabinoid receptor 1 (CB1R) and cannabinoid receptor 2 (CB2R) that are identical in 44% of the total sequence and show 68% sequence similarity in their transmembrane region (**Figure 2**) (Hua et al., 2020). Due to their sequence and structural similarities, the major challenge concerning drug targeting of cannabinoids is ensuring receptor selectivity of the ligand. Besides their structural similarity, they differ in function, tissue distribution, and signalling (Hua et al., 2020; Zou and Kumar, 2018).

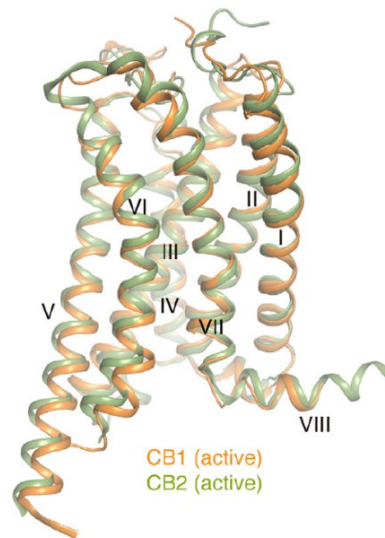


Figure 2. Comparison of active CB1, orange; and CB2, green. Adapted from *Hua et al., 2020*.

1.2.2 Signalling pathways

CB1R couples primarily to $G_{i/o}$ but also to G_s , $G_{q/11}$ -proteins opening a wide range of physiological responses, whereas CB2R only couples $G_{i/o}$ -protein (Glass and Felder, 1997; Lauckner et al., 2005). Moreover, β -arrestins interactions and other signalling pathways are assumed to be affected due to CB1R or CB2R activation, and not all signalling mechanisms are sufficiently explained so far (Bosier et al., 2010; Hua et al., 2020).

1.2.3 Tissue distribution

The CB1R is one of the most common GPCRs in the brain and its high density in the central nervous system is responsible for the control of motor function, cognition, memory, and analgesia (Herkenham et al., 1990; Hua et al., 2016). The function is to inhibit neurotransmitter

release in the central and peripheral neurons. Further, CB1R is also expressed in the periphery, but not at this high density compared to the central nervous system (Hua et al., 2016, Hua et al., 2020).

The CB2R can be found particularly in peripheral organs with an immune function such as tonsils, thymus, and lungs and a higher expression of CB2R at the central nervous system is found to play an important role in diseases including Alzheimer's disease and multiple sclerosis (Hua et al., 2020).

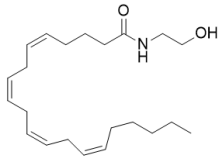
1.2.4 Endogenous and exogenous cannabinoids

Cannabinoids are lipophilic ligands binding to CB1R and/or CB2R. A distinction is made between endogenous and exogenous ligands and it has to be pointed out that cannabinoids can interact with different receptors or proteins besides CB1R and CB2R such as the transient receptor potential (TRP) channels or orphan GPCRs GPR3, GPR6, and GPR12 (Haspula and Clark, 2020; Muller et al., 2019; Morales and Reggio 2017).

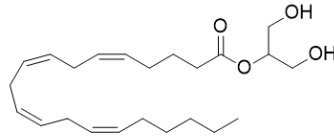
Typical representatives of endogenous cannabinoids are the eicosanoids 2-arachidonoylglycerol (**1**) and anandamide (**2**) (Devane et al., 1992; Mechoulam et al., 1995; Sugiura et al., 1995). They are orthosteric ligands and 2-arachidonoylglycerol is a full agonist while anandamide is a partial agonist for both CB1R and CB2R (Zou and Cumar, 2018). Besides, there are fewer known orthosteric ligands such as virodhamine (**3**), a full agonist at the CB2R and an antagonist at the CB1R (Haspula and Clark, 2020; Porter et al., 2002). Lipoxin A4 (**9**) is a representative of potent endogenous allosteric modulators functioning as a positive allosteric modulator of CB1R and CB2R (Bauer et al., 2012; Haspula and Clark, 2020; Pamplona et al., 2012). Moreover, cholesterol (**10**) is an allosteric modulator of CB1R. (Haspula and Clark, 2020; Hua et al., 2020).

Exogenous cannabinoids are divided into natural and synthetic ligands. The best known natural phytocannabinoid is Δ -9-tetrahydrocannabinol (**4**) with a high affinity to CB1R and CB2R. Representatives of the synthetic cannabinoids are HU-210 (**5**), R-(+)-WIN55212 (**6**), and CP55940 (**7**), also binding CB1R and CB2R (Haspula and Clark, 2020). Another important synthetic ligand for the CB1R is rimonabant (**8**) which is used as a starting point for the design of a variety of selective inverse agonists (**Figure 3**) (Grant et al., 2019).

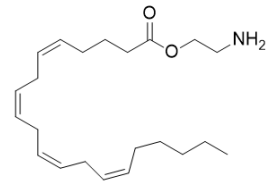
Other important ligands at the CB1R and the CB2R are so called high-affinity ligands that are used to stabilize the receptor during sampling techniques such as cryo-EM and crystallisation. At the CB1R there are the high-affinity ligands AM6538 (**11**) and AM841 (**12**) (Hua et al., 2016; Hua et al., 2020) and at the CB2R there are the high-affinity ligands AM10257 (**13**), AM12003 (**14**) (**Figure 4**) (Hua et al., 2020; Li et al., 2019). The respective binding affinities are given in **Table 1**.



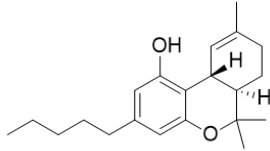
Anandamide (1)



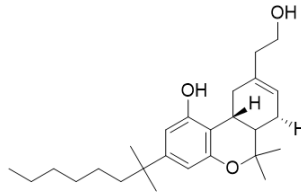
2-Arachidonoylglycerol (2)



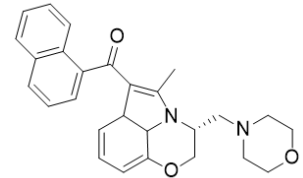
Virodhamin (3)



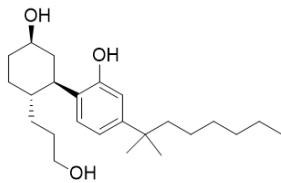
Δ-9-Tetrahydrocannabinol (4)



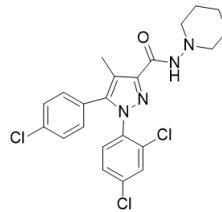
HU-210 (5)



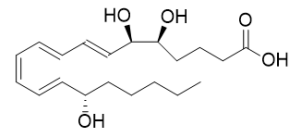
R-(+)-WIN552121 (6)



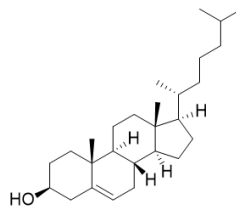
CP55940 (7)



Rimonabant (8)

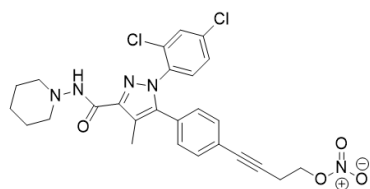


Lipoxin A4 (9)

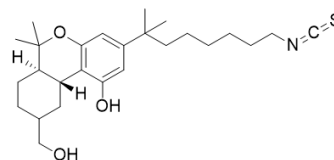


Cholesterol (10)

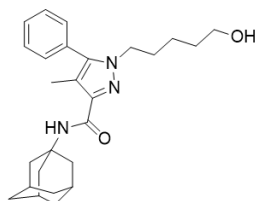
Figure 3. Molecular structure of OTR ligands (1-8) and the allosteric modulators (9-10)



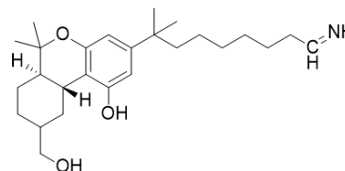
AM6538 (11)



AM841 (12)



AM10257 (13)



AM12003 (14)

Figure 4. Molecular structure of high-affinity ligands for the CB1R (11-12) and CB2R (13-14)

Table 1. Binding affinity of the high-affinity ligands 11 and 12 towards CB1R and 13 and 14 toward CB2R. These ligands are used to stabilize the receptors during crystallization.

Receptor	Ligand	Binding affinity ($K_i \pm \text{SEM}$ nM)	Ref
CB1R	AM6538	5.1 ± 0.9	Hua et al., 2016
	AM841	$3,12 \pm 0,27$	Hua et al., 2020
CB2R	AM10257	5.1 ± 0.9	Li et al., 2019
	AM12003	$0,37 \pm 0,03$	Hua et al., 2020

1.2.5 Structure of cannabinoid receptors

Cannabinoid receptors CB1R and CB2R have the same fundamental structure. They belong to the class A GPCR subfamily with seven transmembrane helices, three extracellular and three intracellular loops, an extracellular N-terminal, an intracellular C-terminus, and an amphiphilic helix 8 (Al-Zoubi et al. 2019).

Some conformational and structural differences between CB1R and CB2R are found to be responsible for their differences in function and signalling (Hua et al., 2016; Li et al., 2019). First of all, the extracellular and intracellular domains of CB1R undergo large conformational changes when changing from inactive to an active state, whereas it is shown for the CB2R that the extracellular domain only changes minimal while activation and a single residue difference

in ICL2 can be held responsible for the difference in G-protein coupling (Hua et al., 2020; Shao et al., 2016).

The orthosteric binding pocket has a very interesting conformation. The non-truncated N-terminus of the CB1R functions as a V-shaped plug, which can restrict access to the orthosteric binding pocket from the extracellular side. Moreover, the N-terminus is shown to be in an ordered form, which is important for the function of CB1R (Hua et al., 2016; Li et al., 2019; Shao et al., 2016). The ELC2 folds into a structure that projects four residues into the binding pocket that are very important for the interaction of certain ligands and there is evidence that two cysteines in ECL2, forming an intraloop disulfide bond (Cys257 and Cys264), are important for the function of CB1R too. What is quite different from other receptors of the class A GPCR, is a missing disulfide bond between ECL2 and TMH3 (Hua et al., 2016; Mallipeddi et al., 2017).

1.2.5.1 Available structure of inactive cannabinoid receptor 1

The PDB-ID of the inactive cannabinoid receptor 1, found at the Protein Data Bank, is **5TGZ**. To get this representation of the CB1R's structure, the wild-type sequence of the receptor is co-crystallized with AM6538 to enable crystallization of the CB1R, and further adaptations had to be done. Therefore, Flavodoxin was inserted into the ICL3 at Val 306 and Pro 332 to gain higher receptor stability. Moreover, the N- and C-termini were truncated by 98 and 58 residues, and mutations were introduced due to improvement of the expression and thermostability of the receptor. The following mutations were done: Thr2103.46Ala, Glu2735.37Lys, Thr2835.47Val, and Arg3406.32Glu (Hua et al., 2016).

1.2.5.2 Available structure of active cannabinoid receptor 1

The structure of the active cannabinoid receptor 1, obtained from the Protein Data Bank, is **6KPG** and it is based on a cryogenic electron microscopy (cryo-EM) sample with the agonist AM841 in the binding pocket. When the sample was prepared, cryo-EM images were taken *via* direct electron camera, and movies were made. To process the images and reconstruct a 3D representation, 5577 movies were collected and contrast transfer function parameters were valued. Further, particle selection and 2D and 3D classification were done. The best 3D representation was then used for further steps, such as final 3D classification and refinement to finally generate a 3,0Å map of the receptor (Hua et al., 2020).

For model generation, the cryo-EM structure of the CB1-FUB-Gi complex was used as a template for comparison against the electron density map. In a further step, the model was docked into the EM-density map, adjustments, as well as rebuilding, were performed and the final statistic parameters were evaluated (Hua et al., 2020).

1.3 Oxytocin receptor

The oxytocin receptor (OTR) is assigned to the class A GPCRs and it is an attractive drug target since it is involved in several disorders such as cancer, pain, and autism (Busnelli et al., 2018; Liu et al., 2020). The endogen ligand oxytocin plays an important role in various physiological functions as a central neurotransmitter and in the periphery reaching from cognitive effects and bonding behaviour to the control of lactation and parturition. (Busnelli et al., 2016; Walterspühl et al., 2020).

The oxytocin receptor is part of the oxytocin/vasopressin receptor system which is important for the modulation of complex social behaviour and bonding (Donaldson et al., 2008; Veenema and Neumann, 2008). The three vasopressin (VP) receptors V1aR, V1bR, and V2R share high structural similarity with the oxytocin receptor as they are also part of the class A GPCRs. (Gimpl et al., 2008; Veenema and Neumann, 2008).

1.3.1 Signalling pathways

A lot of signalling pathways are mediated by the oxytocin receptor whereby the most important pathways are mediated by the G-proteins $G_{\alpha i}$, $G_{\alpha q}$, and $G_{\beta \gamma}$ whereby $G_{\alpha q}$ plays an essential role in the upregulation of the Ca^{2+} level. Further, oxytocin receptor plays an important role in the activation of MAP kinases ERK1, ERK2 and ERK5 as well as β -arrestins. (Devost et al., 2008; Gimpl et al., 2008).

1.3.2 Tissue distribution

The OTR is expressed throughout different tissues in different concentrations. For example, tissues such as the kidney, heart, thymus, pancreas, adipocytes, uterus, and brain are found to express the OTR in different levels. In the brain, certain areas are claimed to have higher levels of the receptor such as the *nucleus accumbens*, and prelimbic cortex of prairie voles. (Mitre et al., 2018).

1.3.3 Oxytocin and exogenous ligands

The neurohypophysial hormone oxytocin is the only endogenous agonist of the OTR. Its hallmark is the presence of a disulfide bridge between cysteines on position one and six leading to the typical structure of a nonapeptide with a cyclic part of six residues and an aminated C-terminal tail comprising three residues. (Gimpl and Fahrenholz, 2001; Richard et al., 1991, Walterspühl et al., 2020). Oxytocin itself is administrated in terms to induce labour (Gimpl et al., 2008; Walterspühl et al., 2020).

Antagonists are essential in the treatment of preterm labour and for the reduction of myometrial contractions. The representatives atosiban (**15**), barusiban (**16**) (peptide ligands) and retosiban (**17**) (non-peptide ligand) are used clinically for the prevention of preterm labour since they have a high affinity to the OTR (**Figure 5**) (Gimpl et al., 2008; Åkerlund et al, 1999; Nilsson et al., 2003; Pierzynski et al., 2004).

Additionally, cholesterol (**10**) is predicted to be an allosteric modulator for many GPCRs and so it is found to play an important role concerning the function and thermostability of the OTR, with the ability to create a higher affinity for ligands. Moreover, divalent cations are found to be important allosteric modulators, due to their ability to increase the affinity of oxytocin for the OTR (Waltenspühl et al., 2020).

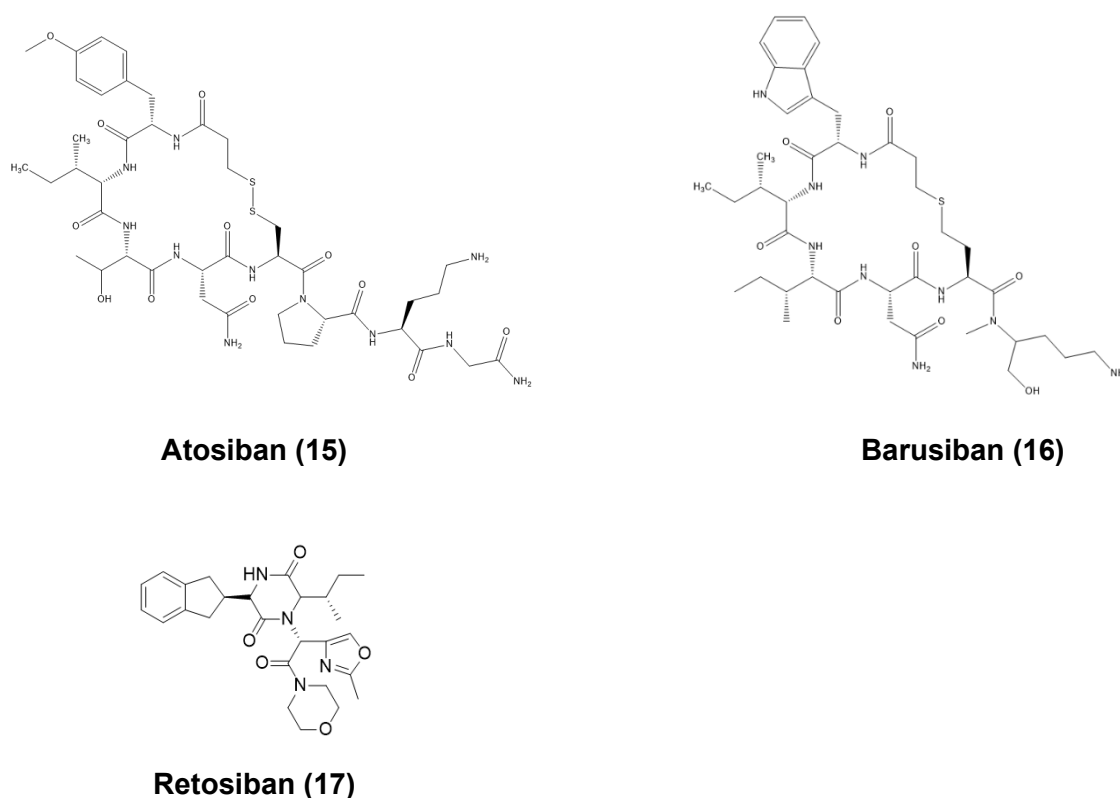


Figure 5. Molecular structure of OTR antagonists Atosiban (**15**), Barusiban (**16**) and Retosiban (**17**).

1.3.4 Relationship to vasopressin

Caused by the high structural similarity between the OTR and the VP receptors, their endogenous ligands oxytocin (**18**) and vasopressin (**19**) are structurally closely related (**Figure 6**). They differ in two of the eight amino acids: residue 3 (Ile/Phe) and residue 8 (Leu/Arg) which are responsible for the similar but yet different affinity to the OTR and VP receptor (Frantz et al.,

2010). Therefore, ligands with peptide structures comparable to oxytocin and vasopressin address both OTR and VP receptor with similar affinity and the goal of receptor selectivity is often challenging (Dekan et al., 2021; Goodson et al., 2013; Hammock et al., 2015).

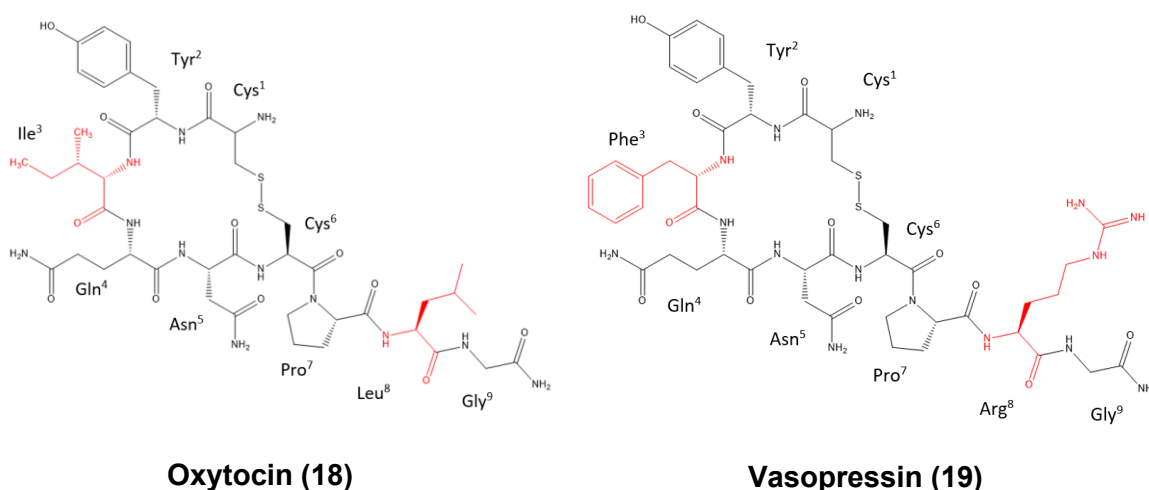


Figure 6. Molecular structure of A: oxytocin in comparison to B: vasopressin. Different residues at positions 3 and 8 are coloured red.

1.3.5 Structure of oxytocin receptor

The Oxytocin receptor is characterized by seven transmembrane helices (TMH 1-7), three intracellular loops (ICL), three extracellular loops (ECL), and an amphiphilic helix 8 at the C-terminus. It has to be highlighted that similar to other receptors in the class A GPCRs the ECL2 is typically formed to an extended β -hairpin, locally anchored to TMH3 due to a disulfide bridge (Hilger et al., 2018; Oldham and Hamm, 2008; Waltenspühl et al., 2020).

The orthosteric binding pocket contains a polar hemisphere located at TMH2 and TMH4 and a larger hydrophobic hemisphere at TMH5 to TMH6. A notable difference to other class A GPCRs is given as the extracellular ends of helices 2, 3, 5, 6, and 7 are moved away from the central axes of the receptor which results in an enlargement of the extracellular binding pocket when compared with other receptors of the class A GPCRs (Waltenspühl et al., 2020).

1.3.5.1 Available structure of inactive oxytocin receptor

The PDB-ID regarding the inactive oxytocin receptor, found at the Protein Data Bank, is **6TPK**. The modifications of this receptor structure are diverse. To get adequate purification of the receptor, directed evolution in *saccharomyces cerevisiae* was performed on the wild-type OTR in two rounds achieving eight mutations. Moreover, the wildtype had to undergo three further changes to enable crystallization in the lipidic cubic phase. All these mutations lead to no change in the binding affinity of the co-crystallized antagonist retosiban. First, it was necessary

to replace a total of 34 residues with the thermostable *Pyrococcus abyssi* glycogen synthase domain, secondly, 30 residues of the flexible C-terminus were truncated, and thirdly two residues were substituted with alanine (Waltenspühl et al., 2020).

1.3.5.2 Available structure of active oxytocin receptor

The structure of the active oxytocin receptor was not available at the Protein Data Bank but in the study of *Busnelli et al., 2016*. There it is described that the β -adrenergic 2 receptor crystal structure presented in an active conformation and interaction with Gs was used as a template for the OTR. The receptors show great similarity in the amino acid sequence (Busnelli et al. 2016).

Modifications for protein preparation had to be done. Therefore, the G-protein, the extracellular fused T4 Isozyme, and the ligand were removed. Moreover, the loop length was reduced and the ECL2 was completely deleted because the amino acid sequence and length were too different compared to the OTR. Only the C-terminal part of the ECL2 was retained. However, the ECL2 of the opsin receptor is assumed to be more identical to the OTR, thus the crystal structure of this loop was merged into the modified β -adrenergic 2 receptor (Busnelli et al. 2016).

1.4 GPCR dimerization

GPCRs were first postulated to form dimers by *Agnati et al. in 1982* but not little attention was paid to this. Only decades later interest in GPCR dimers arose due to the better insight into receptor cross-talk and many studies focused on this topic (Agnati et al., 1982; Angers et al., 2000; George et al., 2000).

Together with new insight of GPCR dimerization, it was predicted that not only the receptors dimerize but also the downstream processes of the dimers are different from their monomeric states (Gurevich and Gurevich, 2008; Wang et al., 2018). Nowadays the importance of receptor dimerization in certain tissues and the novel signalling mechanisms and functions are widely known and many research teams have the goal of further understanding and revealing new insight concerning this topic (Terrillon and Bouvier, 2004). As mentioned in chapter 1.1.4.5, there are three different categories of dimerization-induced activation of GPCRs (Wang et al., 2018).

1.4.1 Methods to study dimerization

Important experimental methods used to reveal the existence of GPCR dimers in cells are cross-linking, immunoprecipitation, and bioluminescence resonance energy transfer (BRET) or fluorescence resonance energy transfer (FRET) (Rios et al., 2001).

Cross-linking methods use a variety of different linkers to connect the two receptors of interest which are assumed to form dimers and to detect these complexes subsequently (Guo et al., 2005; Shah et al., 2020). Immunoprecipitation makes use of antigens that bind antibodies attached to a protein or a dimeric receptor of interest so these molecules can be isolated by methods such as gel filtration or density gradient sedimentation (Bonifacino et al., 1999; Rios et al., 2001; Waldhoer et al., 2005). FRET and BRET studies are the methods of choice for evaluating receptor dimerization. They are based on fluorescence and luminescence emission respectively caused by high proximity of energy donors and acceptors for detection of dimers (Carriba et al., 2008; Cotte et al., 2012; Masuho et al., 2015).

Further computational studies are important to gain further insight into the interaction mode between the receptors forming a dimer and the characteristics of the receptors as they exist as dimers. Therefore, docking approaches together with mutational analyses are the key methods used (Filizola et al., 2005; Gouldson et al., 2000; Meng et al., 2014).

1.4.2 Cannabinoid receptor 1 and Oxytocin receptor dimerization

Due to the increasing interest in GPCR oligomerization, different research teams published their findings regarding receptor dimerization of OTR or CB1R. Literature research was carried out concerning the homodimerization and heterodimerization of OTR and CB1R and the results are presented in subchapters below. Unfortunately, hardly any detailed information concerning involved residues in protein-protein interaction were published, since research was mostly concentrated on proving dimerization in cell studies (Rios et al., 2001), but no computational experiments to research specific protein-protein interactions between the human CB1R and the human OTR were performed.

1.4.2.1 Cannabinoid receptor 1 dimerization

CB1 receptors are known to form both homodimers and heterodimers. Examples of receptors known to build heterodimers with CB1R are cannabinoid receptor 2 (CB2R), dopamine 2 (D2) receptor, adenosine receptor, angiotensin (AT1) receptor, orexin (OX1) receptor, and opioid μ 1 receptor (Callen et al., 2012). Further, opioid δ receptor is proven to form heterodimers with CB1R (Rozenfeld et al., 2012).

1.4.2.2 Oxytocin receptor dimerization

Regarding homodimerization of OTRs, the interactions between TMH1-TMH2-helix8 or TMH5-TMH6 were taken for further investigations since these interactions are assumed to be possible. When docking bivalent ligands, the TMH1-TMH2-helix8 interface is seen as the better one because a channel-like passage between TMH1 and TMH2 makes enough place for the linker of the bivalent ligand and enables both moieties to bind at the orthosteric binding pockets of

the two OTRs (**Figure 7**). TMH5-TMH6 interface would require the usage of a larger linker (Busnelli et al., 2016).

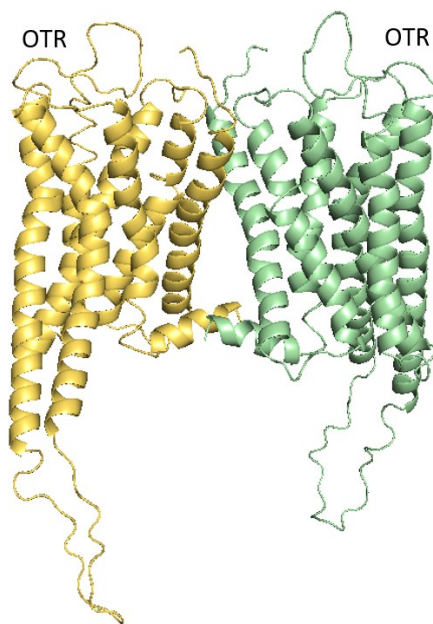


Figure 7. Molecular structure of OTR-OTR homodimer. PDB-ID obtained from *Busnelli et al., 2016*. Interface formed between TMH1-TMH2-helix8 of both OTRs.

Further investigations revealed the existence of dopamine (D2) receptor-oxytocin receptor heterodimerization (Romero-Fernandez et al., 2013) and dimerization of the OTR with the vasopressin receptors V1a and V2 (Busnelli et al., 2016), but no suggestions of interacting residues are made.

1.5 Bivalent ligands

Due to increasing interest in homodimeric and heterodimeric receptors, the development of bivalent ligands is essential to simultaneously stimulate dimeric receptors (Grant et al., 2019). Bivalent ligands can be defined as “molecules that contain two discrete recognition units linked through a spacer”. The two ligand moieties can either interact with two components of a receptor dimer or with two binding sites at the same receptor (Zhang et al., 2010).

Two types of bivalent ligands exist. Heterobivalent ligands, where both ligands are different from each other, and homobivalent ligands, where the ligands are the same (Busnelli et al., 2016).

Bivalent ligands for many receptor dimers, such as opioid receptors, adrenergic receptors, dopamine receptors, serotonin receptors, and muscarine receptors are already developed and there is high interest in developing further bivalent ligands for other receptor dimers too (Grant et al., 2019).

The development of bivalent ligands comprises four general steps. At first, a ligand has to be chosen, which binds selectively to the receptor and has attachment sites for the linker. Then, in the second step, a linker is chosen which can link the two ligands and in the third step, the linker has to be proven to not disturb the receptor-ligand interaction. In the fourth and last step, the linker has to be adapted in length, so an optimal ligand-receptor interaction is guaranteed (Shonberg et al., 2011; Zhang et al., 2007).

There is a wide range of different linkers that can be used for the synthesis of bivalent ligands. The decision, which linker is taken, can be quite challenging and depends on the properties of the ligands and receptors. Two common types of linkers are mainly used for the synthesis of bivalent ligands. The first class are polyethylene glycol (PEG) linkers and the second class are small peptides (Bonger et al., 2007; Grant et al., 2013; Portoghese et al., 2001; Rajeswaran et al., 2001). An example for other, more complex linkers, is a linker, consisting of a series of triamines and a protonable nitrogen atom, which is used for bivalent ligands at the CB1R (Zhang et al. 2010).

1.6 Molecular docking and ranking methods in the theory

In this chapter, the protein-protein docking and protein-ligand docking, as well as ranking methods are described in detail.

1.6.1 Protein-protein docking

Protein-protein docking is an essential computational tool for identifying possible binding interfaces for receptor dimers and estimating possible interactions between them (Kaczor et al., 2018; Lyskov et al., 2008). Due to growing interest in these interactions and the resulting biological processes, many sampling algorithms and scoring functions were developed over the last decade and it can be challenging to compare the results and to choose the right method for a certain structure (Huang, 2015; Porter et al., 2019).

Protein-protein docking typically consists of two consecutive stages, the docking stage, and the ranking stage (Huang, 2015).

1.6.1.1 Docking stage

The docking stage is also called sampling stage and is done using different search algorithms. Two different proteins called A and B or receptor and ligand are docked in two steps, first the rigid docking and then the refinement step (Zhang et al., 2016). At the rigid docking stage, the proteins are treated as rigid bodies with no flexibility, and protein B or ligand is translated and rotated on three translational and three rotational axes in search for relative orientation to pro-

tein A or receptor. Further, a refinement step with energy minimization takes place where specific residues, side-chains, and the backbone are free to move to incorporate small conformational changes (Huang, 2015; Vakser et al., 2014; Zhang et al., 2016).

The search algorithms used in this docking stage are challenging and have high computational cost. Direct docking algorithms can be divided into three broad categories: (i) global systematic rigid body docking, (ii) medium-range docking methods, and (iii) restraint-based docking (Kozakov et al., 2017; Vajda et al., 2009; Zhang et al., 2016).

The global systematic rigid body docking methods can be used without prior information of the complex since the whole translational and rotational conformational space has to be sampled. Only minimal conformational changes are allowed since the rigid complexes are modelled. (Zhang et al., 2016; Kozakov et al., 2017).

The medium range method samples only specific regions of the complexes thus requiring further information about the modelled proteins in advance, and it is especially helpful for homology models, where certain parts of the receptor are known to identify the regions of interest (Zhang et al., 2016). The Monte Carlo search algorithms are examples of the medium-range docking methods and they are based on the Monte Carlo method (Read et al., 1995). This is a statistical concept that uses individual random events that have no order and don't follow a pattern to draw conclusions for deterministic systems. Thereby random sampling is conducted repeatedly to obtain numerical results for investigated parameters (Kroese and Rubinstein, 2012). In the case of protein-protein docking, the translational and rotational orientations of one of the proteins are the variables that are changed randomly to obtain different interaction modes (Harrison, 2010; Zhang et al., 2016). Further, the Acceptance-Rejection Method can be used to identify whether the random binding conformations are possible and therefore accepted or rejected (Kroese and Rubinstein, 2012). The Monte Carlo method is also used for Monte Carlo minimization. Here the method is applied to refine the docking partners poses is a refinement step used for example by the Memdock server (Gray et al., 2012; Hurwitz et al., 2016). Thereby a certain level of flexibility, especially at the side-chains is considered. (Gray et al., 2012).

The restrain based docking methods uses interactions restraints to achieve a search, which is limited to specific conformational space. To achieve good results, sufficient restraints have to be available (Kozakov et al., 2017).

Notable docking algorithms which are quite important for the refinement step are the genetic algorithms which are classified as non-deterministic search algorithms. Two genetic operations are the basis of the algorithms, first, the crossover and mutation, and second, a fitness function (Zhang et al., 2016).

1.6.1.2 Ranking stage

Following the sampling stages ranking and scoring takes place. Typically, the results are already ranked in the docking stage, but to get better results a re-scoring and re-ranking is done. All in all, two widely used scoring functions can be distinguished. First, there are force field-based scoring functions and secondly, there are knowledge-based scoring functions. Further description can be found in chapter 3.3 (Zhang et al., 2016; Gromiha et al. 2017).

1.6.1.3 Benchmarks of protein-protein docking methods

Due to the fact that so many different search algorithms and scoring functions are available, comparison and evaluation are necessary to select the best method suited for a specific task. Benchmarks are essential for the comparison of different docking methods. Protein-protein docking benchmarks are collections of protein dimers shown in different binding modes. There is a wide range of benchmarks available containing different sets of complexes and they are used for comparing docking algorithms systematically (Hwang et al., 2010; Porter et al., 2019). One benchmark has to fulfil two important criteria: First, to reduce bias, unnecessary information has to be eliminated and the interactions of the protein dimers have to be diverse to show a wide range of interactions. Second, it has to be guaranteed that the resolution is high enough so the results show reliable data (Zhang et al., 2016).

Two essential criteria for ranking the different kinds of scoring functions are root mean square deviation (RMSD) and f_{nat} (Zhang et al., 2016; Janin et al., 2003). Two modes of application of the RMSD are the absolute RMSD and the relative RMSD. The absolute RMSD is used to measure the average distance between atoms of the two aligned proteins without taking coordinate translation and rotation into account, and the relative RMSD includes an alignment step before the actual calculation of the RMSD so all coordinates of the protein complex are aligned (Kirchmair et al., 2008). f_{nat} defines the fraction of native protein-protein contacts that are correctly predicted in the docking model (Zhang et al., 2016).

1.6.2 Protein-ligand docking

Protein-ligand docking methods are used for identifying the binding mode of ligands within the binding pocket of macromolecular targets. They play a major role in structure-based drug design and the identification of structure-activity relationships (SAR) (Ferreira et al., 2015).

It is important to have ligands in a stereochemically defined geometry and the correct protonation state and a higher overall size of the ligands and therefore a higher number of rotatable bonds leads to a higher number of degrees of freedom, causing increased computational cost and less docking accuracy (Brooijmans and Kuntz, 2003; Torres et al., 2019). Often, the location of the binding pocket at the target is known, but if not, it is possible to predict the most

probably binding pocket by different softwares or a “blind docking” simulation is done (Torres et al., 2019).

The main applications of protein-ligand docking are target fishing and profiling to predict certain targets on basis of complementarity, the prediction of adverse drug reactions, the identification of simultaneous modulations of a broad range of receptors called polypharmacy, drug repositioning, identification of the essential structural properties for ligand-receptor binding and virtual screening for identification and optimization of certain compounds (Pinzi and Rastelli, 2019).

To identify the best docking pose, search algorithms are used for conformational search and docking while scoring functions are used for evaluation of binding energies and ranking them (Ferreira et al., 2015; Torres et al., 2019).

1.6.2.1 Conformational search and docking

In the stage of the conformational search, the structural features of the ligand, such as torsional, translational, and rotational degrees of freedom are modified to evaluate different ligand-receptor conformations (Ferreira et al., 2015; Torres et al., 2019).

Different search algorithms pursue different strategies that can be divided into three classes: systematic strategy, stochastic strategy, deterministic strategy (Guedes et al., 2014; Morris et al., 2008; Torres et al., 2019). Systematic search algorithms examine each degree of freedom of the ligand incrementally, which means a high number of calculations are found. They can be shown as conformational ensembles or incremental constructions based on ligand fragmentation (Morris et al., 2008; Torres et al., 2019). Stochastic search algorithms make the ligand undergo random changes in the degrees of freedom. Thus, it cannot be guaranteed to receive the overall best docking result (Torres et al., 2019). For deterministic search algorithms, the conformation of the ligand in each step depends on the conformation in the previous step and the new conformational state has either the same or lower energy values. These algorithms are widely used for energy minimization and molecular dynamics simulations (Guedes et al., 2014).

1.6.2.2 Evolution of binding energies and ranking

In the step of evaluating the binding energies, scoring functions are used for estimating the binding energy of the previously found conformations for ligand-receptor complexes (Guedes et al., 2014). Mostly, the scoring functions rely on a consensus scoring scheme and re-scoring approaches and the results are ranked from best to worst concerning their binding free energy (Torres et al., 2019). The major types of scoring functions are empirical scoring, force field-based functions, and knowledge-based functions (Guedes et al., 2014, Eldridge et al., 1997; Kitchen et al., 2004). They are described in detail in chapter 3.3.

1.6.2.3 Benchmarks of protein-ligand docking methods

Benchmarking sets are as important for protein-ligand docking as for protein-protein docking. They are used to compare experimental data to assess the performance and accuracy of the programs and they help in choosing the right program for certain tasks (Torres et al., 2019). There are many different benchmark datasets of targets and ligands available at databases that also provide further information such as true binding affinity or active/inactive distinction (Huang et al., 2006). The goal of the benchmarking datasets is to group as much high-quality data as possible. Benchmarks are different for pose prediction, binding affinity calculations, and virtual screening (Irwin, 2008; Torres et al., 2019; Wang et al., 2004).

For pose prediction, the comparison of RMSD calculations are used and to compare binding affinity, root mean square residual correlations (RMSD) calculations and the Pearson correlation coefficient can be taken. (Janin et al., 2003; Torres et al., 2019).

1.6.3 Ranking

Scoring functions are used to rank the results of the docking step so the near-native structures are the highest results. This is very challenging and important to guarantee the reliability of the docking results because it is worth nothing having an excellent docking run when the results are not appropriately represented at the end. Due to intensive research over the years, four scoring functions were developed. The three classical force field-based scoring functions, knowledge-based scoring functions, empirical scoring functions and advanced machine learning-based scoring functions (Li et al., 2019).

1.6.3.1 Force field-based scoring functions

These scoring functions can calculate interactions between atoms of the protein-protein complex or protein-ligand complex directly. A set of parameters such as van der Waals interactions, electrostatic interactions, the standard bond angles, and many more are used to calculate various potential terms. By summing them up, the energy of each conformation can be calculated. To improve the accuracy, torsion, entropy, solvation and desolvation effects, and solvent modes are incorporated. There are many different force fields based on different parameter sets and energy formulas. To improve physics-based scoring functions, quantum mechanics can be used (Zhang et al., 2016; Li et al., 2019).

1.6.3.2 Knowledge-based scoring functions

Knowledge-based scoring functions are not only part of the ranking but also part of the docking stage, so more native-like conformations can be generated. They are characterized by taking the best weights of each scoring term into account and they are based on training sets for comparison (Zhang et al., 2016; Liu et al., 2011). Underlying inverse Boltzmann approaches,

desired pairwise potentials between two atoms of a 3D structure of a large set of protein-protein complexes or ligand-protein complexes are defined. They can be used to predict the interaction of the paired atoms by taking the frequency of the atoms into account (Chuang et al., 2008). Further, they are used to improve the f_{nat} , which means the interaction of ligand and protein is more relatable to the interaction of the native structures (Zhang et al., 2016).

1.6.3.3 Empirical scoring functions

Empirical scoring functions refer to structure-activity relationships and previously known binding affinity parameters are used for the prediction of accurate binding affinities. Therefore, a training set with given binding affinities is used to get better weights of the energetic factors. Empirical scoring functions usually employ simple energy terms that are used for the prediction of binding affinities, ligand poses, and virtual screening (Torres et al., 2019; Li et al., 2019).

1.6.3.4 Machine learning-based scoring functions

These scoring functions are not classical like the previous ones since they make use of different machine-learning algorithms. Usually, they are not used as common scoring functions but for re-scoring, so the accuracy of the results can be further improved. The workflow comprises data selection, data representation, and feature selection to predict the best binding modes and evaluation of the performance (Li et al., 2019).

2 Aims and significance

So far, little is known about the structural characteristics and interactions of this CB1R-OTR receptor complex, since the crystal structure of the CB1R-OTR complex has not been investigated yet. Our in-house data (collaboration with Center of Brain Research, Medical University of Vienna, Austria) however demonstrate presence of the mRNA for both receptors on the same cells within distinct brain regions, as determined by the FISH (*Fluorescent in situ hybridisation*) method. Fundamental for investigations are the individual structures of the oxytocin receptor (Waltenspühl et al., 2020; Busnelli et al., 2016) and cannabinoid receptor 1 (Hua et al., 2016; Hua et al., 2020)

To further improve the understanding of the CB1R-OTR dimeric complex this thesis focuses on creating a molecular model of this receptor complex, investigating the stability and structure of the complex and examining the interface built by the two receptors. Further heterobivalent ligands with different linker lengths are designed and the stability of the ligands at the receptor complex is analyzed computationally. This aim was addressed step-wise in the following five stages consecutively:

- I. Generating a model of the CB1R-OTR heterodimeric complex by molecular docking of the CB1R and OTR.
- II. Docking selective ligands to the receptors' orthosteric binding pockets and linking them with linkers of different length to design heterobivalent ligands.
- III. Embedding the complexes comprising of a dimeric protein complex and the respective heterobivalent ligand into a lipid bilayer.
- IV. Evaluating the lipid-bilayer consistent behaviour of the complexes in the membrane during molecular dynamic simulation.
- V. Investigating the protein complex by alanine scan and the evaluation of stabilizing hydrogen bonds between the receptors.

3 Methods: Databases Software and Programs

In this chapter, the different databases, software, and programs used in this work are listed.

3.1 RCSB-Protein Data Bank

The Research Collaboratory for Structural Bioinformatics Protein Data Bank (RCSB-PDB) (accessible at www.rcsb.org) is a website providing PDB files defining coordinates for specific molecules and further information about the molecules are given. The structure of receptors as well as their ligands, but also nucleic acids, and complex assemblies are available and can be downloaded and uploaded to other programs for further investigations (Website accessed at www.rcsb.org; 08-09-2021).

3.2 CHARMM-GUI

CHARMM (Chemistry at HARvard Macromolecular Mechanics; accessible at www.charmm.org) is a molecular simulation program using all-atom classical potential energy functions, quantum mechanical energy functions, and mixed quantum mechanical-molecular mechanical force fields for the simulation of different molecules (Brooks et al., 1983; Brooks et al., 2009).

Primarily biomolecules such as proteins, peptides, lipids, nucleotide acids, carbohydrates, and small molecular ligands are used in this program (Brooks et al., 2009; Guvench et al., 2009). The wide range of available tools includes conformational and path sampling methods, free energy estimators, molecular minimization, molecular dynamics, various analysis techniques, and model-building options. Thus, this program is widely used and extremely versatile (Brooks et al., 2009; Zhu et al., 2012).

CHARMM-GUI (accessible at www.charmm-gui.org) is a web-based graphical user interface to generate different molecular systems and standardized input files, usable in CHARMM. The Input Generator of CHARMM-GUI is used to generate input files that can be modified, read, and downloaded (Lee et al., 2016). When the input files are generated, calculations are done, ensuring that the inputs and systems are properly functional. If they are not, the calculations are stopped (Jo et al. 2008).

The PDB-reader is a basic module of CHARMM-GUI, used for converting a PDB file into input files for CHARMM (Jo et al., 2014). The PDB file can be saved from previous research or downloaded from the Protein Data Bank and uploaded to the PDB reader subsequently. As described in Jo et al., 2007 and 2008 the following options are available after the upload: (1) partial selection of protein chains as well as model selection in the case of NMR structures, (2) modification of engineered residues, (3) terminal group selection, (4) protonation selection, (5)

disulfide bond selection, (6) phosphorylation selection, (7) generation of a biological functional unit, and (8) generation of a crystal packing (Jo et al. 2008).

The Membrane Builder is a module of CHARMM-GUI, used to generate a protein-membrane complex (Lee et al., 2018; Wu et al., 2014). The building process of the complex is automatized and consists of six steps. At first, the protein structure is uploaded and read, then the protein is orientated in the membrane, and in case the protein has a pore, the pore water is generated. In the following step, the system size is defined and components such as ions, bulk water, and the lipid bilayer are generated. In the last two steps, assembly and equilibration are done. (Jo et al. 2008).

Lipid molecules supported by Membrane Builder that are important to build a human-like membrane, are POPC, POPE POPS, POPI, and PSM (Wu et al., 2014). The system shapes available are hexagonal and rectangular and the lipid bilayer can be generated either by the insertion method or the replacement method. For the insertion method, a hole of a certain size is given and the protein is inserted into the membrane. The replacement method uses lipid-like pseudo atoms that are replaced by lipid proteins one by one so a membrane is built around the protein (Jo et al. 2008, Jo et al., 2017).

3.3 PPM Server

The PPM-Server (accessible at https://opm.phar.umich.edu/ppm_server) can be used to get the arrangement of membrane proteins in the lipid bilayer of membranes. It is a web server in which the atomic coordinates of a protein are uploaded as a PDB file and the output are orientational parameters of the membrane proteins, given as a new PDB file. Further, the positions of hydrophobic core boundaries can be shown by dummy atoms in the new PDB file (Lomize et al., 2011).

3.4 Memdock Server

Memdock (at <http://bioinfo3d.cs.tau.ac.il/Memdock/>) is a computational tool for docking α -helical membrane proteins whilst taking the lipid bilayer environment into account (Hurwitz et al., 2016). The Docking algorithms usually include a rigid docking, conformational refinement, and ranking by an energy score stage. Memdock is characterized by additionally including the lipid bilayer environment (Halperin et al., 2002).

3.4.1 Docking

The algorithm for rigid docking is based on the PatchDock algorithm, using the geometric hashing method (Schneidman-Duhovny et al., 2005). The movement of the proteins was restricted inside the lipid bilayer. Therefore, the proteins have to be orientated so that the z-axis is parallel to the membrane plane normal and the centroid of the proteins is at zero. This can be achieved

during the patch matching stage, where the translations along the z-axis are limited to a threshold of 8Å and the rotational tile angle from the x-axis is limited to a threshold of 0,4 radians (Hurwitz et al., 2016).

A refinement algorithm is used to perform flexible refinement on the docking candidates. The algorithm is based on the FiberDock algorithm and both, side-chain and backbone flexibility, are modelled and the orientation of the rigid protein is optimized (Hurwitz et al.2016). Monte Carlo minimization of the binding score function was used to refine the relative position of the binding proteins (Gray et al., 2012). To get the proteins membrane consistent orientation once again the translation along the z-axis and the rotational tilt angle from the x-axis of the original structure were limited to 12Å and 0,8 radians (Hurwitz et al.2016).

3.4.2 Ranking

In the last step, the Memscore energy function, based on knowledge concerning the 3D structure and α -helical membrane proteins is used to re-rank and re-score. The energy functions include atomic softened van der Waals interactions energy, partial electrostatics, estimations of the binding free energy, and further, environment energy of the membrane were also taken into account (Hurwitz et al., 2016; Yarov-Yarovoy,V. et al., 2006).

3.5 Pymol

“Pymol Molecular Graphics System” (Schrödinger LLC .“The PyMOL Molecular Graphics System, Version 4.6.” 2021) is a cross-platform molecular graphics tool written in Python (Yuan et al., 2017). It is widely used for 3D visualization of different molecules such as proteins, nucleotide acids, and small molecules in different representations such as ribbons, sticks, and surfaces. Moreover, electron density and surfaces can be shown. Pymol is further capable of making movies, editing molecules, and ray tracing (Yuan et al., 2017). Due to the Python programming language, many Python plugin tools are available and it can easily be used for drug design, protein-ligand modelling, molecular simulations, and virtual screening. (Yuan et al., 2017; Seeliger and Groot, 2010).

3.6 ChemDraw

ChemDraw is a chemical drawing package, which allows drawing molecules and chemical interactions. These can be saved as different file types and used in different display programs or docking programs (Nancy Mills, 2006).

3.7 Protein-ligand docking with LigandScout *via* AutoDock Vina

LigandScout is a molecular modelling and design software site published in 2005 and improved since then, so many different features are available (Wolber and Langer, 2004). These features

range from virtual screening and 3D conformer generation to pharmacophore modelling, molecular docking, ligand binding affinity estimation, and much more. Further, it is important for *in-silico* screening of a large database in the early stage of drug discovery (LigandScout Version 4.3, 2018).

Ligands and known X-ray or NMR structures of receptors as BDP files and can be uploaded to LigandScout. After different possible adjustments and ligand docking, the interactions modes between ligand and receptor can be inspected as a 3D model (Wolber and Langer, 2005).

Ligand-based and structure-based pharmacophore models are constructed by defining specific chemical features and volume limitations. Pharmacophore models are based on hydrogen bonds, charge transfers, electrostatic and hydrophobic interactions since these interactions are mainly observed in drug-receptor interactions. They are used to identify certain binding modes (LigandScout Version 4.3, 2018; Wolber and Langer, 2005).

AutoDock Vina is a docking program used for protein-ligand docking and virtual screening and is among others implemented to LigandScout (Wolber and Langer, 2005; Jaghoori et al., 2016). A search algorithm for generating possible binding modes, stochastic global optimization approaches, and a scoring function for predicting the protein-ligand affinity are essential tools for showing the different interaction modes of receptor and ligand. From the resulting binding modes, certain ones can be selected and used for further investigations (Trott et al., 2009; Wolber and Langer, 2005).

3.8 Maestro

Maestro is part of the physics-based computational platform Schrödinger and provides access to all Schrödinger's computational technologies. It can be used for a broad range of features such as model generation, flexible visualization, data management and organization, quantitative structural analysis, and much more. Especially the modification and adaption of molecules for different purposes is very practicable (Website accessed at <https://www.schrodinger.com/products/maestro>; 17-10-2021).

3.9 OpenMM molecular dynamics toolkit

OpenMM (accessible at: <http://openmm.org>) is an open-source, high-performance, molecular dynamics simulation toolkit with high flexibility in adding new features such as new simulation protocols and integrated algorithms. OpenMM is set up as a layered architecture and it is capable of different tools. It can be used as a library for calculations concerning molecular modelling, and simulation, for implementing new algorithms for molecular modelling, and for running a molecular dynamics simulation (Eastman et al., 2017; website accessed at <http://openmm.org>; 17-10-2021).

3.10 Visual molecular dynamics (VMD)

VMD is a program used for analyzation and visualization of biomolecules, such as proteins, lipid bilayers, and nucleic acids (Hsin et al., 2008). Besides many other useful functions, it is mainly used for 3D visualizations of different representations and colouring styles of molecules, the analysis of trajectories of MD simulations as well animation and movie making of MD simulations (Hsin et al., 2008; Humphrey et al., 1996).

The RMSD Trajectory Tool is an important tool used for measuring the RMSD in Angstrom (Å) and therefore the stability of molecules during the MD-simulation. The result is shown in a plot and the average RMSD of the protein together with the standard deviation and the minimum and maximum of RMSD are shown in a Table (Hsin et al., 2008; Humphrey et al., 1996).

3.11 PyRosetta - Alanine scan

PyRosetta (accessible at www.pyrosetta.org) is Python-based and part of the Rosetta molecular modelling package. At the PyRosetta website, scripts for alanine scanning, protein and small-molecule docking, protein design and all-atom relaxation, and many more are available (Chaudhury et al., 2010).

Alanine scan is a molecular-biological analysis method used for the characterisation of the interface between two proteins. Important amino acids at the interface are systematically mutated to alanine and the effect on binding free energy is estimated. Thus, the importance of certain protein residues to the binding free energy of two receptors can be identified. During this process, the backbone is static and the side-chains of the amino acid mutants are re-packed. As a result, the changes in the residues' binding free energy can be measured (Kortemme and Baker, 2002).

4 Results and discussion

In this chapter, the results of the computational experiments are described in detail in the order in which they were performed.

4.1 Protein preparation and protein-protein docking via Memdock

Receptors used for the protein-protein docking are selected and prepared in this chapter. The proteins are orientated in a membrane, and protein-protein docking was performed using Memdock. Further, the results were visually inspected using Pymol.

4.1.1 Structures of the receptors

The crystal structure of inactive CB1R (Hua et al., 2016), the cryo-EM structure of active CB1R (Hua et al, 2020), and the crystal structure of inactive OTR (Waltenspuehl et al., 2020) were available at “The Research Collaboratory for Structural Bioinformatics Protein Data Bank”. The crystal structure of the active OTR was not available there, so it was taken from the paper *Busnelli et al., 2016*.

The following PDB-IDs were found and are listed in **Table 2**.

Table 2. Receptor structures and corresponding PDB codes used for generation of models in this study.

Receptor type and activation state	PDB-ID
Inactive CB1R	5TGZ
Active CB1R	6KPG
Inactive OTR	6TPK

The final selection of the receptors relied on the fact that primarily receptors in their active conformations tend to form dimers, so the active receptors were taken for modelling instead of the inactive receptors. Modelling the combination of active OTR/inactive CB1R, inactive OTR/active CB1R, and inactive OTR/inactive CB1R would additionally be very interesting but it would go beyond the scope of this master’s thesis.

4.1.2 Selection and restoring missing amino acids of the receptor

The PDB file of the CB1R had to be modified for the needs of further experimental steps. The PDB file of the OTR had to undergo no such modifications since it already fulfils the requirements. Different amino acids missing in the CB1R’s PDB file, downloaded from the database, had to be reinserted and the structures of the G-protein, ligand AM841, and scFv16 antibody had to be removed. This was done using the CHARMM-GUI PDB reader.

The PDB file (6KPG) was obtained from the RCSB and the chain “D” was extracted (containing only residues with ID 106 – 411) In the following step, missing amino acid residues with the residue ID 314 – 334 were added.

4.1.3 PPM Server

PPM web-server was used to calculate the orientation of the proteins in the membrane. The prepared PDB files of CB1R and OTR were uploaded. The number of membranes was selected to be 1 and the type of the membrane was selected to “undefined membrane”. The allowed curvature was “non” and the topology of the N-terminus was selected to point towards the extracellular side. As a result, the modified PDB file could be downloaded and the orientation of the proteins in the membrane is described for each receptor as shown in **Table 3** and **Table 4**. The membrane-embedded residues are described in **Table 5** and **Table 6**.

Table 3. Parameters concerning the orientation of the CB1R in the membrane

Depth/Hydrophobic Thickness	$\Delta G_{\text{transfer}}$	Tilt Angle
$28,2 \pm 2,0\text{\AA}$	-52,7 kcal/mol	$5 \pm 1^\circ$

Table 4. Parameters concerning the orientation of the OTR in the membrane

Depth/Hydrophobic Thickness	$\Delta G_{\text{transfer}}$	Tilt Angle
$30,0 \pm 2,5\text{\AA}$	-51,2 kcal/mol	$15 \pm 1^\circ$

Table 5. The membrane embedded residues with allocation to the TMHs of the CB1R

Subunits	Tilt	Segments
P	10	Embedded residues: 118-142, 152-153, 155-172, 174, 191-212, 233-251, 253, 255, 268, 274-295, 345-365, 367-368, 378-400, 404, 408
P	5	Transmembrane secondary structure segments: 1(119-142), 2(155-172), 3(191-212), 4(233-251), 5(274-295), 6(345-365), 7(378-400)

Table 6. The membrane embedded residues with allocation to the TMHs of the OTR

Subunits	Tilt	Segments
C	35	Embedded residues: 38-59, 61, 79, 81-101, 105-132, 134-135, 156-172, 174-177, 187, 195-221, 225, 271, 274-300, 309-329, 344
C	15	Transmembrane secondary structure segments: 1(38-61), 2(81-101), 3(109-132), 4(157-172), 5(195-221), 6(274-297), 7(310-329)

4.1.4 Memdock Server

Memdock was used for docking CB1R and OTR while taking the lipid bilayer environment into account. The prepared PDB files of CB1R and OTR were uploaded to the server, docking was performed and the 20 best docking results were obtained. Docking positions were ranked by Memscore, as shown in **Table 7** Res0 was the best docking pose and res19 the worst. The results were then visually inspected in Pymol.

Table 7. Representation of the Memscores regarding each docking position

Docking position	Memscore	Docking position	Memscore
res0	-628,62190128	res13	-268,561740283
res1	-432,024959178	res14	-261,713098606
res2	-417,474060123	res15	-257,110361241
res3	-368,314832148	res16	-245,019826337
res4	-324,114497125	res17	-235,259050359
res5	-323,193414909	res18	-232,861114302
res6	-322,401392262	res19	-230,372255909
res7	-309,80194985		
res8	-303,780702814		
res9	-298,634399389		
res10	-289,830128116		
res11	-270,586545027		
res12	-269,976389164		

4.1.5 Pymol visualization of the Memdock results

To visualize and interpret the docking results, Pymol software was applied. The OTR is coloured yellow and its presumed interacting TMH are shown in dark yellow; the CB1R is coloured green and its interacting TMHs are shown in dark green. The best docking result is res0 and it is shown in **Figure 8** and **Figure 9**. The four best results were further investigated with focus on the TMHs of the CB1R and OTR.

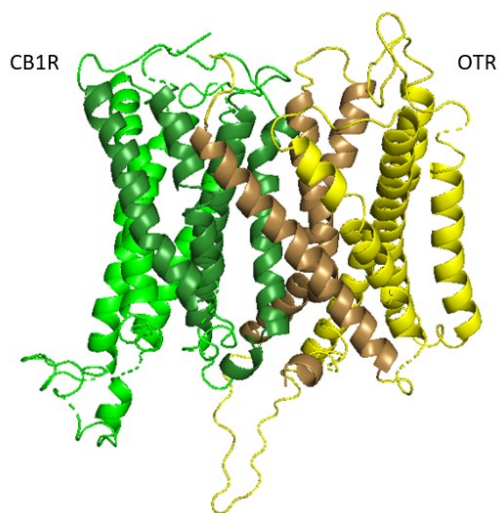


Figure 8. The front view of the best docking pose res0.

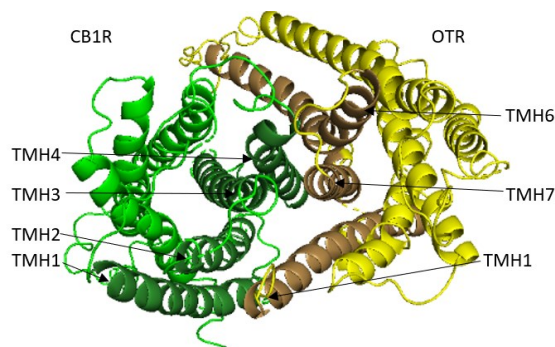


Figure 9. The top-down view of the best docking pose res0.

The best docking result res0 showed interactions between CB1R TMH1/2/3/4 and OTR TMH1/6/7. Docking result res1 showed interactions between CB1R TMH1/2/3/4 and OTR TMH3/4/5, docking result res2 showed interactions between OTR CB1R TMH1 and TMH1/6/7 and docking result res3 showed interactions between CB1R TMH6/7 and OTR TMH1/6/7. **Figure 10** and **Figure 11** show the aligned structures of the four docking poses.

Summing up, the results were similar. Res0, res2, and res3 showed the same docking position of OTR, but res1 displayed a completely different docking position. For the CB1R, res0 and res1 showed the same docking position and res2 also displayed interaction with TMH1 whereas res3 seemed to be completely different from the others.

The overlay of the four best docking positions showed how diverse the interactions are. For further investigations, the best docking position res0 was selected.

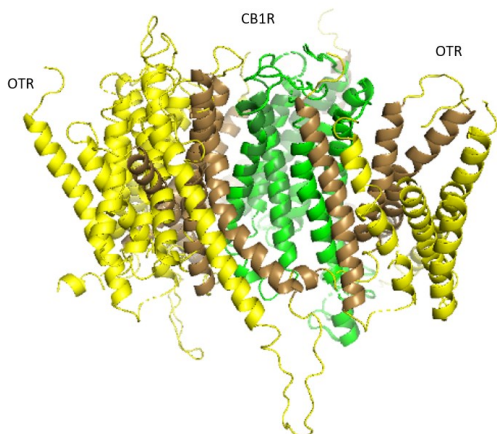


Figure 10. The front view of the four best docking poses res0-res3

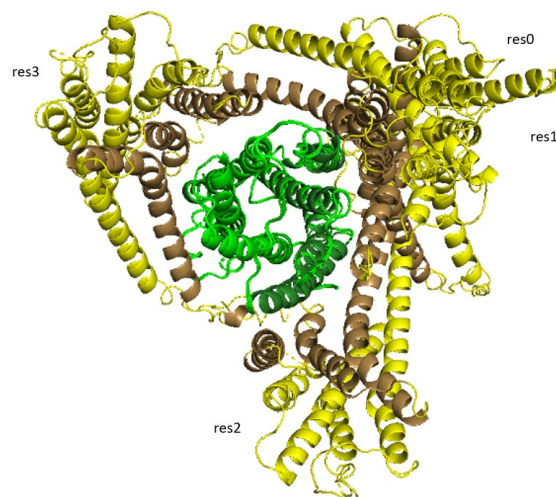


Figure 11. The top-down view of the four best docking poses res0-res3

4.2 Protein-ligand docking and design of bivalent ligands

In this chapter, ligands for the CB1R and OTR are chosen and the procedure of protein-ligand docking is shown. Further, linkers are selected for generating bivalent ligands.

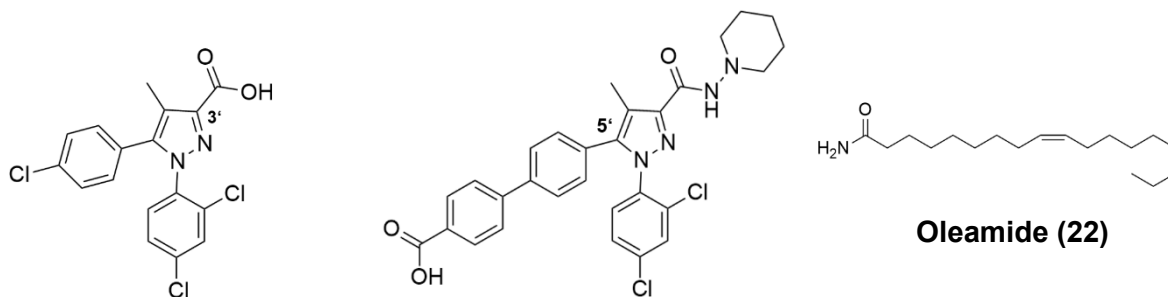
4.2.1 Ligand selection

To perform protein-ligand docking, five ligands were chosen. Two inverse agonists and one agonist of CB1R and one antagonist and one agonist for OTR.

The two inverse agonists of CB1R selected for this thesis were first described by *Grant et al.*, 2019. For both, the selective inverse agonist rimonabant (SR141716A) was taken as a starting point and two attachment sites were identified for them: the C3 and C5 position of the central pyrazole ring.

The carboxylic acid derivate of rimonabant has the attachment site at position 3 (rimonabant derivate 3') of the pyrazole ring and in the following, it is called compound **20** and the derivate of rimonabant with the attachment site, at the biphenyl at position 5 (rimonabant derivate 5') of the pyrazole ring is called compound **21** in the following (**Figure 12**) (Grant et al., 2019).

The selective endogenous agonist oleamide (Cis-9,10-octadecanoamide) was taken as a CB1R agonist for modelling and in the following, it is called compound **22** (**Figure 12**) (Leggett et al., 2004).



Rimonabant derivate 3' (20) Rimonabant derivate 5' (21)

Figure 12. Molecular structures of selective CB1R ligands from literature (20 - 22). Possible attachment positions are labeled with number and prime.

For OTR the ligand dOTK, described by *Busnelli et al., 2016*, was selected as agonist. It is similar to oxytocin and only a few modifications were made. First, it was deaminated at position 1 (dCys) and a lysine (K) was added at position 8 instead of leucine. In the following it is called compound **23 (Figure 13)**.

The OTR antagonist was taken from the study *Manning et al., 1995*, where it is described as component 5 “desGly-NH₂,d(CH₂)₅[D-Tyr²,Thr⁴]OVT”. In the following, this compound is called compound **24 (Figure 13)**.

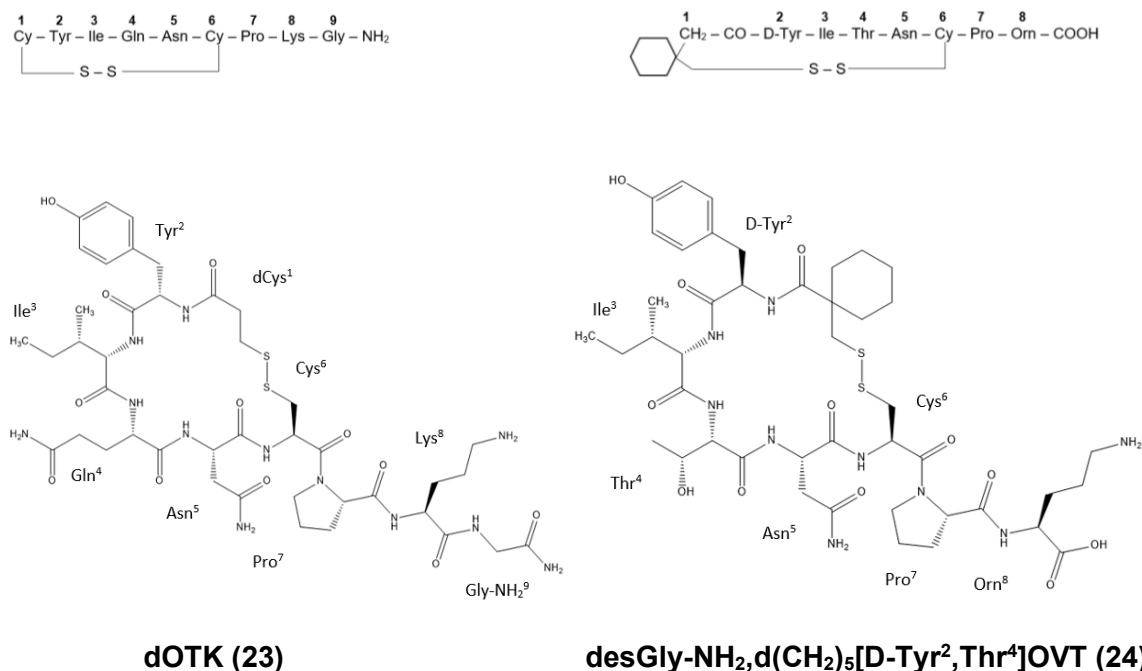


Figure 13. Molecular structures of selective OTR ligands from literature (23-24)

4.2.3 Protein-ligand docking via LigandScout and AutoDock Vina

After generating the ligands using ChemDraw, I used LigandScout (LS) to perform protein-ligand docking. To perform protein-ligand docking with LS the first step was to generate a binding pocket using the standard parameters (buriedness of 0,50 and threshold of 0,30) for binding pocket create in LS. In the next step, the ligand structures were minimized using the MMFF94 force field. The binding pocket of the receptor was selected and the ligand was inserted into the binding pocket. Docking was performed using AutoDock Vina. For the docking run, standard parameters were used with an exhaustiveness level of 8, the maximum number of modes was set to 9 and the maximum energy difference was set to 3 kcal/mol.

The docking results were ranked using their binding affinity. To identify the best docking result, in addition to the binding affinity the orientation of the ligands played an important role since the residue for linker attachment had to be accessible without steric clashes.

This procedure was repeated for all five ligands. Each of them was visually inspected to the best docking pose of the ligands using Pymol. The best poses are illustrated in **Figure 7** to **Figure 12**.

Ligands of the CB1R (shown in green) are coloured as followed: Compound **20** is coloured light blue, compound **21** is coloured magenta and the oleic acid as an initial substance for oleamide (**22**) is coloured yellow. Regarding the OTR (shown in yellow), compound **23** is coloured violet and the compound **24** is coloured blue.

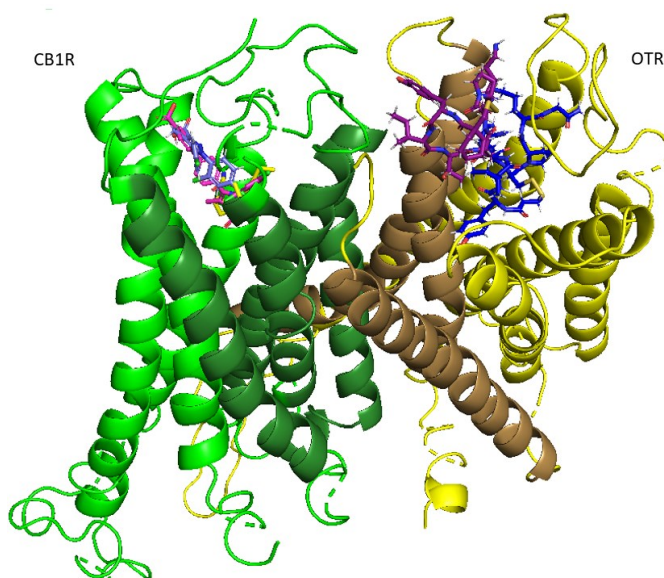


Figure 14. Front view of the receptor complex and the five ligands at CB1R and OTR.

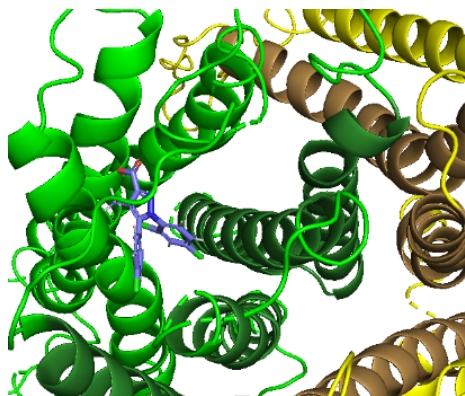


Figure 15. Top-down view of compound **20** bound to CB1R

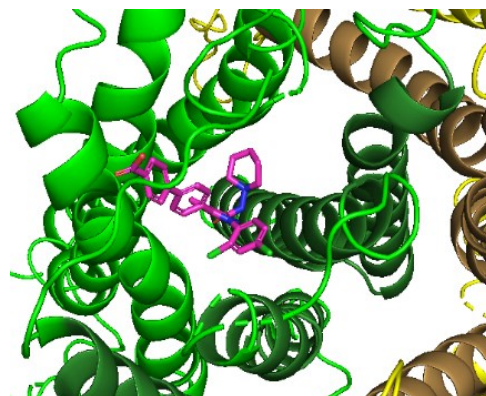


Figure 16. Top-down view of compound **21** bound to CB1R

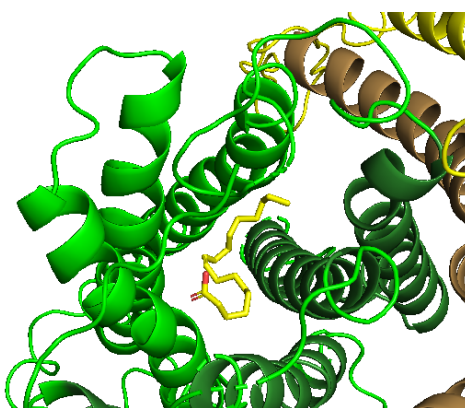


Figure 17. Top-down view of oleic acid bound to CB1R

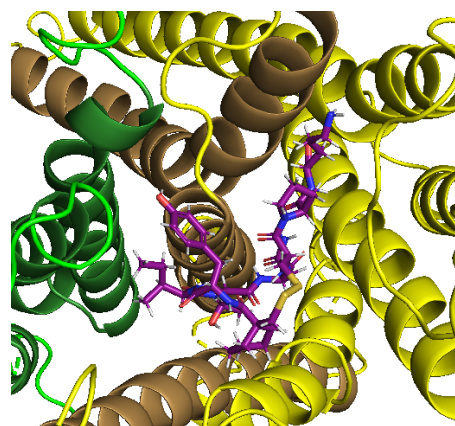


Figure 18. Top-down view of compound **23** bound to OTR

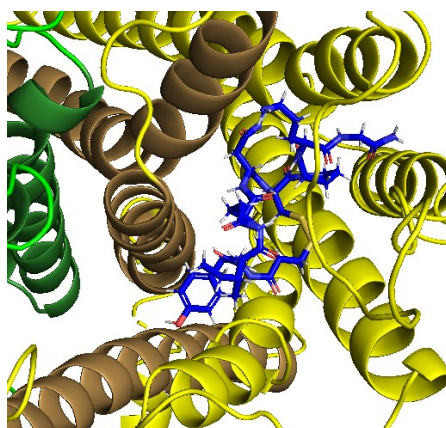


Figure 19. Top-down view of compound **24** bound to CB1R

4.2.4 Linker design

To design heterobivalent ligands, the individual ligands of OTR and CB1R were linked with linkers of different lengths. For this purpose, the linkers COOH-PEG5-NH-Fmoc (**Figure 20**), COOH-PEG10-NH-Fmoc (**Figure 21**), and COOH-PEG15-NH-Fmoc (**Figure 22**) were chosen, because they are the promising linkers concerning CB1R ligands mentioned in *Grant et al., 2019*.

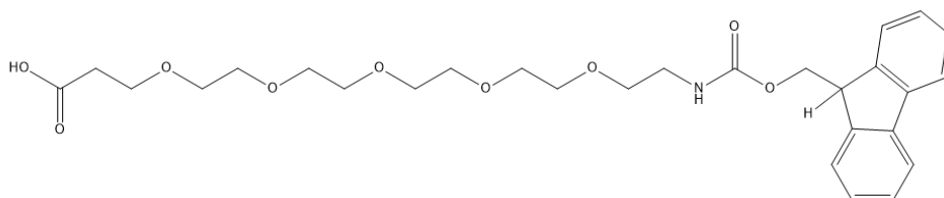


Figure 20. Linker COOH-PEG5-NH-Fmoc

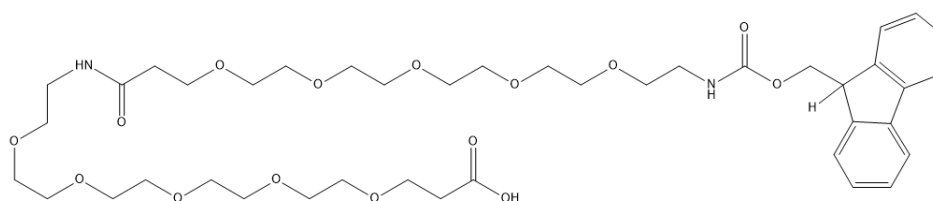


Figure 21. Linker COOH-PEG10-NH-Fmoc

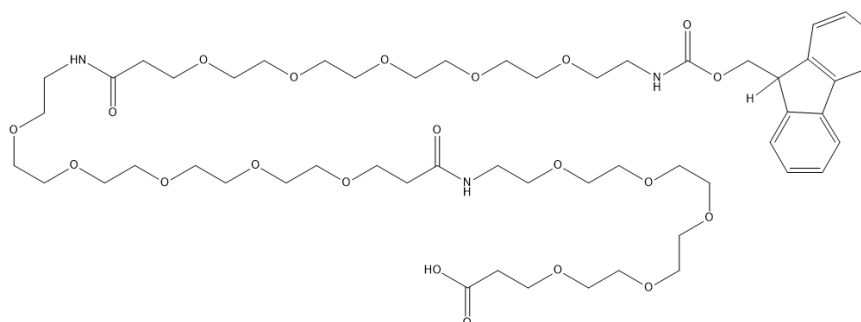


Figure 22. Linker COOH-PEG15-NH-Fmoc

The length of the linker depends on the distance between the ligands bound to their receptor inside the binding pocket. Therefore, the distance between the ligands, in their best scored docking pose res0, was measured *via* Pymol and a spacer-length between 40Å and 60 Å was suggested. Thus, the COOH-PEG5-NH-Fmoc linker with an average length of 20Å was discarded and the linkers COOH-PEG10-NH-Fmoc with ~40Å and COOH-PEG15-NH-Fmoc with ~60Å were taken to design twelve heterobivalent ligands with the previously chosen ligands. They were then considered for further inspection.

By connecting the ligands with a linker in lab, the carboxyl group of the CB1R ligands interact with the amino group of the linker building an amide bond formation between the linker and the ligands. For oleamide (**22**), the oleic acid was taken as an initial substance so by linking the carboxyl group of the oleic acid and the amine group of the linker, the amide of the oleamide results. The OTR's ligands are attached to the linker by an amide bond formation between the amine group of the ligand and the carboxyl group of the linker. The fluorenylmethoxycarbonyl (Fmoc) is used as a protecting group at the amine of the linker and it can be cleaved off with piperidine in dimethylformamide so the CB1R's ligands can interact with the linker's amino group (Chan et al., 1999).

Here, the Maestro software was used for building the linkers between the docked ligands and subsequently energy minimization.

4.3 Membrane building via CHARMM-GUI

To embed the receptor dimer into an authentic lipid-bilayer CHARMM-GUI's Membrane Builder was used. Membrane composition was chosen as described in *Van Meer et al., 2008* and shown in **Table 8**. The water box was generated with 60Å on both sides to bury the whole receptors in water. The protein was added using replacement and the physiological salt concentration was represented by potassium and chloride ions in a concentration of 0.15M KCl.

Table 8. Components of the human membrane and their concentration in the upper and lower leaflet.

Molecules in the membrane	Upper Leaflet	Lower Leaflet
Cholesterol	106	105
POPC (Phosphatidylcholine)	45	42
POPE (Phosphatidylethanolamine)	25	24
POPS (Phosphatidylserine)	10	10
POPI (Phosphatidylinositol)	4	4
PSM (Sphingolipids)	26	25

The results were visually inspected in Pymol (**Figure 23** to **Figure 34**). The CB1R is shown in green and the OTR is shown in yellow. The membrane is shown in green and the heterobivalent ligands are shown in blue.

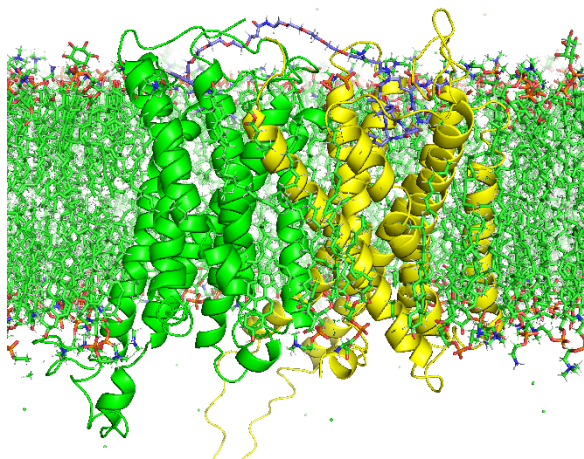


Figure 23. Receptor complex with ligand "compound **20** - PEG10 - compound **23**" (complex 1) in the membrane.

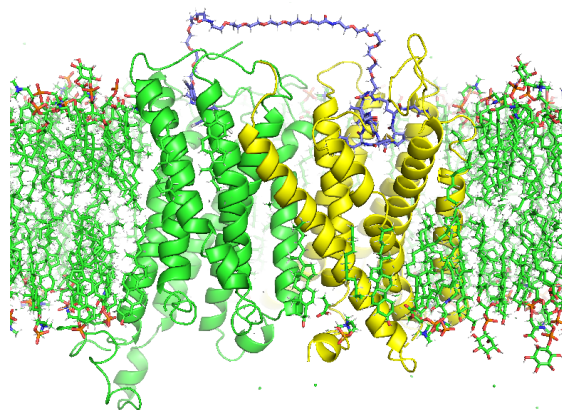


Figure 24. Receptor complex with ligand "compound **20** - PEG15 - compound **23**" (complex 2) in the membrane.

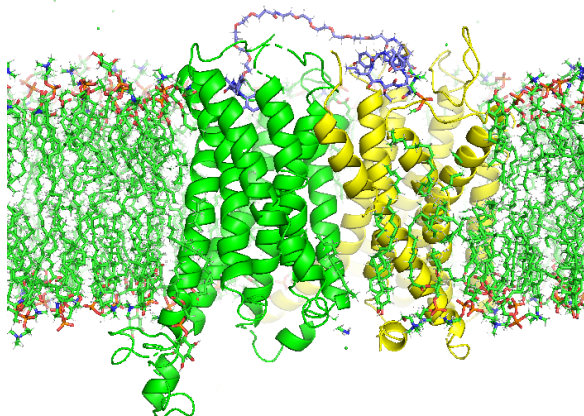


Figure 25. Receptor complex with ligand "compound **20** - PEG10 - compound **24**" (complex 3) in the membrane.

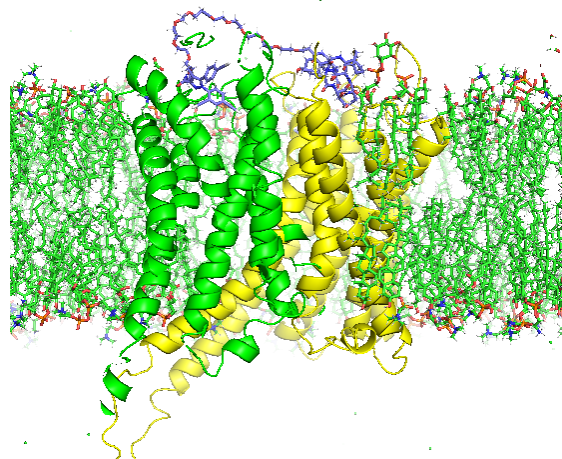


Figure 26. Receptor complex with ligand "compound **20** - PEG15 - compound **24**" (complex 4) in the membrane.

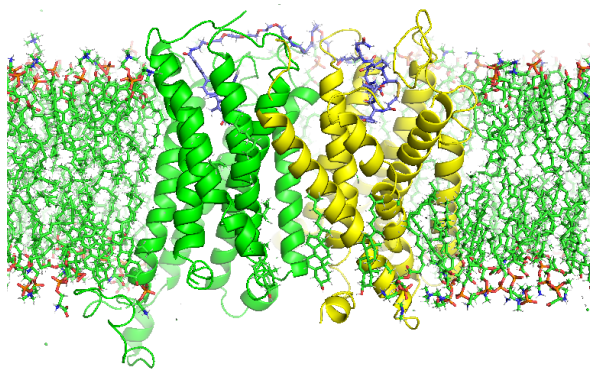


Figure 27. Receptor complex with ligand “compound 21 - PEG10 - compound 23” (complex 5) in the membrane.

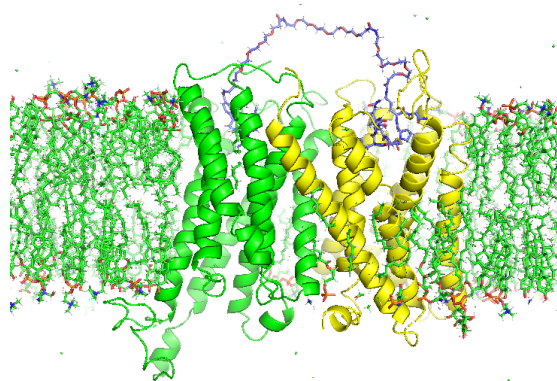


Figure 28. Receptor complex with ligand “compound 21 - PEG15 - compound 23” (complex 6) in the membrane.

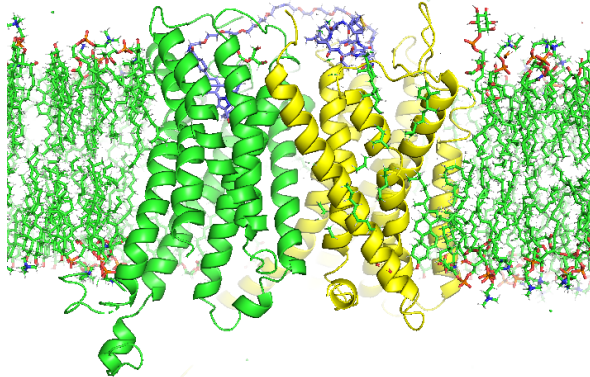


Figure 29. Receptor complex with ligand “compound 21 - PEG10 - compound 24” (complex 7) in the membrane.

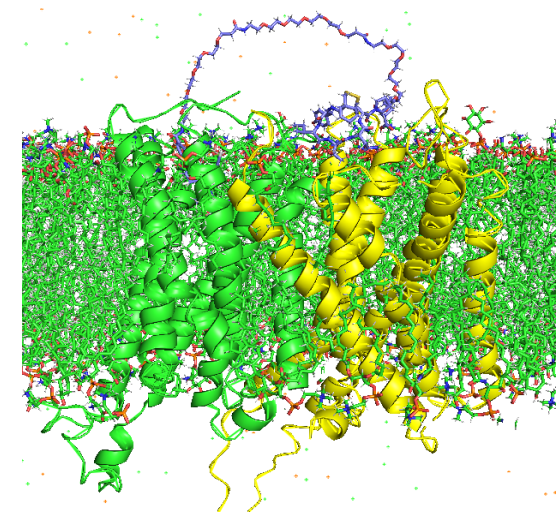


Figure 30. Receptor complex with ligand “compound 21 - PEG15 - compound 24” (complex 8) in the membrane.

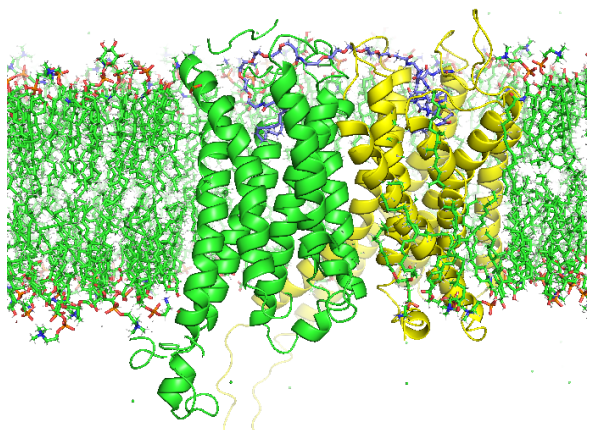


Figure 31. Receptor complex with ligand “compound 22 - PEG10 - compound 23” (complex 9) in the membrane.

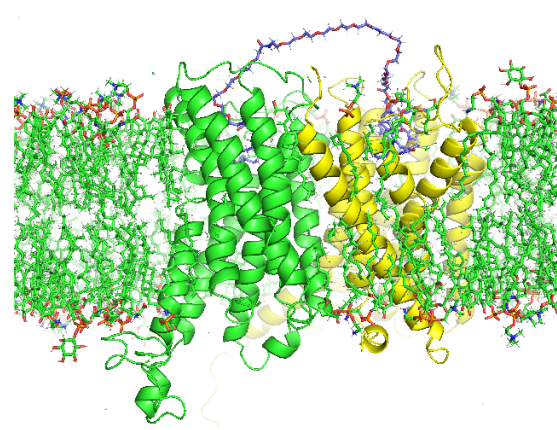


Figure 32. Receptor complex with ligand “compound 22 - PEG15 - compound 23” (complex 10) in the membrane.

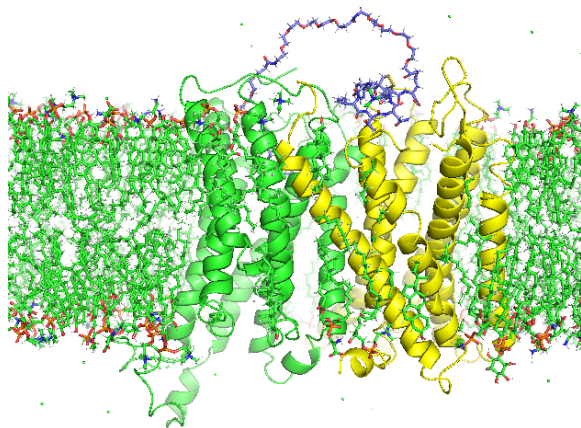


Figure 33. Receptor complex with ligand “compound **22** - PEG10 - compound **24**” (complex 11) in the membrane.

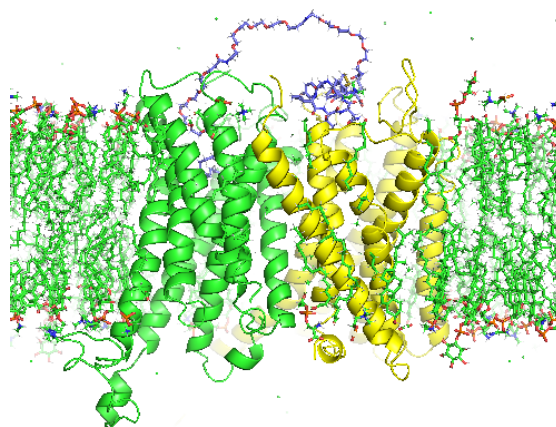


Figure 34. Receptor complex with ligand “compound **22** - PEG10 - compound **24**” (complex 12) in the membrane.

4.4 Molecular dynamics simulation

Molecular dynamics (MD) simulations are used to investigate the behaviour of biomolecules, especially proteins, in full atomic detail and fine resolution. Since atoms are in constant motion molecular functions and intermolecular interactions depend on the dynamics of a molecule. The basis of MD simulation is calculating the force exerted on the atoms of a molecule when it is given in a biomolecular system such as a lipid bilayer. The result is a trajectory, which describes the conformation of the molecule along the simulation (Hollingsworth and Dror, 2018).

MD simulations are used for elucidating the function of biomolecules besides conformational changes, ligand binding, and the mechanisms of protein aggregation. Therefore, they play an important role in discovering causes for diseases and further creating new drugs in this regard (Hollingsworth and Dror, 2018).

In this master’s thesis, the results of the MD simulation were used for gaining additional information about the stability of each receptor complex with its respective ligand and about the receptor complexes’ interfaces.

To perform MD simulation, the openMM MD simulation toolkit was used and the MD simulation was performed in the CHARMM force field. The 10 ns simulation was done in 5 million steps and after every 5.000 steps, coordinates were saved.

4.4.1 Root mean square deviation

The calculation of the root mean square deviation (RMSD) of the protein backbones is important for the analyses of the MD simulation since the conformational stability of the protein complex can be predicted.

In this thesis, the relative RMSD was measured, so all coordinates of the protein complex are aligned to the first frame. Therefore, only the internal structural changes of the protein's backbone are considered and the movement of the protein complex in the membrane is excluded from the calculations.

After measuring the RMSD of the proteins backbone for all frames in relation to the first frame, for each complex results are shown in **Table 9** and **Table 10** and **Chart 1 - Chart 12**. Then the results were additionally visually inspected (**Figure 35 - Figure 46**) All these tasks were performed using VMD.

The results of the RMSD analysis regarding all interfaces are summarized below.

The average RMSD scores suggest high stability of the complexes. This could be confirmed by visually inspecting the MD simulation of each complex, with three exceptions.

The first unstable complex was protein complex 3 with heterobivalent ligand "compound **20** - PEG10 - compound **24**". Here the MD simulation was terminated very early at frame 32 of 1000. By visually inspecting the protein complex, it is seen that the compound **24** moiety of the bivalent ligand is no longer bound to the OTR. This might be caused by the too-small linker lengths of PEG10 because the same complex was shown to be stable when the enlengthened linker PEG15 was used in the next complex 4 (**Figure 37 B**).

The second unstable complex was protein complex 10 with heterobivalent ligand "compound **22**- PEG15 - compound **23**". Here, the MD-simulation was determinate at frame 189 of 1000 because of insufficient stability. This was shown best by the high fluctuation at the RMSD plots (**Chart 10**)

The third unstable complex was protein complex 12 with heterobivalent ligand "compound **22**- PEG10 - compound **24**". The MD simulation was terminated at frame 636 of 1000 because the compound **24** moiety of the bivalent ligand popped out of the OTR's binding pocket (**Figure 46 C**).

The RMSD plots showed a high fluctuation at the beginning of each MD simulation caused by the adaption of the proteins to the force field since the proteins undergo an energy minimization. Then, the RMSD values reached a plateau out and the system was quite stable. Regarding the OTR it could be seen that a higher fluctuation took place compared to the CB1R. This could lead to the assumption that the CB1R is more stable compared to the OTR. Major variations in the RMSD values were caused by intracellular and extracellular loops that resulted in

a shift of the RMSD values to a higher level. Especially ICL3 and H8 of the OTR caused higher fluctuation because of their movement. ICL3 is quite long and therefore it has high flexibility to move towards or away from the protein complex or to twist around itself, causing high jumps in the RMSD values. At the CB1R, ICL3 showed extremely high flexibility during the MD simulation comparable to ICL3 of the OTR, due to its length causing changes in the RMSD values. The transmembrane regions showed less change in their conformation due to the high conservation of these regions. The following small structural changes at the TMH were noticeable: Complexes 2, 4, 5, 6, 8, 9, and 10 showed a small lateral drift of the receptors, complex 12 showed a small inward drift of the receptors, and complex 7 showed a small outward drift of the receptors. What has to be mentioned is that the simulation time of 10ns might not be long enough to reach the global minimum.

For each receptor complex (Complex 1 to 12), the average RMSD was measured. In **Table 9** the results concerning the CB1R are shown, and in **Table 10**, the results concerning the OTR are shown.

Table 9. The average RMSD scores of the backbones in relation to frame 0 (avg), standard deviations (sd), minimal (min) RMSD scores, and maximal (max) RMSD scores of each protein complex and the respective ligand were calculated for the CB1Rs.

Complexes	RMSD CB1R			
	avg.	sd.	min.	max.
Complex 1	5,043	0,761	1,220	6,230
Complex 2	3,478	0,321	1,191	4,033
Complex 3	1,760	0,425	0,872	2,383
Complex 4	3,478	0,321	1,191	4,033
Complex 5	3,368	0,629	0,837	4,153
Complex 6	3,066	0,453	1,168	4,255
Complex 7	4,429	0,599	1,401	5,626
Complex 8	3,283	0,412	0,915	3,885
Complex 9	3,993	0,386	1,121	4,526
Complex 10	3,079	0,455	1,122	4,154
Complex 11	3,959	0,892	0,914	4,904
Complex 12	2,578	0,527	1,263	3,682

Table 10. The average RMSD scores of the backbones in relation to frame 0 (avg), standard deviations (sd), minimal (min) RMSD scores, and maximal (max) RMSD scores of each protein complex and the respective ligand were calculated for the OTRs.

Complexes	RMSD CB1R			
	avg.	sd.	min.	max.
Complex 1	3,956	0,664	1,418	6,026
Complex 2	4,703	0,862	1,242	6,859
Complex 3	2,803	0,855	1,247	3,893
Complex 4	4,703	0,862	1,242	6,859
Complex 5	5,336	0,664	1,314	6,434
Complex 6	4,425	0,456	1,184	5,083
Complex 7	5,780	0,624	1,433	6,990
Complex 8	5,820	1,138	1,452	7,939
Complex 9	6,071	1,729	1,149	8,825
Complex 10	4,132	0,802	1,172	5,999
Complex 11	4,572	0,633	1,181	5,476
Complex 12	4,028	0,749	1,141	5,346

In the following sections, the results of each complex's RMSD plot, regarding CB1R and OTR, as well as the last frame in complex with the respective ligand and the representation of the alignment of the first and last frame are demonstrated. For complex 3 and complex 12, the visual representations of the unstable complexes are given. These results are listed from complex 1 to complex 12.

Complex 1:

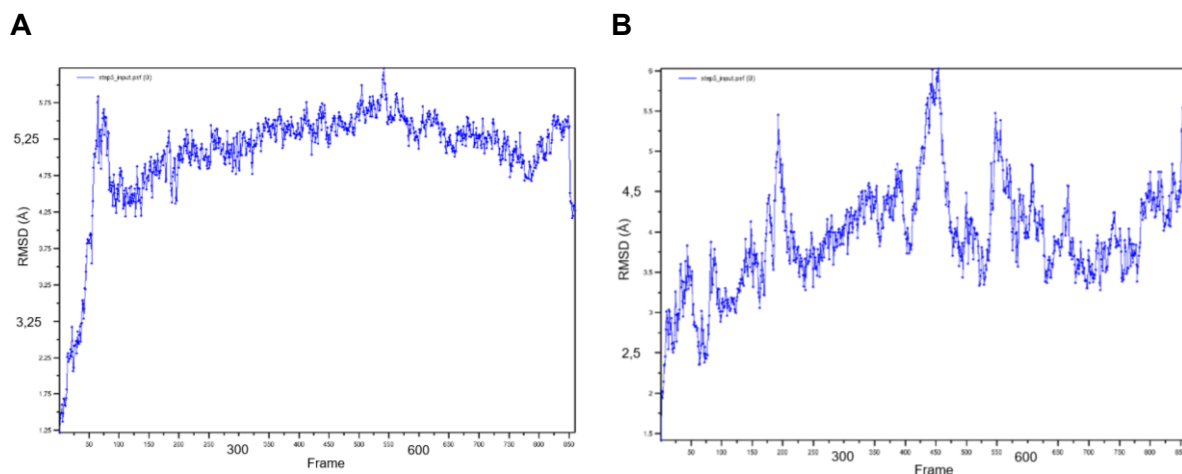


Chart 1.: RMSD plots of the protein complex with ligand “compound **20** - PEG10 - compound **23**” **A:** RMSD plot of CB1R **B:** RMSD plot of OTR.

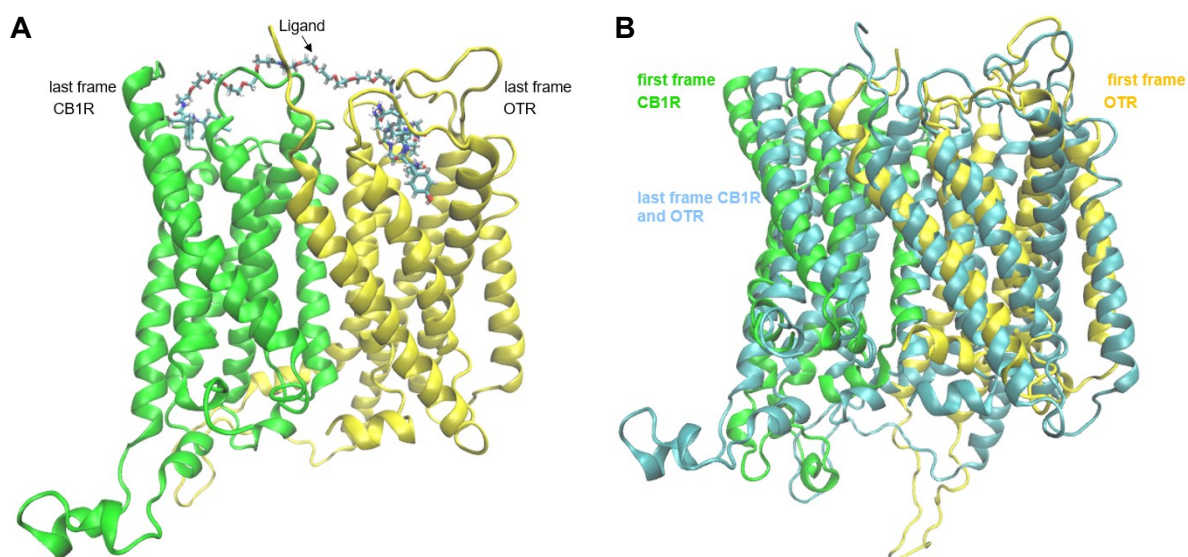


Figure 35. A: Last frame of MD simulation with bivalent ligand “compound **20** - PEG10 - compound **23**”; **B:** Alignment of the first frame and last frame of the MD simulation.

Complex 2:

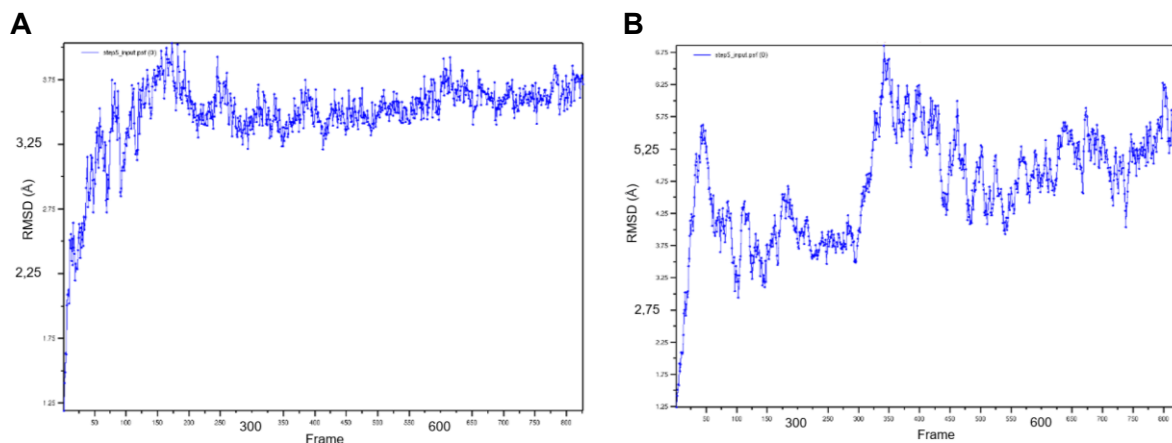


Chart 2. RMSD plots of the protein complex with ligand “compound 20 - PEG15 - compound 23” **A:** RMSD plot of CB1R **B:** RMSD plot of OTR.

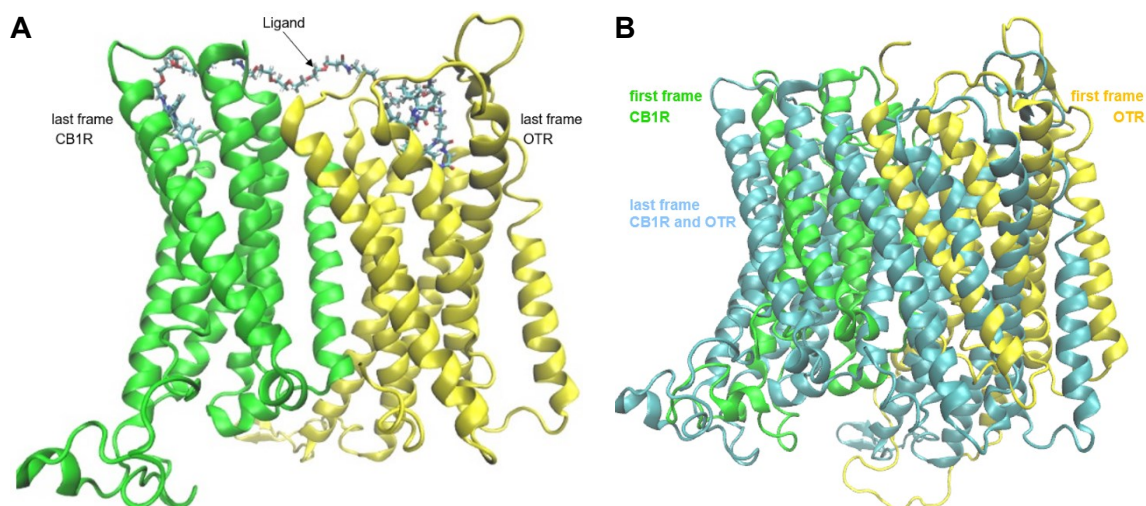


Figure 36. **A:** Last frame of MD simulation with bivalent ligand “compound 20 - PEG15 – compound 23”; **B:** Alignment of the first frame and last frame of the MD simulation.

Complex 3:

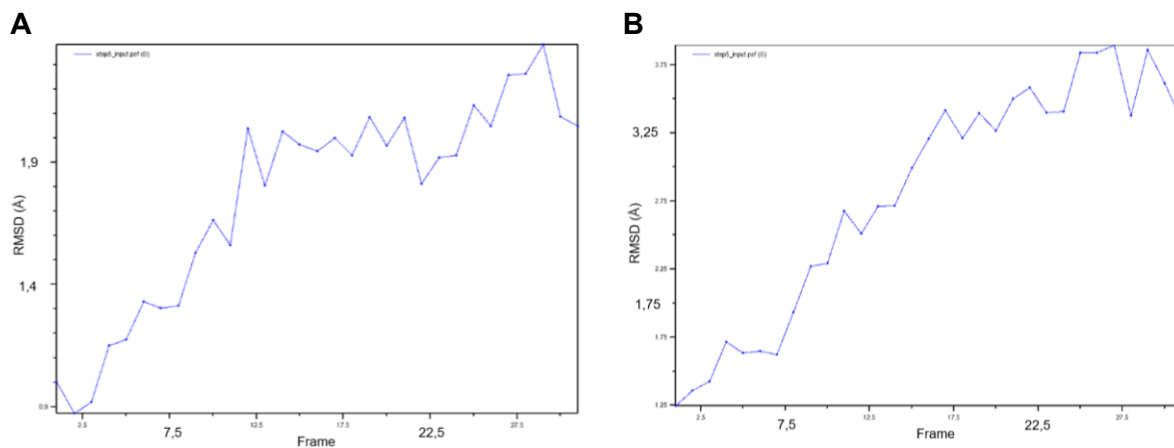


Chart 3. RMSD plots of the protein complex with ligand “compound 20 - PEG10 - compound 24” **A:** RMSD plot of CB1R **B:** RMSD plot of OTR.

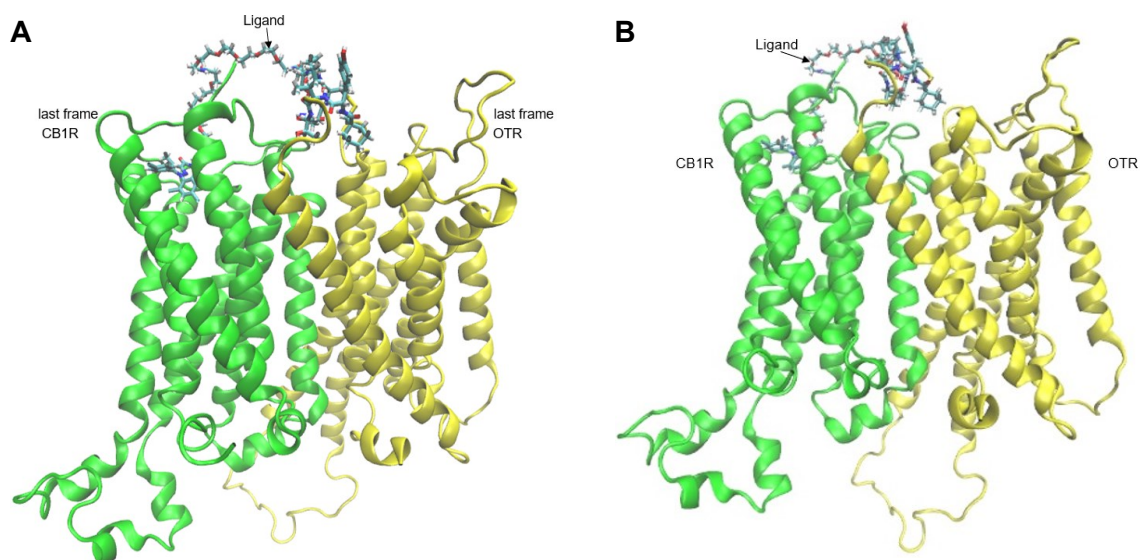


Figure 37. A: Last frame of MD simulation with bivalent ligand “compound 20 - PEG10 - compound 24”; **B:** Unstable frame of MD-simulation with bivalent ligand “compound 20 - PEG10 - compound 24”.

Complex 4:

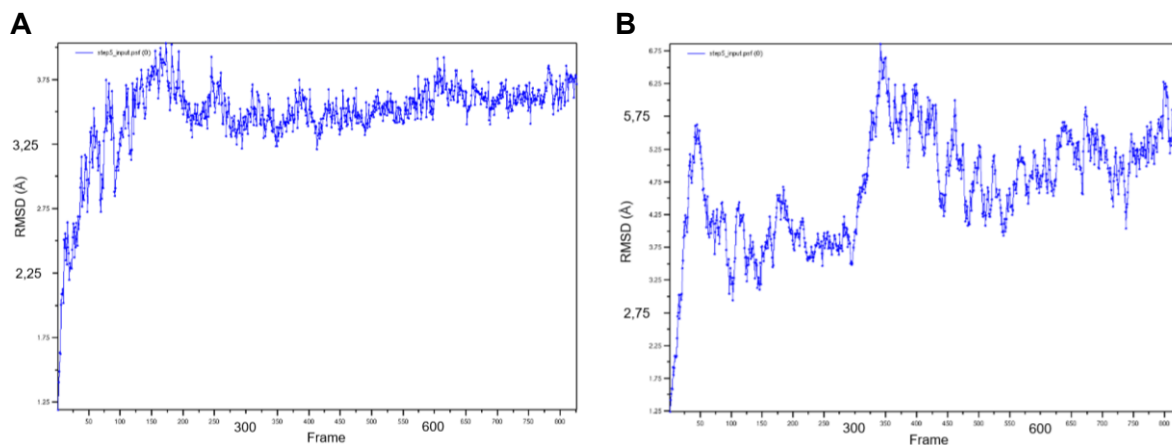


Chart 4. RMSD plots of the protein complex with ligand “compound 20- PEG15 - compound 24” **A:** RMSD plot of CB1R **B:** RMSD plot of OTR.

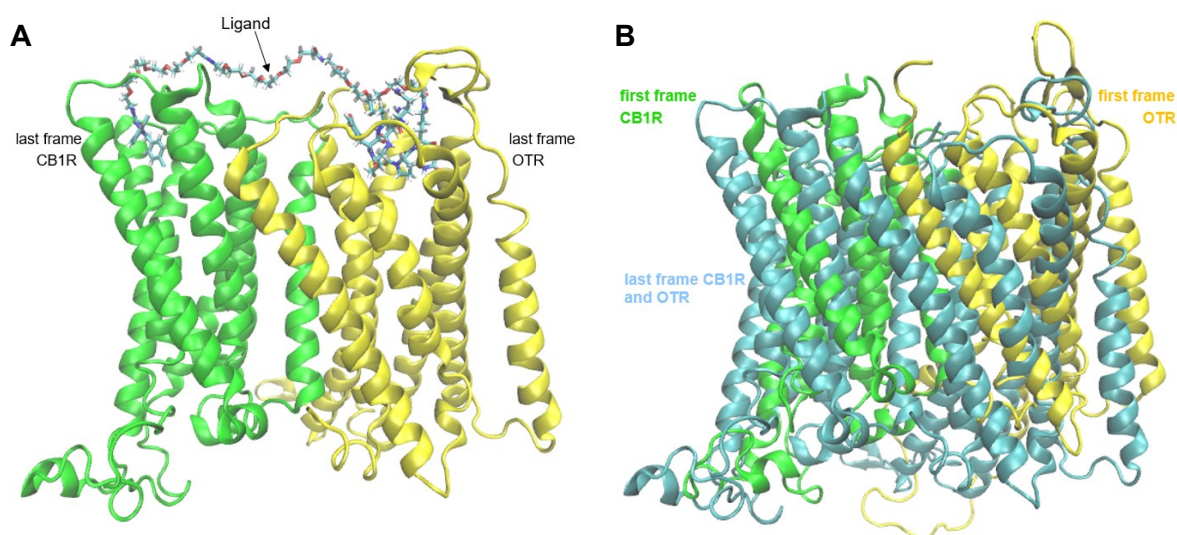


Figure 38. **A:** Last frame of MD simulation with bivalent ligand “compound 20 - PEG15 - compound 24”; **B:** Alignment of the first frame and last frame of the MD simulation.

Complex 5:

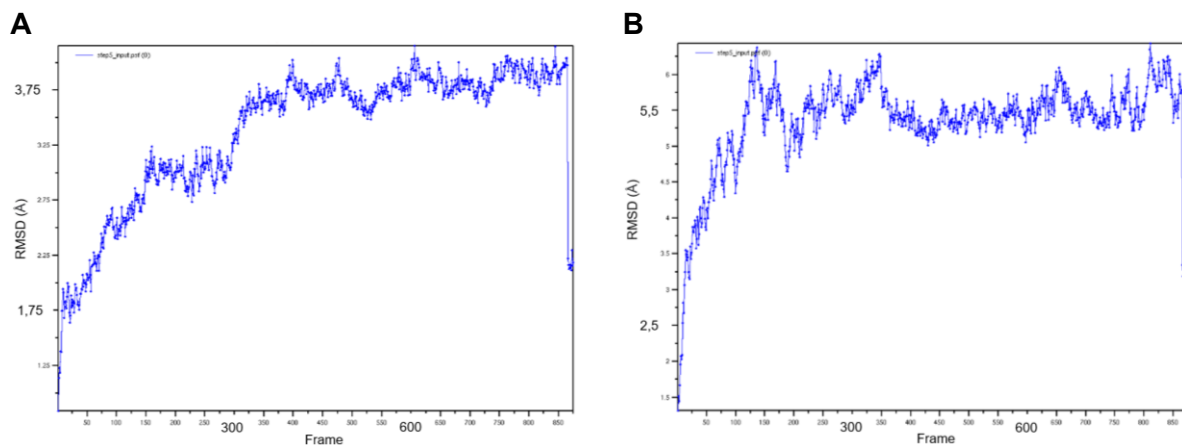


Chart 5. RMSD plots of the protein complex with ligand “compound 21- PEG10 - compound 23” **A:** RMSD plot of CB1R **B:** RMSD plot of OTR.

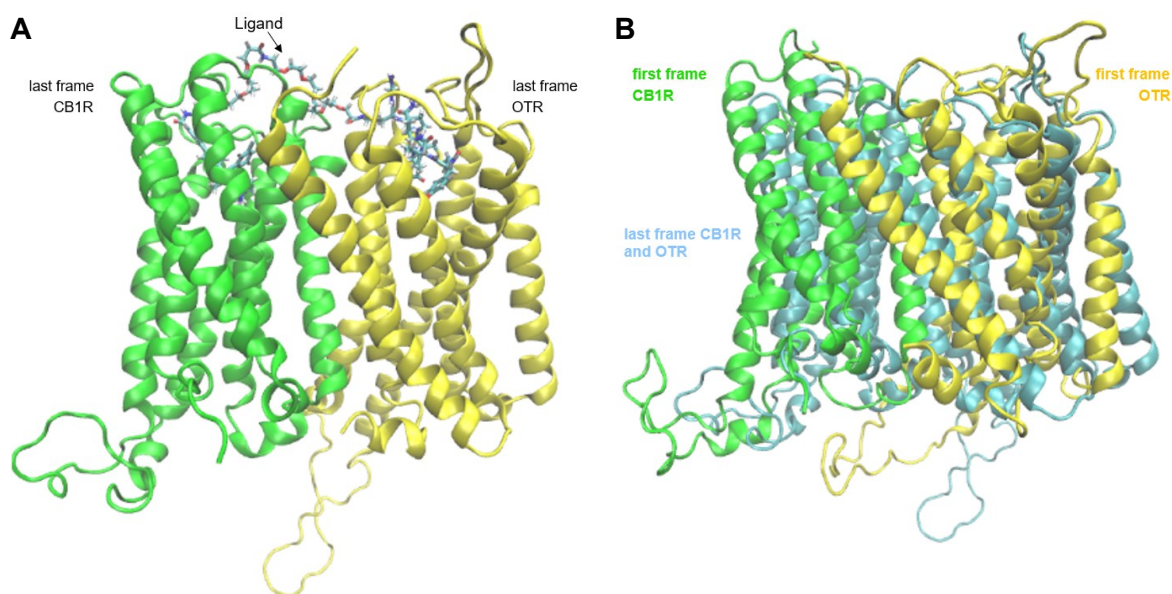


Figure 39. **A:** Last frame of MD simulation with bivalent ligand “compound 21- PEG10 - compound 23”; **B:** Alignment of the first frame and last frame of the MD simulation.

Complex 6:

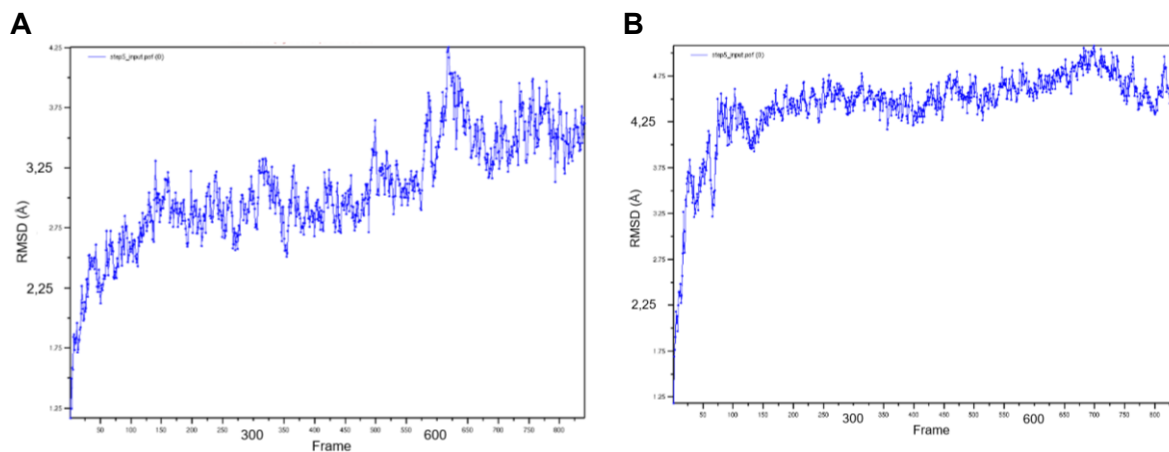


Chart 6. RMSD plots of the protein complex with ligand “compound 21- PEG15 - compound 23” **A:** RMSD plot of CB1R **B:** RMSD plot of OTR.

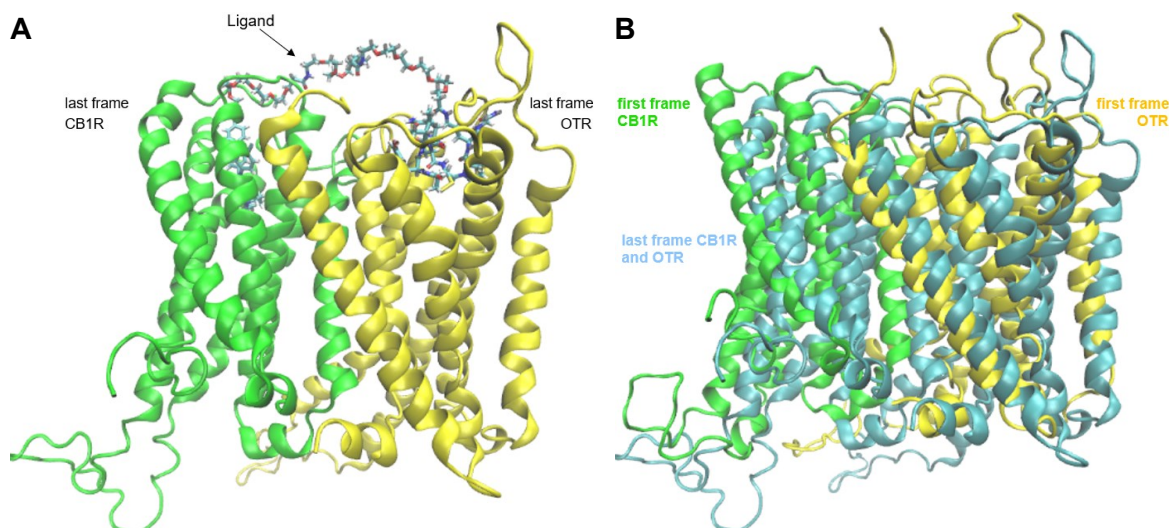


Figure 40. **A:** Last frame of MD simulation with bivalent ligand “compound 21- PEG15 - compound 23”; **B:** Alignment of the first frame and last frame of the MD simulation.

Complex 7:

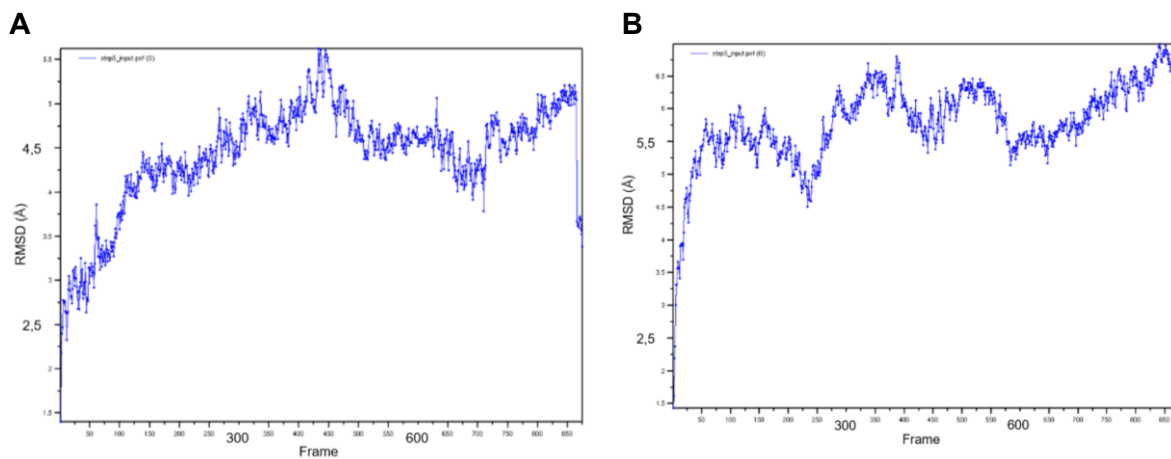


Chart 7. RMSD plots of the protein complex with ligand "compound 21- PEG10 - compound 24" **A:** RMSD plot of CB1R **B:** RMSD plot of OTR.

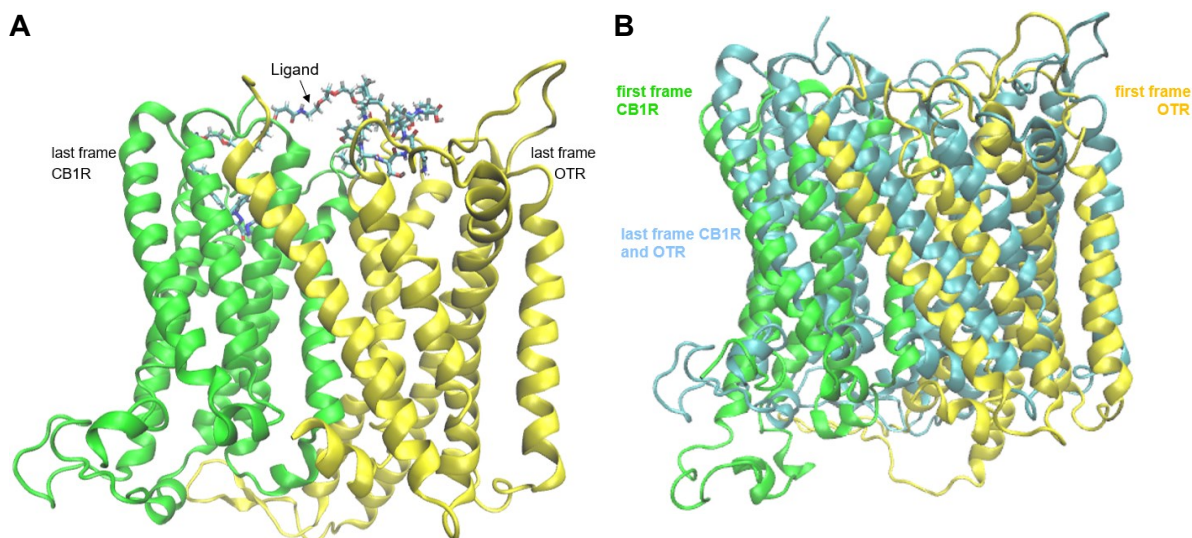


Figure 41. **A:** Last frame of MD simulation with bivalent ligand "compound 21- PEG10 - compound 24"; **B:** Alignment of the first frame and last frame of the MD simulation.

Complex 8:

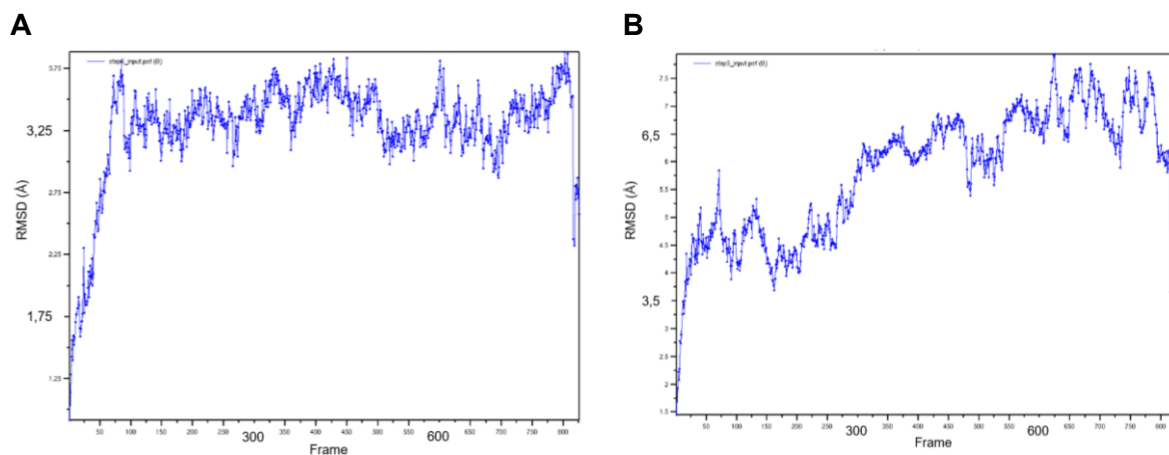


Chart 8. RMSD plots of the protein complex with ligand “compound 21 - PEG15 - compound 24” **A:** RMSD plot of CB1R **B:** RMSD plot of OTR.

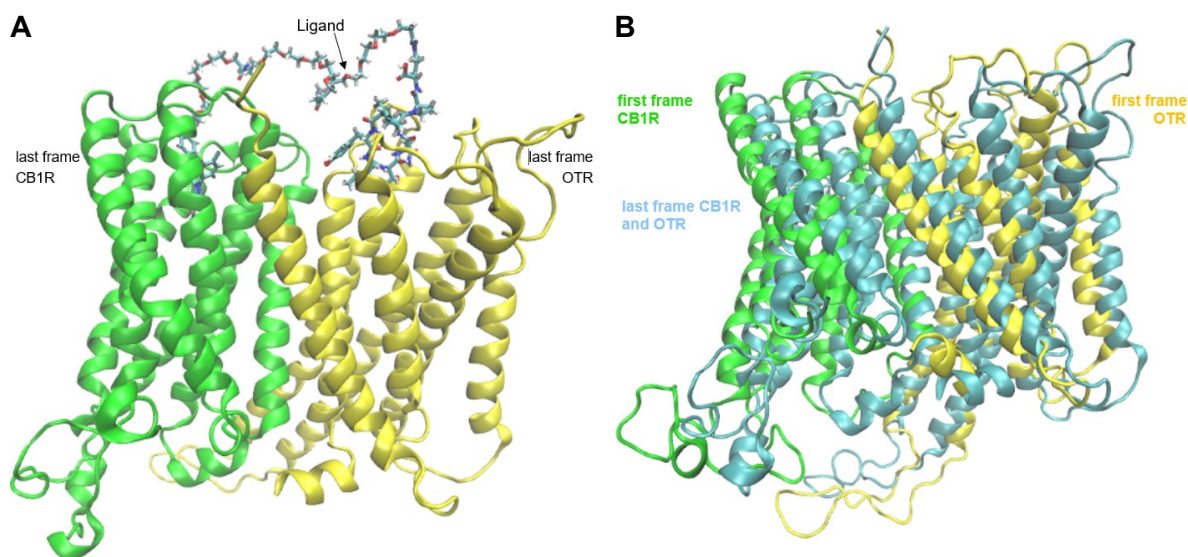


Figure 42. **A:** Last frame of MD simulation with bivalent ligand “compound 21 - PEG15 - compound 24”; **B:** Alignment of the first frame and last frame of the MD simulation.

Complex 9:

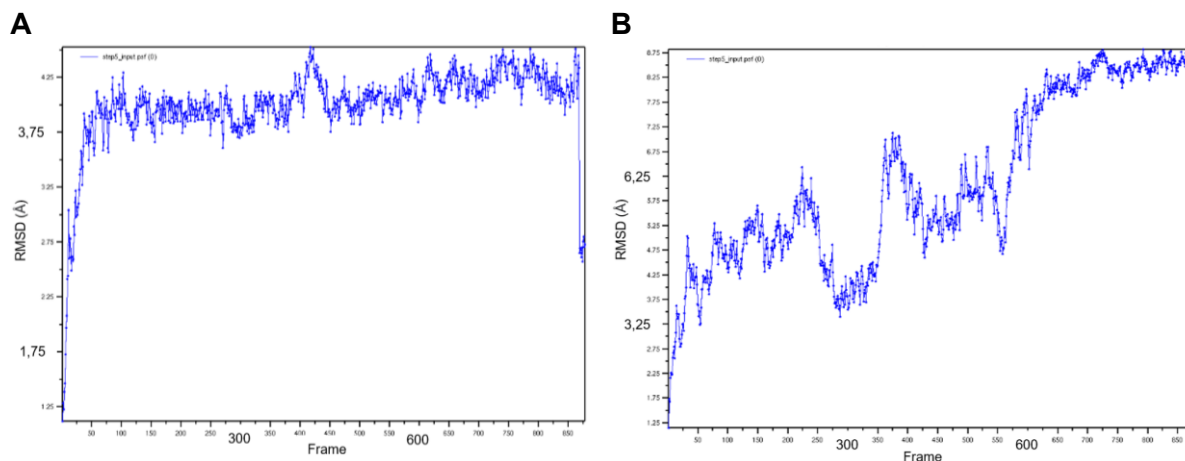


Chart 9. RMSD plots of the protein complex with ligand “compound **22**- PEG10 - compound **23**”. **A:** RMSD plot of CB1R **B:** RMSD plot of OTR

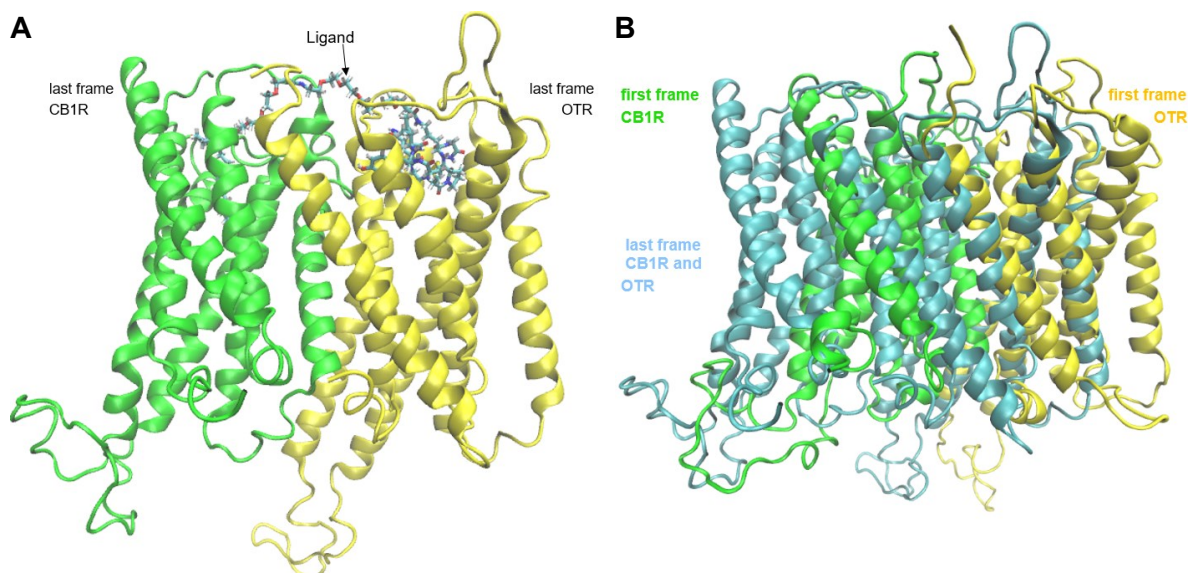


Figure 43. **A:** Last frame of MD simulation with bivalent ligand “compound **22**- PEG10 - compound **23**”; **B:** Alignment of the first frame and last frame of the MD simulation.

Complex 10:

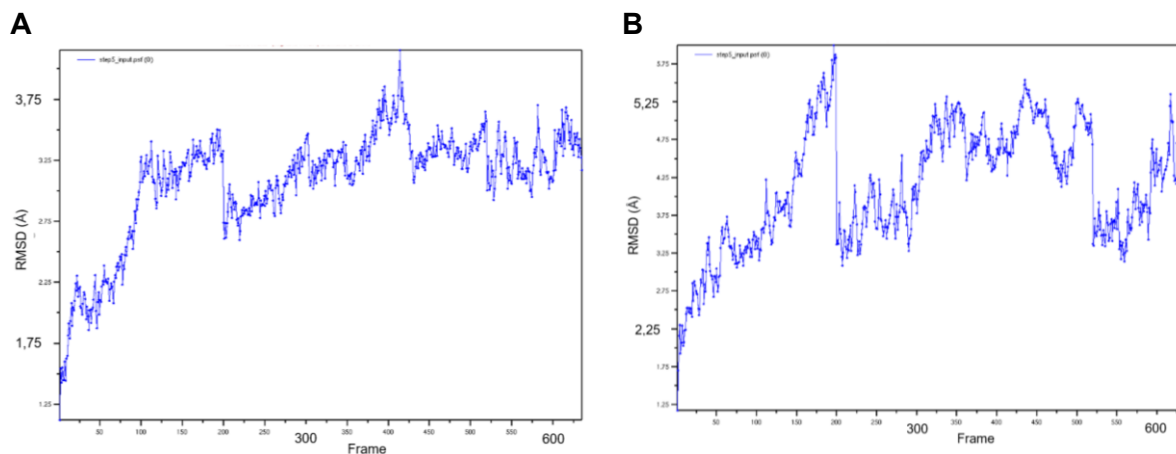


Chart 10. RMSD plots of the protein complex with ligand “compound **22**- PEG15 - compound **23**”**A:** RMSD plot of CB1R **B:** RMSD plot of OTR.

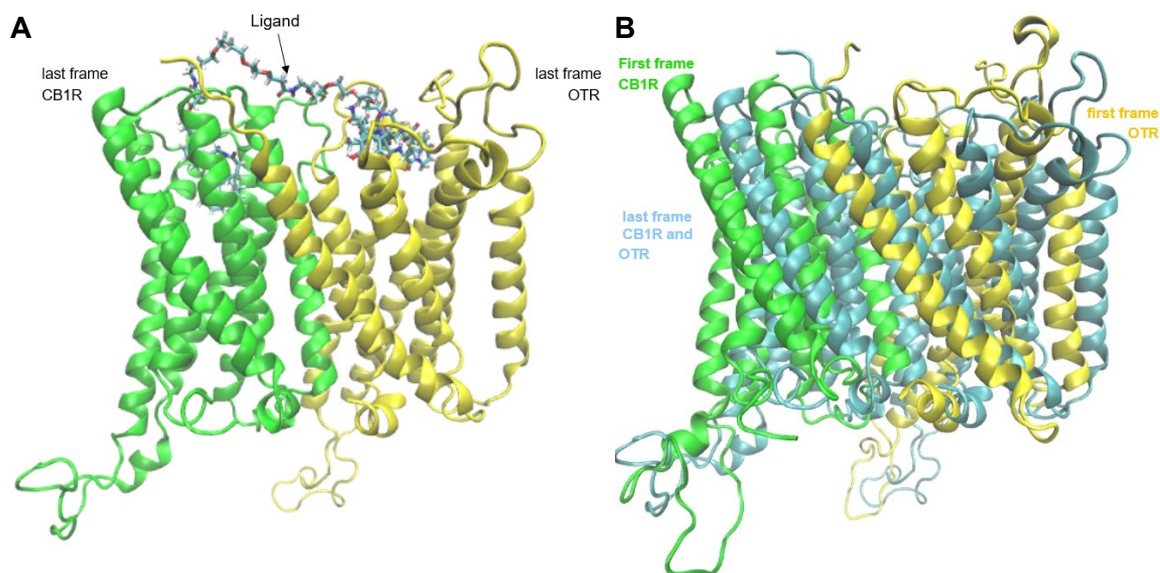


Figure 44. A: Last frame of MD simulation with bivalent ligand “compound **22**- PEG15 - ”; **B:** Alignment of the first frame and last frame of the MD simulation.

Complex 11:

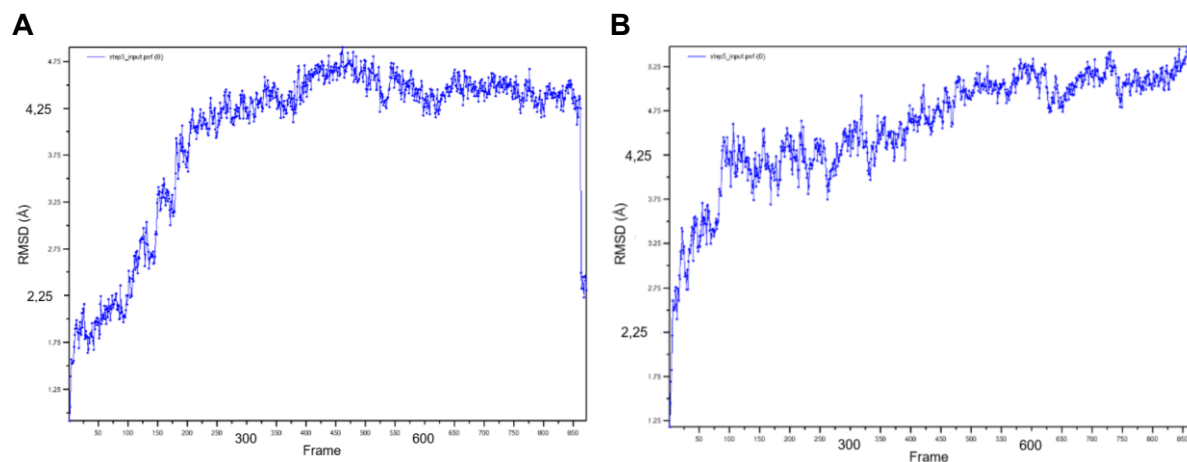


Chart 11. RMSD plots of the protein complex with ligand “compound 22- PEG10 – compound 24” **A:** RMSD plot of CB1R **B:** RMSD plot of OTR.

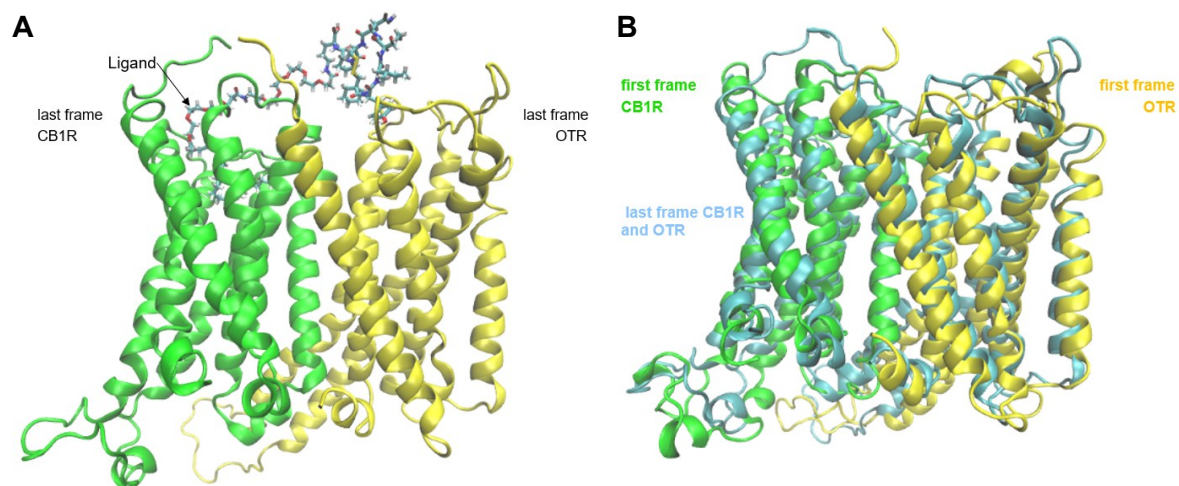


Figure 45. A: Last frame of MD simulation with bivalent ligand “compound 22- PEG10 - compound 24”; **B:** Alignment of the first frame and last frame of the MD simulation.

Complex 12:

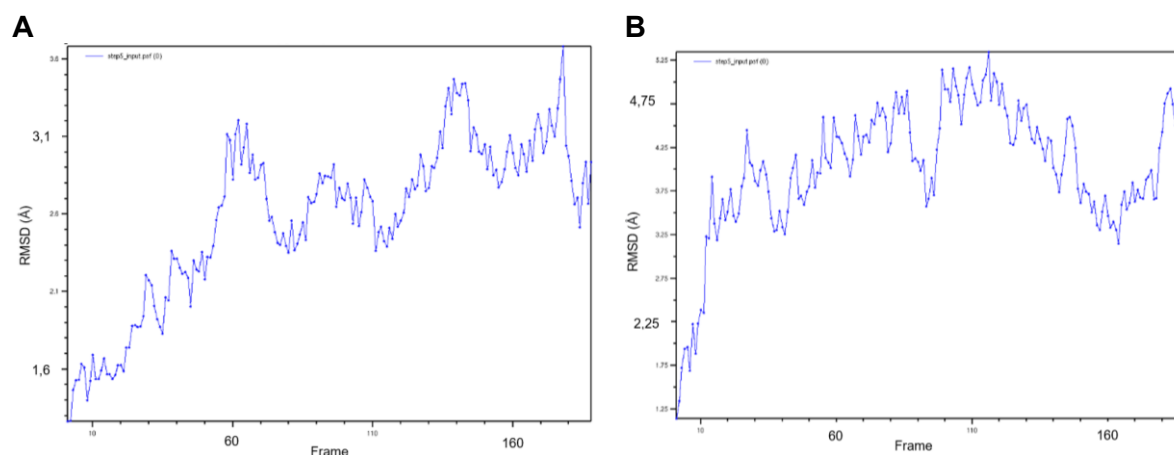


Chart 12. RMSD plots of the protein complex with ligand “compound **22**- PEG15 - compound **24**” **A:** RMSD plot of CB1R **B:** RMSD plot of OTR.

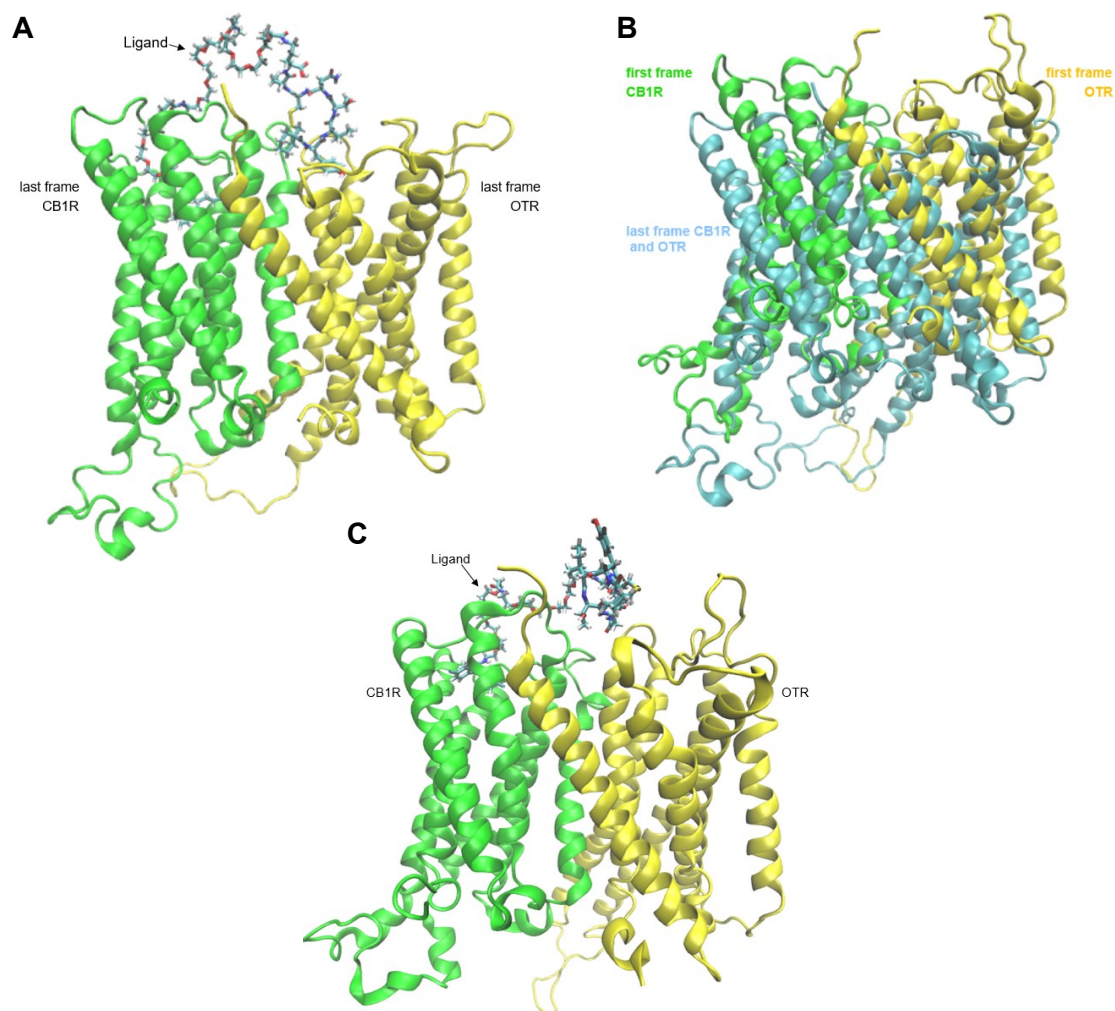


Figure 46. **A:** Last frame of MD simulation with bivalent ligand “compound **22**- PEG15 - compound **24**”; **B:** Alignment of the first frame and last frame of the MD simulation **C:** Unstable frame of MD simulation with bivalent ligand “compound **22**- PEG15 - compound **24**”.

4.4.2 Surface area assessment

Pymol was used for measuring the surface area of the Memdock results before MD simulation and the MD simulations' results of complex 1 to complex 12 via "get surface area".

The accessible surface area (ASA) was calculated for each protein and the complex. Then the ASA of the unbound proteins was calculated for each receptor and the complex by separating the receptors by 100Å along the x-axis. The surface of the interfaces (also called buried surface area (BSA)) was calculated as the difference between the accessible surface area of the bound complex (ASA_{bound}) and the accessible surface area of the unbound complex (ASA_{unbound}). The variation in the ASA provides information about changes in the hydrophobic free energy when the complex is transferred from a polar solvent to a hydrophobic environment (Chothia and Janin, 1975).

$$BSA = \text{all ASA of bound proteins} - \text{all ASA of unbound proteins}$$

Further, the differences between the BSAs (ΔBSA) and the ASAs of the bound complex ($\Delta ASA_{\text{bound}}$) before and after the MD simulation were calculated to demonstrate the impact of the MD simulation on BSA and ASA_{bound} of the dimeric complexes could be demonstrated.

The results are rounded and shown in **Table 11**. It could be seen that changes in the interfaces' surface areas (% ΔBSA) from before MD simulation to after were quite diverse along the different receptor complexes. Some interfaces seem to increase while others showed a loss of their initial size. Especially interface 1 at receptor complex 1 stood out with a massive surplus of 43% of the BSA after MD simulation.

The pictures are different for the accessible surface area. Only marginal differences between the accessible surface area (% $\Delta ASA_{\text{bound}}$) before and after the MD simulations could be observed.

The differences of BSA and ASA_{bound} between complex 1 to complex 12 could be explained by the relatively short simulation time of 10 ns. It is assumed that a simulation time longer than that would result in an adaption of the values to one another and they would level off to a certain value of the BSA and ASA_{bound} before and after MD simulation.

To give an overview of the results, the mean and standard deviation were calculated. The average BSA of complexes 1 to 12 before MD simulation is $3819 \pm 355 \text{ \AA}^2$ and after MD simulation it is $3712 \pm 426 \text{ \AA}^2$ and the average ASA of the bound complexes 1 to 12 is $33506 \pm 195 \text{ \AA}^2$ before MD simulation and $34625 \pm 783 \text{ \AA}^2$ after MD simulation.

Table 11. Overview of the surfaces of the receptor complexes 1 to 12 before and after the MD simulation and the calculation of the BSA, Δ BSA, Δ ASAbound as well as the percentual change of BSA and ASAbound before and after MD simulation.

	ASA before MD (\AA^2)		BSA (\AA^2)	ASA after MD (\AA^2)		BSA (\AA^2)	Δ BSA (\AA^2)	Δ ASA bound (\AA^2)	% Δ BSA (\AA^2)	% Δ ASA bound (\AA^2)
	bound	un-bound		bound	un-bound					
Complex 1										
OTR	18355	19949		19153	21143					
CB1R	15679	16858		15778	17822					
All	34134	37116	2979	35001	38986	3984	+1005	+241	+34%	+0,7%
Complex 2										
OTR	18275	19996		18509	20006					
CB1R	15015	16855		15194	16722					
All	33411	37234	3824	33764	36834	3069	-755	+354	-19%	+1%
Complex 3										
OTR	18316	20097		19834	21459					
CB1R	14919	16757		16026	17813					
All	33554	37859	4304	35957	39475	3518	-786	+2403	-18%	+7%
Complex 4										
OTR	18320	20060		18125	19874					
CB1R	14974	16817		15581	17312					
All	33476	37960	4485	33775	37251	3476	-1009	+299	-22%	+0,8%
Complex 5										
OTR	18276	20023		18309	19917					
CB1R	15005	16838		15535	17245					
All	33408	37157	3750	33950	37337	3387	-363	+542	-9%	+1,6%
Complex 6										
OTR	18311	20041		18765	20530					
CB1R	15001	16845		15650	17485					
All	33441	37431	3989	34517	38177	3660	-329	+1075	-8%	+3,2%
Complex 7										
OTR	18331	20072		17687	19866					
CB1R	15010	16851		15479	17698					
All	33481	37204	3723	33272	37752	4481	+757	-209	+20%	-0,6%
Complex 8										
OTR	18334	20055		19797	1260					
CB1R	14969	16811		15022	16515					
All	33425	37371	3946	34893	37948	3055	-891	+1468	-23%	+4,4%

Complex 9										
OTR	18336	20072		19177	21111					
CB1R	14982	16829		16251	18077					
All	33445	37224	3779	35500	39300	3800	+21	+2054	+1%	+6,1%
Complex 10										
OTR	18376	20105		18353	20442					
Cb1R	15002	16842		15924	18024					
All	33519	37297	3777	34375	38659	4284	+506	+856	+13%	+2,6%
Complex 11										
OTR	18321	20043		18206	20016					
Cb1R	14951	16792		16898	18809					
All	33390	37028	3638	35209	38979	3770	+132	+1818	+4%	+5,4%
Complex 12										
OTR	18321	20042		18886	20874					
Cb1R	14951	16792		16329	18358					
All	33390	37028	3638	35286	39351	4065	+427	+1896	+12%	+5,6%

4.4.3 PyRosetta Alanine scan

Alanine scan was used to identify important protein-protein interactions at the interface of the CB1R and OTR.

The alanine scan identified these interactions by mutating residues to alanine and calculating the impact of this mutation on the binding free energy. It was performed with the protein structure of the MD simulations' last configuration for all complexes 1 to 12. The results showed each mutated amino acid at the interfaces and the respective energy score.

The protein complexes' interfaces 1 to 12 are accordingly named "interface 1" to "interface 12" in the following text.

4.4.3.1 Pymol visual inspection

The interfaces of the CB1R and OTR dimeric complexes after MD simulation were visually inspected using Pymol. Residues found to impact the binding free energy significantly were coloured based on their impact. The residues at the CB1R coloured blue show a positive shift in the binding free energy as well as the residue coloured cyan at the OTR and red shows residues with a negative shift in the binding free energy for OTR and CB1R.

The results of the alanine scan revealed also residues that are not at the interface between the TMH of the two receptors but at the ECLs, N-termini, ICL, and C-termini. These interactions

were also included in the evaluations because they are assumed to play an important role in the receptor complexes' interface.

A few general statements about the interfaces could be made.

The core domain of the interface was shown to be between TMH4 of the CB1R and TMH7 of the OTR. The interface is built between TMH2 of the CB1R and TMH1 of the OTR, TMH3 of the CB1R and TMH7 of the OTR, and TMH4 of the CB1R and TMH6 of the OTR. In some cases, as it was seen at interface 1 and interface 8, interactions between TMH1 of the CB1R and TMH1 of the OTR were noticed. Important residues at the ECL, ICL, N-terminus, and C-terminus of each receptor were shown at ECL1, ECL2, ICL1, ICL2, ICL3, and H8 of the CB1R and the N-terminus, ECL3, ICL3, H8, and C-terminus of the OTR. Interactions between these structures are quite diverse and therefore explained in detail at each interface individually.

Further, some interfaces showed special interactions or residues. Interface 4 and interface 7 displayed interactions between residues at the ICL3 of the OTR and ICL2 or ICL3 of the CB1R. These interactions are caused by the high flexibility of the intracellular loops. Especially ICL3 of the OTR is quite long and therefore a high movement in every direction is possible. So, when ICL3 of the OTR moves towards the CB1R, additional interactions between the receptors are enabled. Moreover, at interface 7, it was shown that H8 of the CB1R might also be involved in interactions at the intracellular side of the receptor complex although this is the only interface showing this interaction. At interface 1, interface 9, and interface 11 it was noticeable that residues at ECL1 of the CB1R are important for interactions with the OTR in contrast to any other interface.

Hydrogen bonds between the CB1R and OTR tend to stabilize the extracellular and intracellular side of the receptors. Only at interface 1, interface 7, interface 8, interface 10, and interface 11 hydrogen bonds between residues at the transmembrane region of the interface were seen. This is explained by the fact that more residues with hydrophobic side-chains are located at the transmembrane region of the interface.

In the following text, interfaces 1 to 12 are inspected in detail and described separately.

Interface 1:

The alanine scan identified 73 to be of importance. 34 residues at TMH1/2/3/4 and ECL1/2 of CB1R, and 39 important residues at TMH1/6/7, N-terminus, ECL3, C-terminus, and H8 of the OTR.

Important residues at the extracellular loops and intracellular loops of each receptor and the N-terminus, C-terminus und H8 of the OTR were found. At the CB1R only extracellular loops showed important residues. These residues are R73, D75, N78 and V79 located at ECL1 and residues N146, E148, and K149 located at ECL2. Regarding important residues at the OTR, important residues P1 and R4 at the N-terminus and residues D268, A269, A271, P272, and

E274 at ECL3 are located extracellularly and residues located intracellularly are residues R308, F309 and L310 at H8 and residue L298 at the C-terminus.

Interactions between TMHs in this interface are generally located between TMH1/2 of the CB1R and TMH1 of the OTR, TMH3 of the CB1R and TMH7 of the OTR and between TMH4 of the CB1R and TMH6/7 of the OTR.

In **Table 12**, the residues are allocated to their localization at the receptors by visually inspecting the dimeric receptor complex.

Table 12. Residues identified by the alanine scan at the receptor.

Receptor	Position	Residues
CB1R	TMH1	L37
	TMH2	V54, L57, L58, V61, I62, Y65
	ECL1	R73, D75, N78, V79
	TMH3	F82, G86
	TMH4	K115, R116, T119, R120, P121, V124, V125, C128, L129, W131, T132, I133, I135, V136, A138, V139, L142, L143
	ECL2	N146, E148, K149
OTR	N-terminus	P1, R4
	TMH1	L8, V11, E12, V15, L18, L21
	TMH6	I246, L249, A250, V253, C254, T256, P257, F260, V261, W264
	ECL3	D268, A269, A271, P272, E274
	TMH7	S276, A277, I280, V281, L283, L284, L287, N288, C290, C291, W294, I295
	C-terminus	L298
	H8	R308, F309, L310

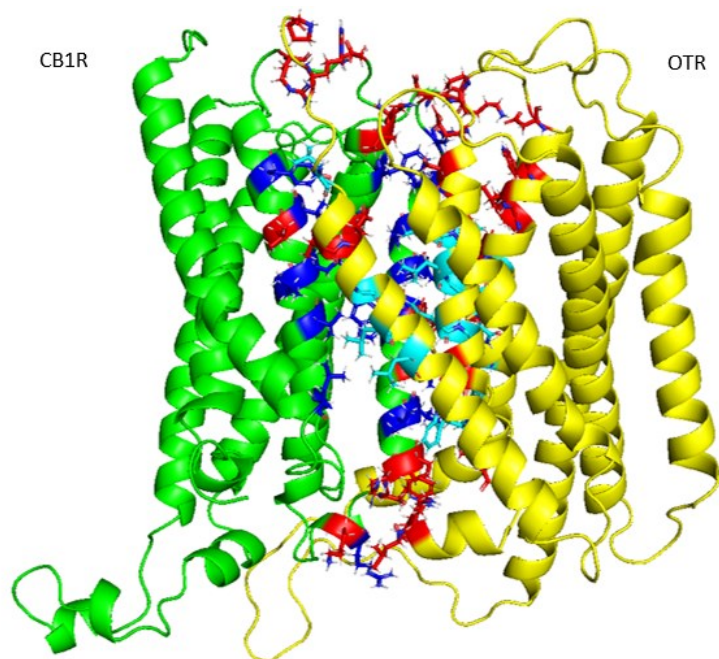


Figure 47. The view of the interface between CB1R (green) and OTR (yellow) after MD simulation.

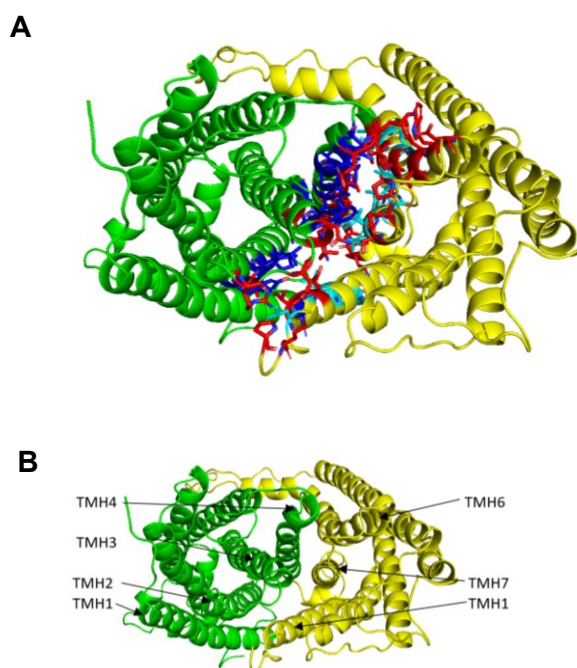


Figure 48. The top-down view of the interface of CB1R (green) and OTR (yellow) after MD simulation. **A:** Interface with highlighted residues **B:** Overview of the TMHs at the interface.

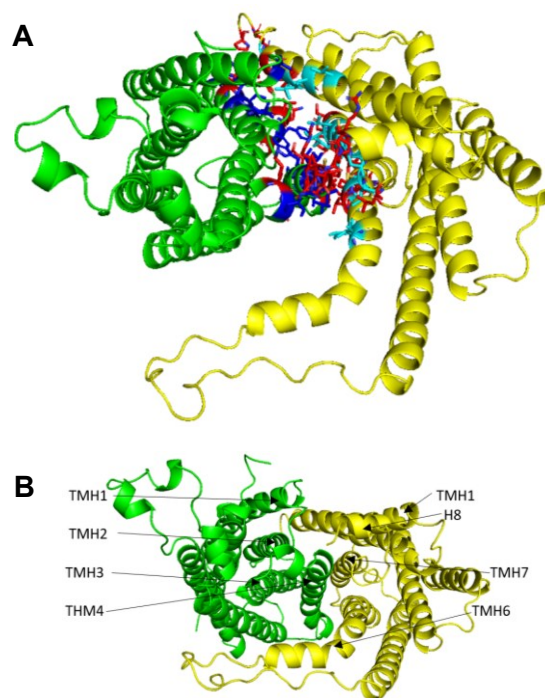


Figure 49. The bottom-up view of the interface of CB1R (green) and OTR (yellow) after MD simulation. **A:** Interface with highlighted residues **B:** Overview of the TMHs at the interface.

A total of nine hydrogen bonds were found between CB1R and OTR. Six of them are located at the extracellular side of the receptor complex, two at the transmembrane region, and one at the intracellular side of the receptor complex.

At the extracellular side, two hydrogen bonds are located between residue K149 at ECL2 of the CB1R and residue D268 at ECL3 of the OTR, one between residue N146 at ECL2 of the CB1R and residue P271 at ECL3 of the OTR, and one hydrogen bond is located between residue N78 at ECL1 of the CB1R and residue E274 at ECL3 of the OTR. Two more hydrogen bonds were found between residues D75 at ECL1 of the CB1R, and N4 at the N-terminus of the OTR (Figure 50). The two hydrogen bonds located towards the transmembrane region of the interface were found between residue K83 at TMH3 of the CB1R and residues E11 at TMH1 of the OTR (Figure 51). Further, the hydrogen bond located at the intracellular side of the receptor complex is built between residue T119 at TMH4 of the CB1R and residue L310 at the C-terminus of the OTR (Figure 52).

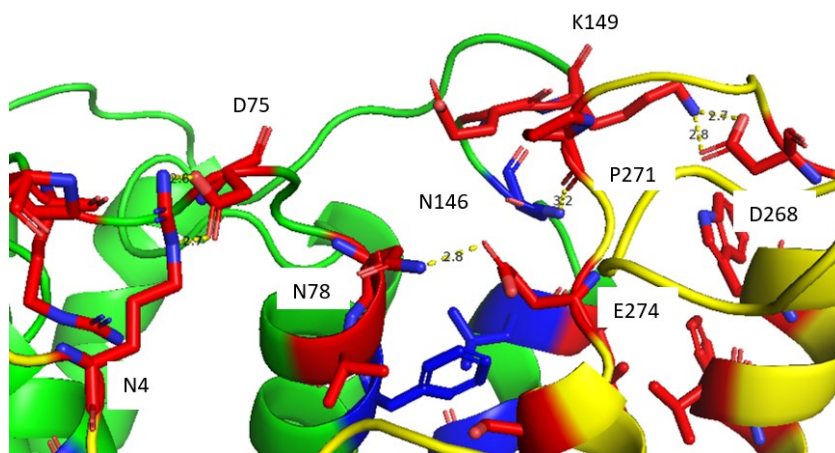


Figure 50. Hydrogen bonds between residue K149 at ECL2 of the CB1R and residue D268 at ECL3 of the OTR, between residue N146 at ECL2 of the CB1R and residue P271 at ECL3 of the OTR, between residue N78 at ECL1 of the CB1R and residue E274 at ECL3 of the OTR and between residues D75 at ECL1 of the CB1R, and N4 at the N-terminus of the OTR.

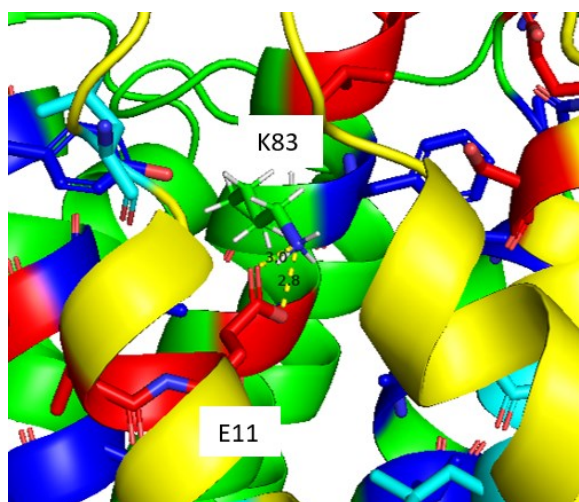


Figure 51. Hydrogen bond between residue K83 at TMH3 of the CB1R and residues E11 at TMH1 of the OTR.

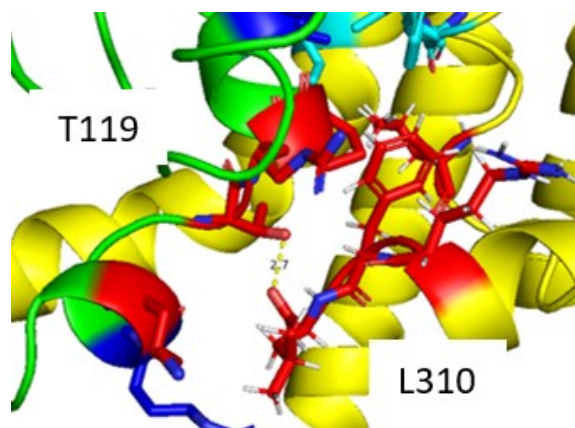


Figure 52. Hydrogen bond between residue T119 at TMH4 of the CB1R and residue L310 at the C-terminus of the OTR.

Interface 2:

At this interface, 60 residues were found to be important for interactions: 28 important residues at TMH2/3/4, ICL1, ICL2, and ECL2 of the CB1R, and 32 important residues at TMH1/6/7, N-terminus, ECL3, H8, and C-terminus of OTR were spread over the interface.

Important residues were found at the extracellular loops and intracellular loops of each receptor and the N-terminus, C-terminus and H8 of the OTR. At the extracellular loops of the CB1R only residue G144 at ECL2 and at the extracellular loops of the OTR, residues R3 and N5 at the N-terminus and S276 at ECL3 were found to be important. Intracellularly, important residues T119, R120, P121, and R42 were found at ICL2 of the CB1R. At the intracellular side of the OTR, residues M297, L298, F309, and L310 at the C-terminus and residue L305 at H8 were found to be important by the alanine scan.

Important interactions between TMHs of the receptors were found between TMH2 of the CB1R and TMH1 of the OTR, TMH3 of the CB1R and TMH7 of the OTR and between TMH4 of the CB1R and TMH6/7 of the OTR.

In **Table 13**, the residues are allocated to their localization at the receptors by visually inspecting the dimeric receptor complex.

Table 13. Residues identified by the alanine scan.

Receptor	Position	Residues
CB1R	ICL1	R42
	TMH2	L58, V61, I62, Y65, S66, D69
	TMH3	V79, F82, K83
	ICL2	T119, R120, P121
	TMH4	K122, V124, V125, C128, L129, W131, T132, I133, I135, V136, A138, V139, L142, L143
	ECL2	G144
OTR	N-terminus	R3, N5
	TMH1	A7, L8, V11, V15
	TMH6	I246, L249, A250, V253, C254, P257, F260, V261
	ECL3	E274
	TMH7	S276, A277, I280, V281, L283, L284, L287, N288, C290, C291, W294, I295
	C-terminus	M297, L298, F309, L310
	H8	L305

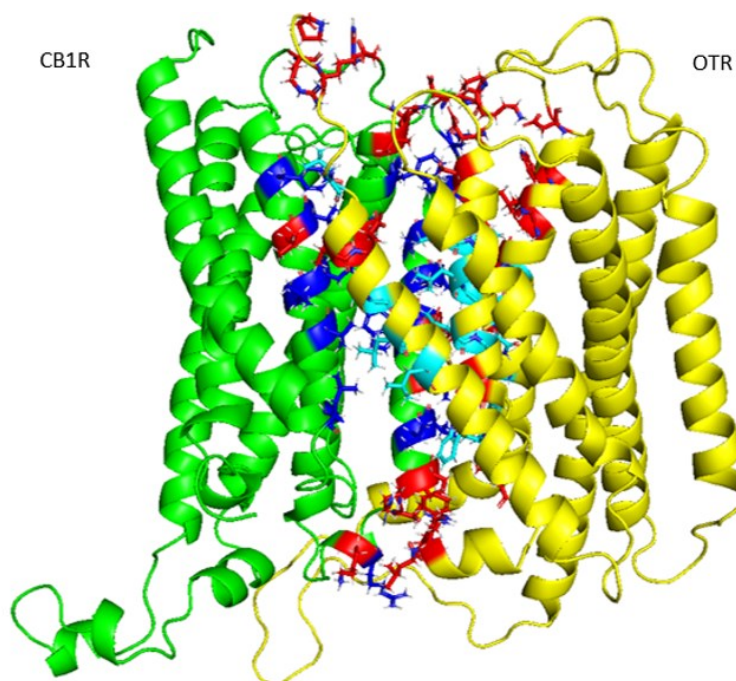


Figure 53. The view of the interface between CB1R (green) and OTR (yellow) after MD simulation.

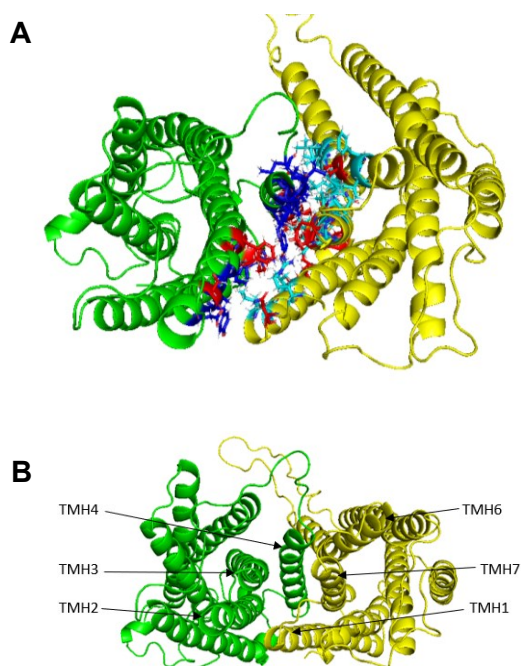


Figure 54. The top-down view of the interface of CB1R (green) and OTR (yellow) after MD simulation. **A:** Interface with highlighted residues **B:** Overview of the TMHs at the interface.

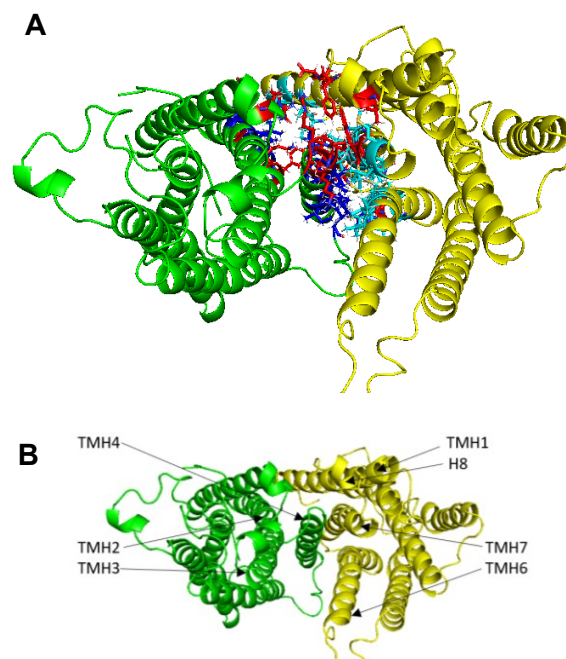


Figure 55. The bottom-up view of the interface of CB1R (green) and OTR (yellow) after MD simulation. **A:** Interface with highlighted residues **B:** Overview of the TMHs at the interface.

A total of five hydrogen bonds were found between five residues, all located at extracellular or intracellular loops. At the extracellular side of the dimeric complex, two hydrogen bonds are located between residue R73 at TMH2 of the CB1R and residue E6 at the N-terminus of the OTR (**Figure 56**). Two intracellularly located hydrogen bonds are built between residue L310 at the C-terminus of the OTR and residue R39 at ICL1 of the CB2R and one more intracellular hydrogen bond is located between residue L310 at the C-terminus of the OTR and R120 at ICL2 of the CB1R (**Figure 57**).

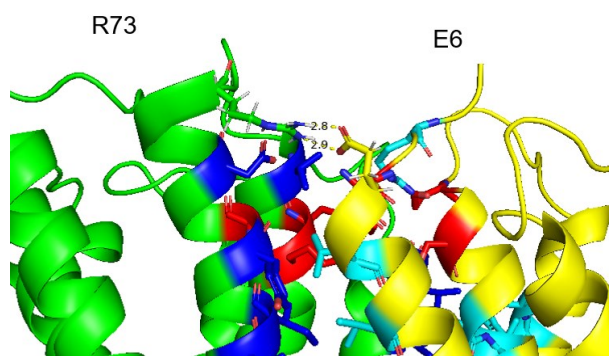


Figure 56. Hydrogen bonds between residue R73 at TMH2 of the CB1R and residue E6 at the N-terminus.

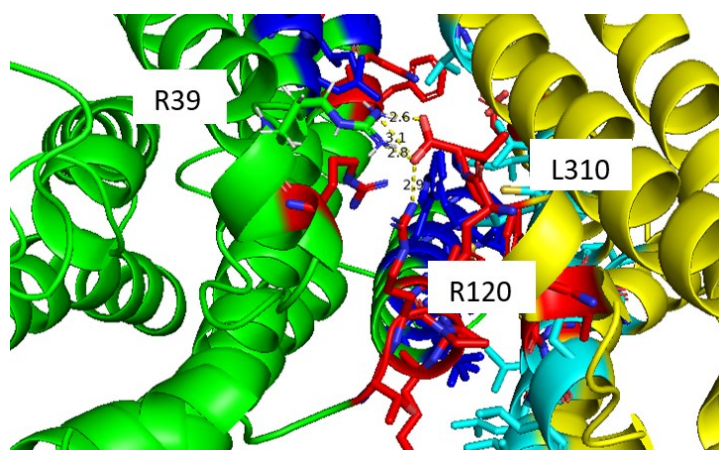


Figure 57. Hydrogen bonds between residue L310 at the C-terminus of the OTR and residue R39 at ICL1 of the CB1R and between residue L310 at the C-terminus of the OTR and residue R120 at ICL2 of the CB1R.

Interface 3:

68 residues were found to be important for interactions by the alanine scan. 29 important residues were found at TMH2/3/4 and ECL2 of the CB1R, and 39 important residues were found at TMH1/6/7, N-terminus, H8, and C-terminus of OTR.

The following important residues at the extracellular loops and intracellular loops of both receptors and the N-terminus, C-terminus, and H8 of the OTR were found. Seven residues, found to be important by the alanine scan, are located at the extracellular loops of the CB1R and OTR. Three of them, residues N146, E148, and K149, are located at ECL2 of the CB1R, three residues D268, N270, and P272 are located at ECL3 of the OTR and one residue N5 is located at the N-terminal of the OTR. At the intracellular loops, residues T119 and R120, located at ICL2 of the CB1R and residues M297, L298, and F303, located at the C-terminus of the OTR and residue L305, located at H8 of the OTR, were shown to be important.

Interactions between TMHs of the receptors were found to be mainly between TMH2 of the CB1R and TMH1 of the OTR, TMH3 of the CB1R and TMH7 of the OTR and between TMH4 of the CB1R and TMH6/7 of the OTR.

In **Table 14**, the residues are allocated to their localization at the receptors by visually inspecting the dimeric receptor complex.

Table 14. Residues identified by the alanine scan at the receptor.

Receptor	Position	Residues
CB1R	TMH2	V54, L58, G59, V61, I62, Y65, D69
	TMH3	F82, K83
	ICL2	T119, R120
	TMH4	P121, K122, V124, V125, C128, L129, W131, T132, I133, I135, V136, A138, V139, L142, L143
	ECL2	N146, E148, K149
OTR	N-terminus	N5
	TMH1	A7, L8, R10, V11, A14, V15, L18
	TMH6	F245, I246, L249, A250, V253, C254, T256, P257, F260, V261, W264
	ECL3	D268, N270, A271, P272
	TMH7	S276, A277, I280, V281, L283, L284, L287, N288, C290, C291, W294, I295
	C-terminus	M297, L298, F303
	H8	L305

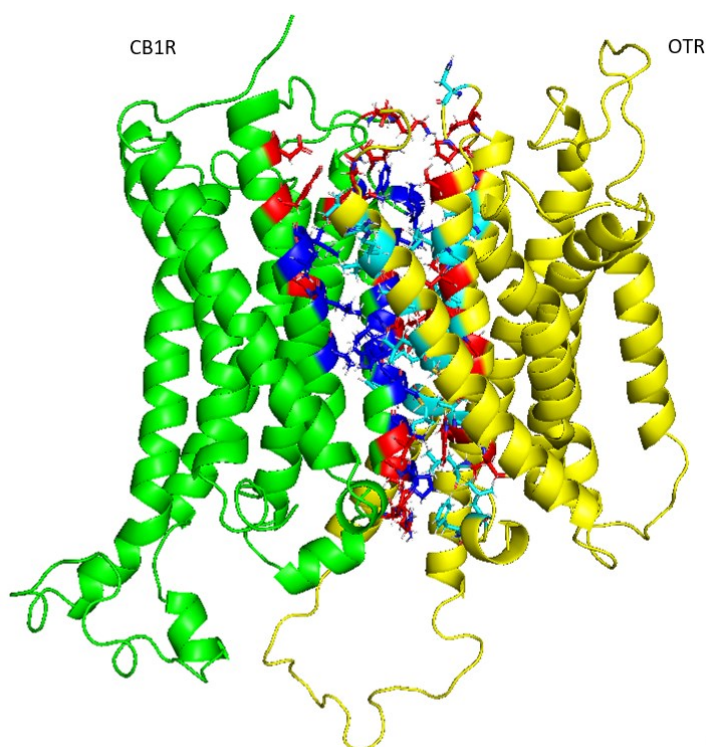


Figure 58. The view of the interface between CB1R (green) and OTR (yellow) after MD simulation.

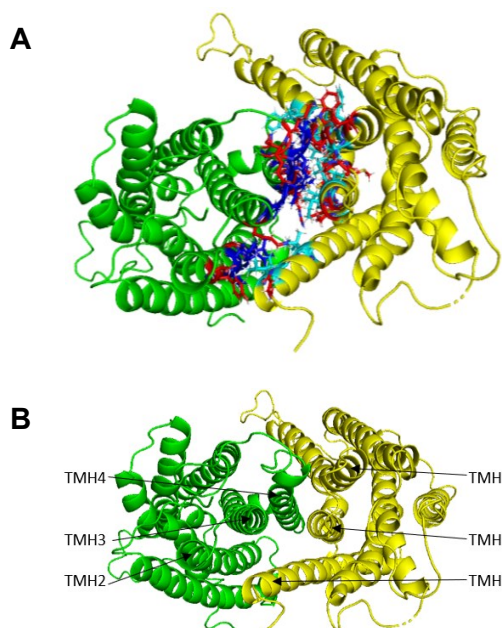


Figure 59. The top-down view of the interface of CB1R (green) and OTR (yellow) after MD simulation. **A:** Interface with highlighted residues **B:** Overview of the TMHs at the interface.

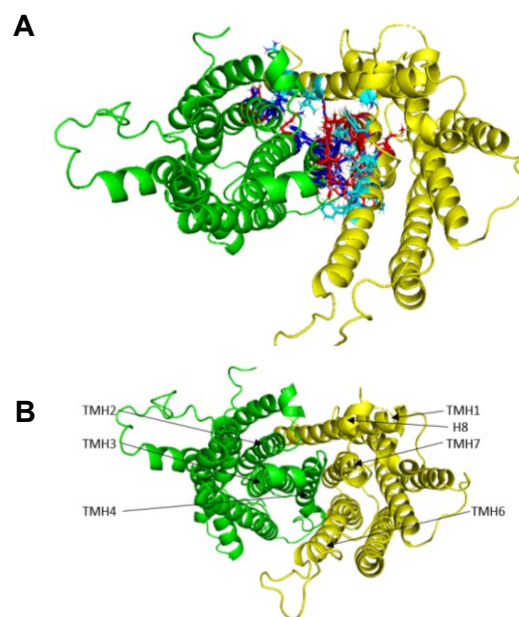


Figure 60. The bottom-up view of the interface of CB1R (green) and OTR (yellow) after MD simulation. **A:** Interface with highlighted residues **B:** Overview of the TMHs at the interface.

Five hydrogen bonds were found, all located at the extracellular side of the receptor dimer. There was one hydrogen bond located between residue R72 at ECL2 of the CB1R and residue N5 at the N-terminus of the OTR, one nearby between residue K83 at TMH3 of the CB1R and residue E12 at TMH2 of the OTR (**Figure 61**). Two hydrogen bonds were found between residue K149 at ECL2 and residue D268 at ECL3 of the OTR and one hydrogen bond is between residue L42 at TMH4 of the CB1R and residue W264 at TMH6 of the OTR (**Figure 62**).

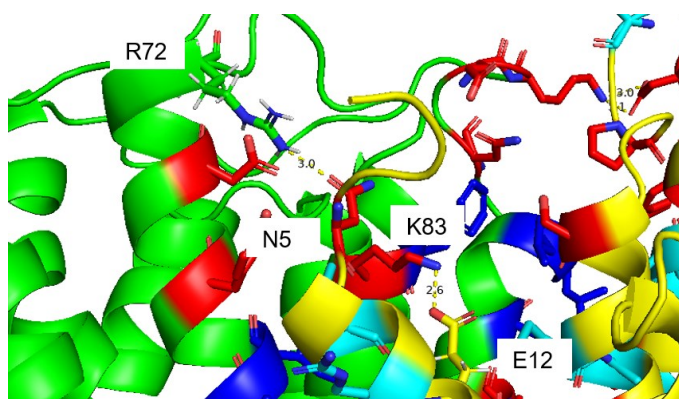


Figure 61. Hydrogen bonds between residue R72 at ECL2 of the CB1R and residue N5 at the N-terminus of the OTR and between residue K83 at TMH3 of the CB1R and residue E12 at TMH2 of the OTR.

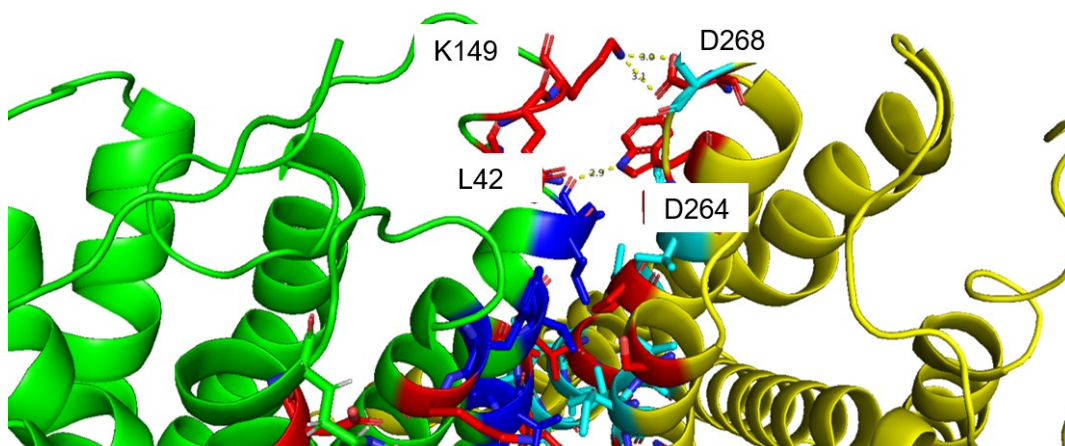


Figure 62. Hydrogen bonds between residue K149 at ECL2 and residue D268 at ECL3 of the OTR and between residue L42 at TMH4 of the CB1R and residue W264 at TMH6 of the OTR.

Interface 4:

At interface 4, 63 residues were found to be important for interactions, by the alanine scan: 29 important residues at TMH2/3/4, ICL1, ICL2 and ECL2 of the CB1R, and 34 important residues at TMH1/6/7, N-terminus, ECL3, ICL3, H8, and C-terminus of OTR.

The following important residues at the extracellular loops and intracellular loops of both receptors and the N-terminus and H8 of the OTR were found. A total of four important residues are located at the extracellular loops of the receptors. Residue G144 is located at ECL2 of the CB1R and concerning the OTR residue N5 is located at the N-terminus and residues E274 and S276 at ECL3. Intracellularly, three residues of the CB1R and four residues of the OTR were found to be important for the binding free energy between the receptors. These three residues found to be important at the CB1R are residues R39 and R42, located at ICL1, and residue R116 at ICL2. Residues A216 and G217 at ICL3, and residues F309 and L310 at the C-terminus are the four residues found at the OTR.

A noticeable characteristic of this interface is the interaction between residue R116 at the ICL2 of the CB1R and residue G217 at ICL3 of the OTR. It is enabled by the high flexibility of the ICLs, especially ICL3 of the OTR is very long causing a high level of flexibility.

The interactions between TMHs of the receptors were as usually found to be between TMH2 of the CB1R and TMH1 of the OTR, TMH3 of the CB1R, and TMH7 of the OTR and between TMH4 of the CB1R and TMH6/7 of the OTR.

In **Table 15**, the residues are allocated to their localization at the receptors by visually inspecting the dimeric receptor complex.

Table 15. Residues identified by the alanine scan at the receptor.

Receptor	Position	Residue
CB1R	ICL1	R39, R42
	TMH2	L58, V61, I62, Y65
	TMH3	V79, F82, K83, G86
	ICL2	R116
	TMH4	T119, R120, P121, K122, V124, V125, C128, L129, W131, T132, I133, I135, V136, A138, V139, L142, L143
	ECL2	G144
OTR	N-terminus	N5
	TMH1	A7, L8, V11, V15, I19
	ICL3	A216, G217
	TMH6	I246, L249, A250, V253, C254, P257, F260, V261, W264
	ECL3	E274, S276
	TMH7	A277, I280, V281, L283, L284, L287, N288, C290, C291, W294, I295, M297, L298
	C-terminus	F309, L310

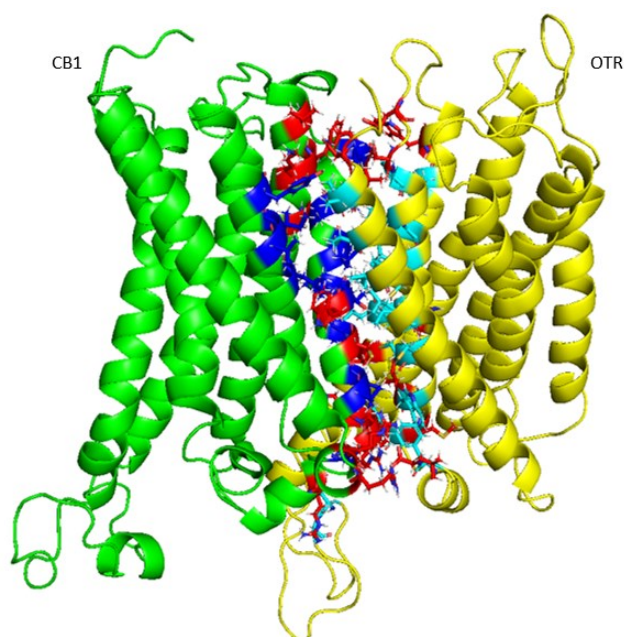


Figure 63. The view of the interface between CB1R (green) and OTR (yellow) after MD simulation.

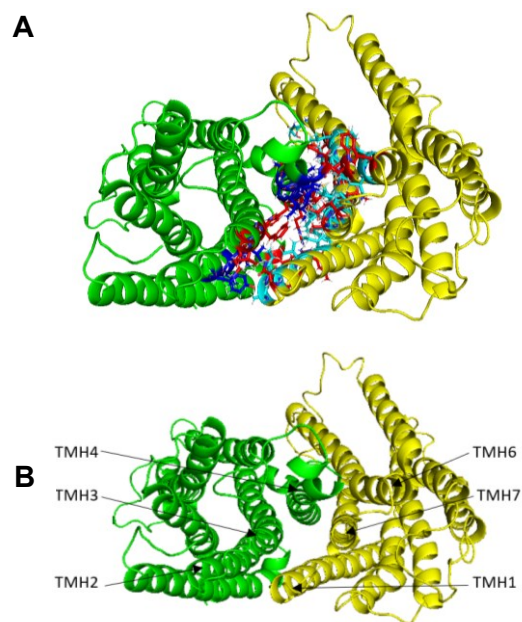


Figure 64. The top-down view of the interface of CB1R (green) and OTR (yellow) after MD simulation. **A:** Interface with highlighted residues **B:** Overview of the TMHs at the interface.

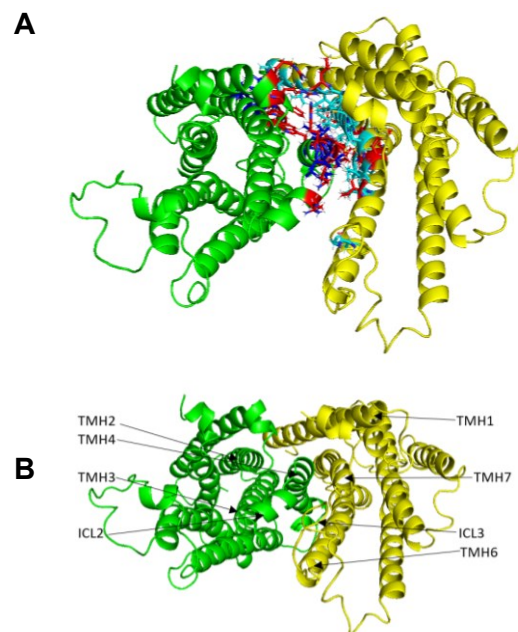


Figure 65. The bottom-up view of the interface of CB1R (green) and OTR (yellow) after MD simulation. **A:** Interface with highlighted residues **B:** Overview of the TMHs at the interface.

Eleven hydrogen bonds were found, all located at the extracellular and intracellular side of the receptor complex. Six hydrogen bonds form between residue L310 at the C-terminus of the OTR forms and three different residues at the CB1R. Further, two hydrogen bonds formed with residue L42 at ICL1, three with residue R120 at TMH4, and one with residue R39 at ICL1 of the CB1R (**Figure 66**). Further, there are two hydrogen bonds between residue I117 at ICL2 of the CB1R and residue R239 at TMH6 of the OTR and one neighbouring between residues R116 at ICL2 of the CB1R and D218 at ICL3 of the OTR (**Figure 67**). At the extracellular side of the receptor complex, two hydrogen bonds were found between residue K149 at ECL2 of the CB1R and residue D268 at ELC3 of the OTR (**Figure 68**).

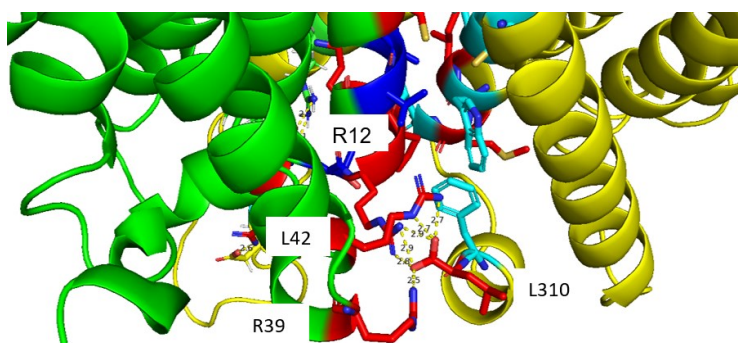


Figure 66. Hydrogen bonds between residue L310 at the C-terminus of the OTR and between residue L42 at ICL1 of the OTR, residue R120 at TMH4, and residue R39 at ICL1 of the CB1R.

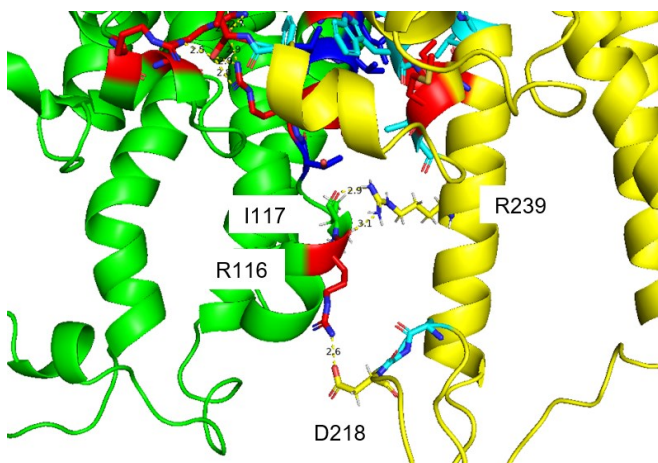


Figure 67. Hydrogen bonds between residue I117 at ICL2 of the CB1R and residue R239 at TMH6 of the OTR and between R116 at ICL2 of the CB1R and D218 at ICL3 of the OTR.

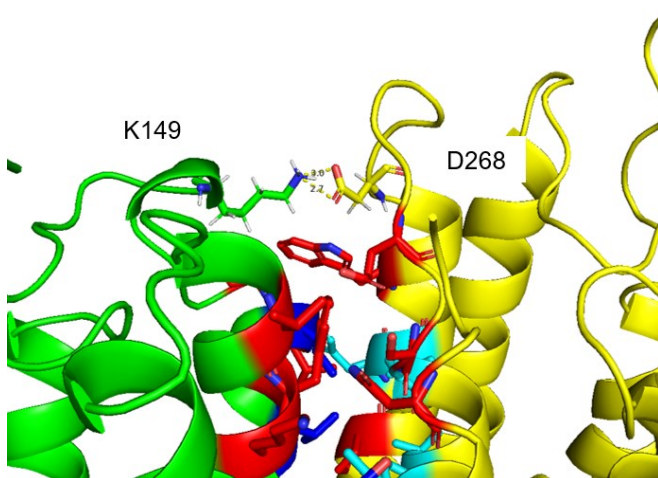


Figure 68. Hydrogen bonds between residue K149 at ECL2 of the CB1R and residue D268 at ELC3 of the OTR.

Interface 5:

At interface 5, 59 residues were found to be important for interactions between the receptor complex. 27 important residues were found to be located at TMH2/3/4 and ICL2 of the CB1R, and 32 important residues at TMH1/6/7, ECL3, and C-terminus of the OTR.

The following important residues at the extracellular loops and intracellular loops of both receptors and the C-terminus of the OTR were found. Concerning the intracellular loops, four residues were found to be important at the interface. Residues T119 and R120 at ICL2 of the

CB1R and residues F309 and L310 at the C-terminus of the OTR. At the intracellular loops, the three important residues W264, P272, and E274 were found at ECL3 of the OTR.

The interactions between TMHs of the receptors were as usually found to be between TMH2 of the CB1R and TMH1 of the OTR, TMH3 of the CB1R, and TMH7 of the OTR and between TMH4 of the CB1R and TMH6/7 of the OTR.

In **Table 16**, the residues are allocated to their localization at the receptors by visually inspecting the dimeric receptor complex.

Table 16. Residues identified by the alanine scan at the receptor.

Receptor	Position	Residues
CB1R	TMH2	V54, L58, V61, I62, Y65
	TMH3	R77, N78, F82, K83, G85
	ICL2	T119, R120
	TMH4	P121, K122, V124, V125, C128, L129, W131, T132, I133, I135, V136, V139, L142, L143, G144
OTR	TMH1	A7, L8, V11, A14, V15, L18, L22
	TMH6	I246, L249, A250, C254, P257, F260, V261
	ECL3	W264, P272, E274
	TMH7	S276, A277, I280, V281, L283, L284, L287, N288, C290, C291, W294, I295, L298
	C-terminus	F309, L310

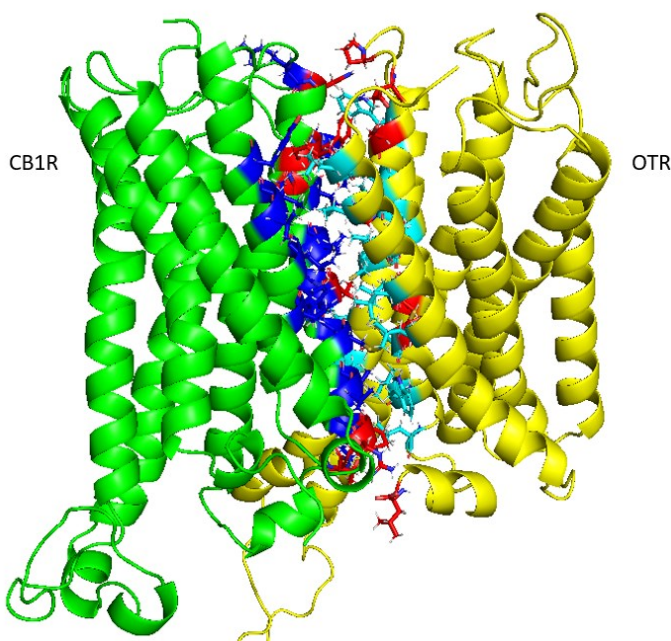


Figure 69. The view of the interface of CB1R (green) and OTR (yellow) after MD simulation.

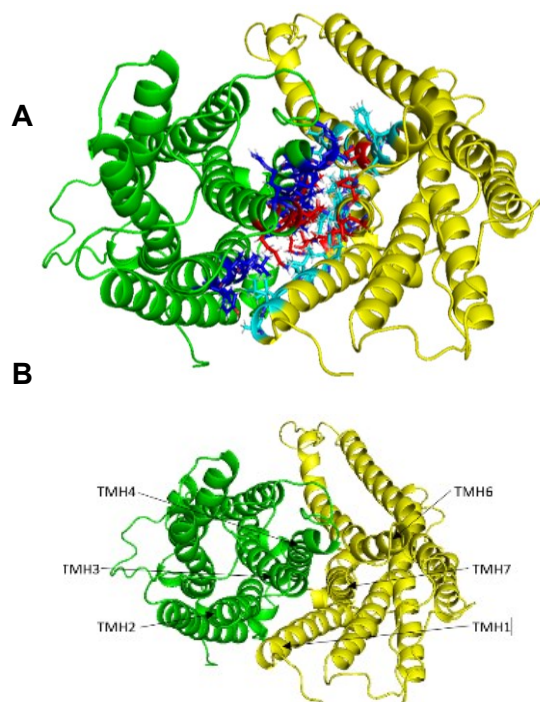


Figure 70. The top-down view of the interface of CB1R (green) and OTR (yellow) after MD simulation. **A:** Interface with highlighted residues **B:** Overview of the TMHs at the interface.

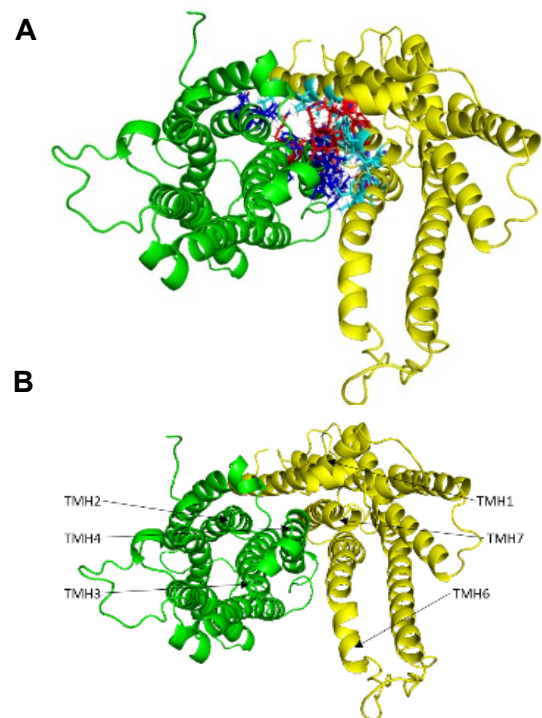


Figure 71. The bottom-up view of the interface of CB1R (green) and OTR (yellow) after MD simulation. **A:** Interface with highlighted residues **B:** Overview of the TMHs at the interface.

Five hydrogen bonds were found, at the extracellular and intracellular side of the receptor dimer. At the extracellular side, one hydrogen bond was found between residue N78 at TMH3 of the CB1R and P272 at ECL3 of the OTR. Another one was found between K83 at TMH3 of the CB1R and E12 at TMH1 of the OTR and one was found to be between R72 at ECL1 of the CB1R, and N4 at the N-terminus of the OTR (**Figure 72**). The two hydrogen bonds found intracellularly are between the two residues R120 at ICL2 of the CB1R and L310 at the C-terminus of the OTR (**Figure 73**).

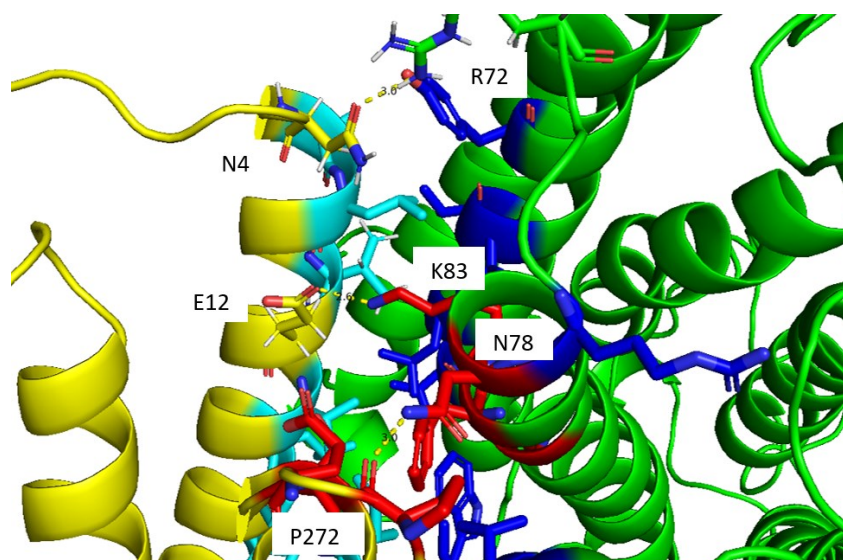


Figure 72. Hydrogen bonds between residue N78 at TMH3 of the CB1R and P272 at ECL3 of the OTR, K83 at TMH3 of the CB1R and E12 at TMH1 of the OTR, R72 at ECL1 of the CB1R, and N4 at the N-terminus of the OTR.

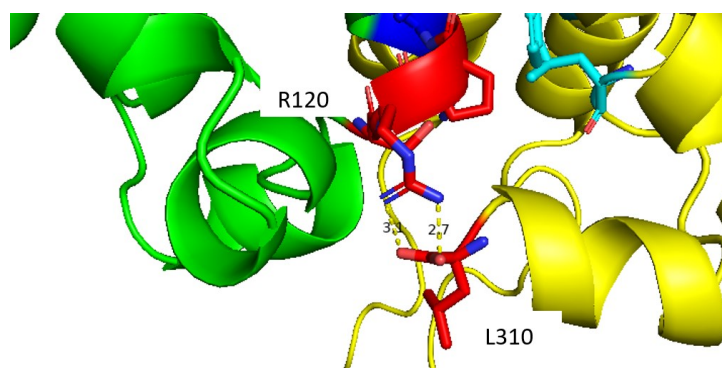


Figure 73. Hydrogen bonds between residue R120 at ICL2 of the CB1R and residue L310 at the C-terminus of the OTR.

Interface 6:

A total of 70 residues were identified to be important for interactions. 30 important residues at TMH2/3/4, ICL1, ICL2 and ECL2 of the CB1R, and 40 important residues at TMH1/6/7, ECL3, C-terminus, and H8 of the OTR.

The following important residues at the extracellular loops and intracellular loops of both receptors and the C-terminus, and H8 of the OTR were found. Regarding the extracellular side, two residues at the CB1R and five residues at the OTR were found to be important. Of these residues, E148 and K149 are located at ECL2 of the CB1R and the five residues W264, N270, A271, P272, and E274 are located at ECL3 of the OTR. At the intracellular side of the receptor complex, residues R42 and C43 are located at ICL1, and residues T119 and R120 are located

at ICL2 of the CB1R. At the OTR, residues L305 and V306 were found at H8, and residues G301, L302, F309, and L310 are located at the C-terminus.

The interactions between TMHs of the receptors were as usually found to be between TMH2 of the CB1R and TMH1 of the OTR, TMH3 of the CB1R, and TMH7 of the OTR and between TMH4 of the CB1R and TMH6/7 of the OTR.

In **Table 17**, the residues are allocated to their localization at the receptors by visually inspecting the dimeric receptor complex.

Table 17. Residues identified by the alanine scan at the receptor.

Receptor	Position	Residues
CB1R	ICL1	R42, C43
	TMH2	L58, V61, I62, Y65
	TMH3	N78, F82
	ICL2	T119, R120
	TMH4	P121, K122, V124, V125, A126, C128, L129, W131, T132, I133, I135, V136, A138, V139, L140, L142, L143, G144
	ECL2	E148, K149
OTR	TMH1	A7, L8, V11, V15
	TMH6	M243, I246, L249, A250, V253, C254, T256, P257, F260, V261, W264
	ECL3	N270, A271, P272, E274
	TMH7	S276, A277, I280, V281, L283, L284, L287, N288, C290, C291, W294, I295, M297, L298, T300
	C-terminus	G301, L302, F309, L310
	H8	L305, V306

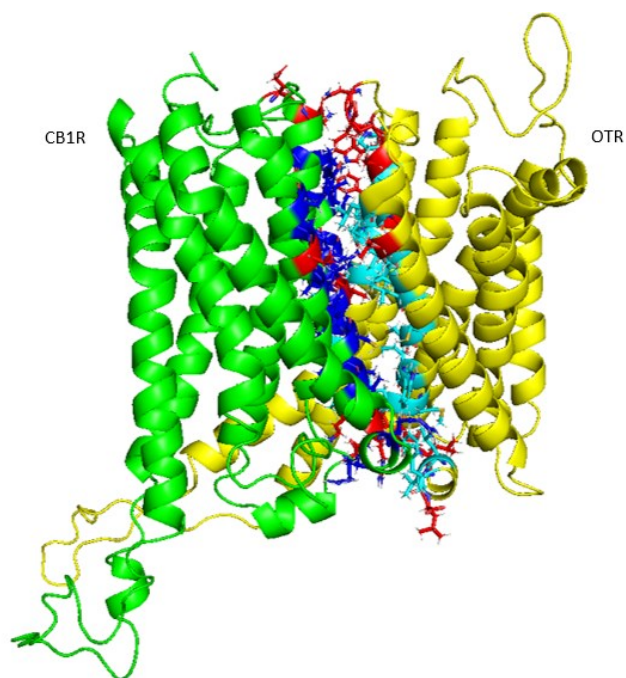


Figure 74. The view of the interface of CB1R (green) and OTR (yellow) after MD simulation.

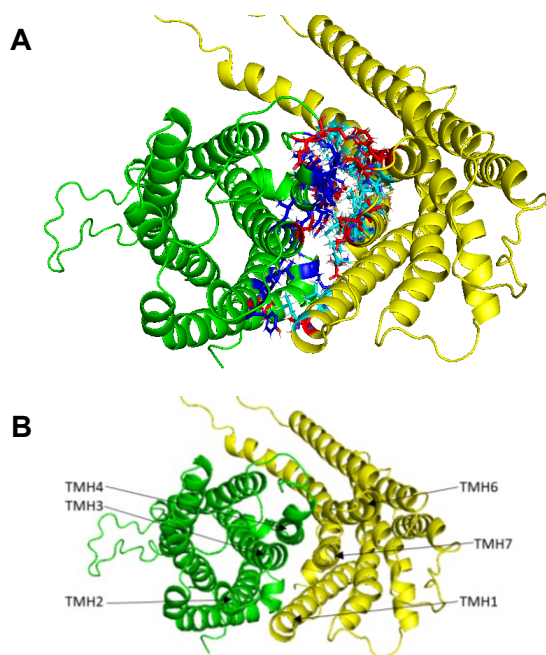


Figure 75. The top-down view of the interface of CB1R (green) and OTR (yellow) after MD simulation. **A:** Interface with highlighted residues **B:** Overview of the TMHs at the interface.

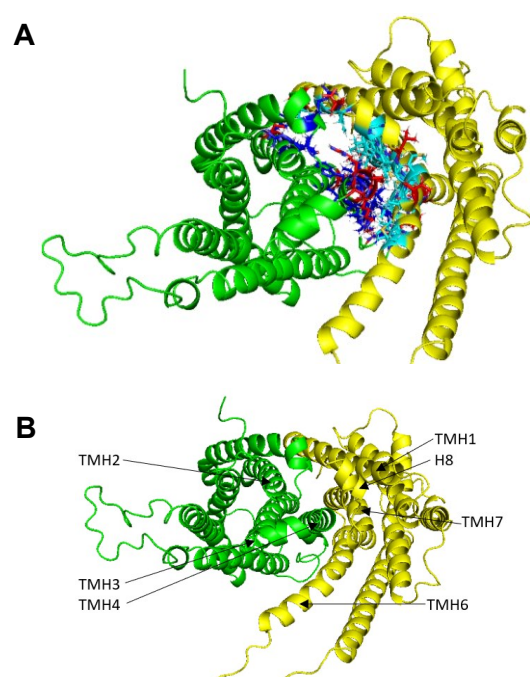


Figure 76. The bottom-up view of the interface of CB1R (green) and OTR (yellow) after MD simulation. **A:** Interface with highlighted residues **B:** Overview of the TMHs at the interface.

Five hydrogen bonds were found at the extracellular and intracellular side of the receptor dimer: Two at the extracellular side, one between residues Y65 at TMH2 of the CB1R and N5 at the N-terminus of the OTR (**Figure 77**) and one between residue K149 at ECL2 of the CB1R and residue D268 at ECL3 of the OTR (**Figure 78**). Intracellularly, three hydrogen bonds were found. Two between residues R39 at ICL1 of CB1R and L310 at the C-terminus of OTR and one between residues Y106 at TMH3 of the CB1R and K235 at TMH6 of the OTR (**Figure 79**).

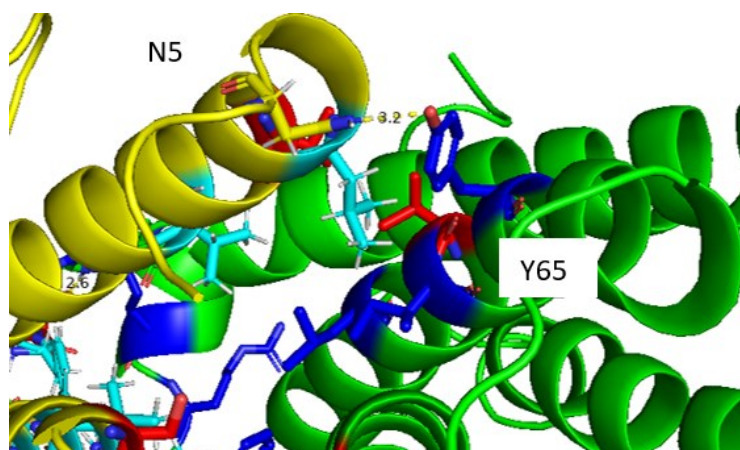


Figure 77. Hydrogen bond between residues Y65 at TMH2 of the CB1R and N5 at the N-terminus of the OTR.

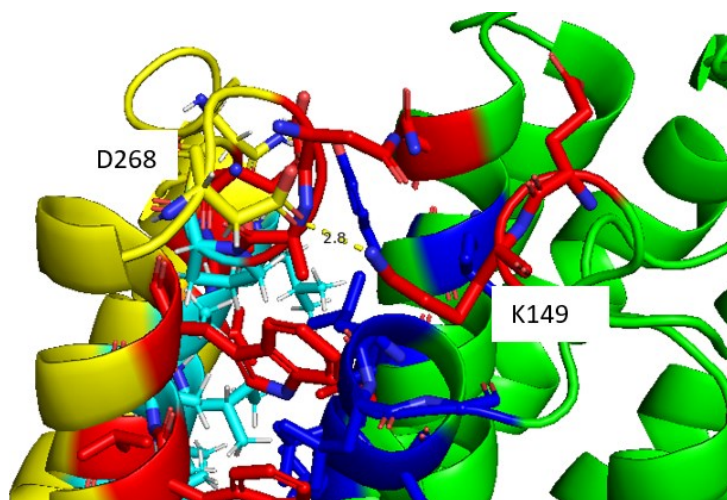


Figure 78. Hydrogen bond between residues K149 at ECL2 of the CB1R and residue D268 at ECL3 of the OTR.

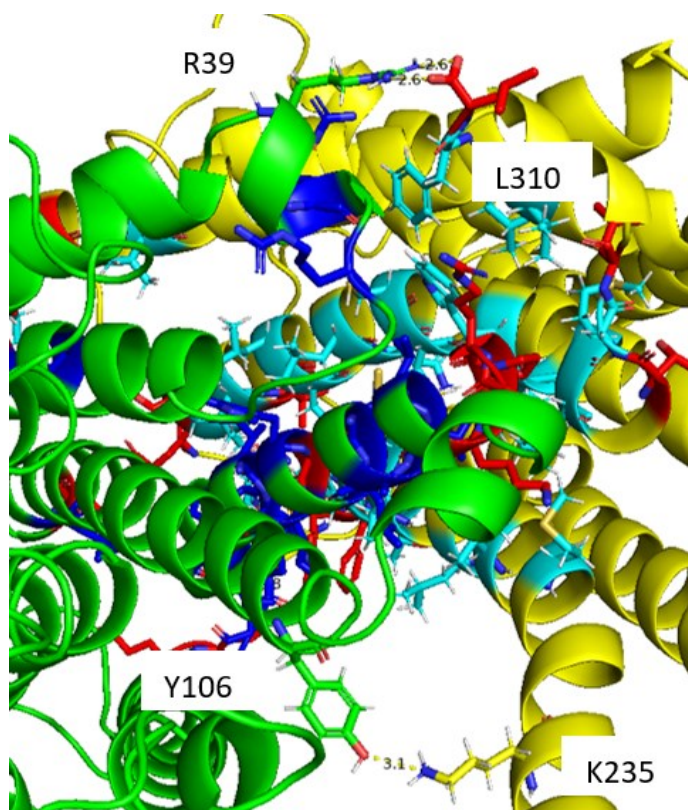


Figure 79. Hydrogen bond between residue R39 at ICL1 of CB1R and residue L310 at the C-terminus of OTR and between residue Y106 at TMH3 of the CB1R and residue K235 at TMH6 of the OTR.

Interface 7:

A total of 81 residues were found to be important for interactions. 38 important residues were identified at TMH2/3/4, ICL1, ICL2, ECL2, ICL3, and H8 of the CB1R, and 43 important residues at TMH1/6/7, N-terminus, ECL3, ICL3, ECL3, C-terminus, and H8 of the OTR.

The following important residues at the extracellular loops and intracellular loops and H8 of both receptors and at the N-terminus and the C-terminus of the OTR were found. At the intracellular side of the receptor complex, nine important residues at the CB1R and eight important residues at the OTR were found by the alanine scan. The residues found at the CB1R are residues R39, R42, and C43 at ICL1, residues A113, I117, and T119 at ILC2, residue S191 at ICL3, and residues V193 and R194 at H8. The residues found at the OTR are residues D218, G219, and G220 at ICL3, residues G301 and L310 at the C-terminus, and residues L305, V306, and F309 at H8. It has to be pointed out that residue S191 at ICL3, and residues V193 and R194 at H8 of the CB1R were seen to be important only at this interface. The interaction of residue S191 at ICL3 of the CB1R and residues D218, G219, and G220 at ICL3 of the OTR seemed to be caused by the high flexibility of ICL3 at the OTR which leads to their proximity.

At the extracellular side of the receptor complex, the three residues N146, E148, and K149 were found at ECL2 of the CB1R and at the extracellular side of the OTR, residue N5 was found at the N-terminus and residues A271, P272, K273, E274, and S276 were found at ECL3.

The interactions between TMHs of the receptors were found to be between TMH2 of the CB1R and TMH1 of the OTR, TMH3 of the CB1R, and TMH7 of the OTR and between TMH4 of the CB1R and TMH6/7 of the OTR.

In **Table 18**, the residues are allocated to their localization at the receptors by visually inspecting the dimeric receptor complex.

Table 18. Residues identified by the alanine scan at the receptor.

Receptor	Position	Residues
CB1R	ICL1	R39, R42, C43
	TMH2	L58, V61, I62, Y65
	TMH3	N78, V79, F82, K83
	ICL2	A113, I117, T119
	TMH4	R120, P121, K122, V124, V125, A126, C128, L129, T132, I133, I135, V136, A138, V139, L140, L142, L143, G144
	ECL2	N146, E148, K149
	ICL3	S191
	H8	V193, R194
OTR	N-terminus	N5
	TMH1	A7, L8, V11, V15, G26
	ICL3	D218, G219, G220
	TMH6	L232, K235, R239, M243, I246, I247, L249, A250, V253, C254, P257, V261
	ECL3	A271, P272, K273, E274, S276
	TMH7	A277, I280, V281, L283, L284, L287, C290, C291, W294, I295, M297, L298
	C-terminus	G301, L310
	H8	L305, V306, F309

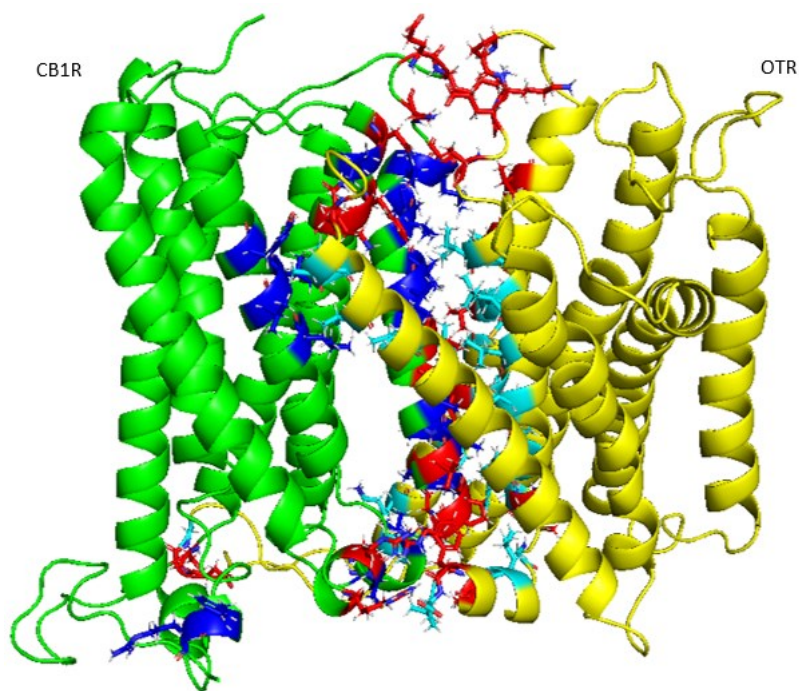


Figure 80. The view of the interface of CB1R (green) and OTR (yellow) after MD simulation.

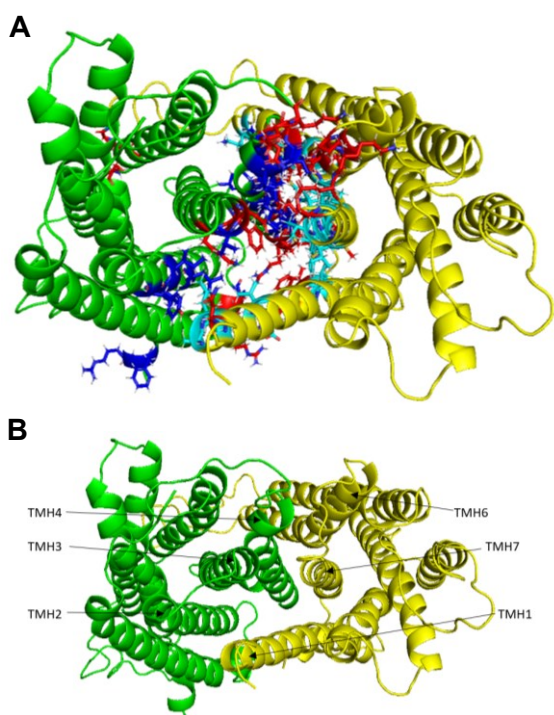


Figure 81. The top-down view of the interface of CB1R (green) and OTR (yellow) after MD simulation. **A:** Interface with highlighted residues **B:** Overview of the TMHs at the interface.

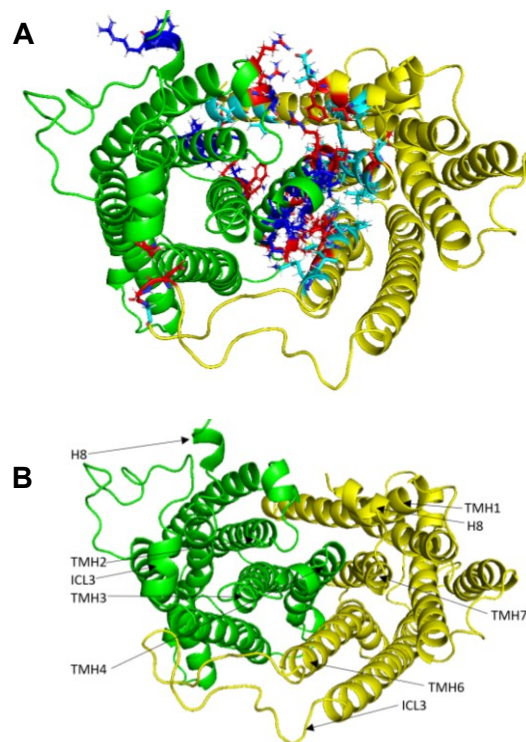


Figure 82. The bottom-up view of the interface of CB1R (green) and OTR (yellow) after MD simulation. **A:** Interface with highlighted residues **B:** Overview of the TMHs at the interface.

Seven hydrogen bonds were found between the CB1R and OTR, four at the extracellular side, one at the transmembrane region of the interface, and three at the intracellular side of the dimeric receptor complex. At the extracellular side of the dimeric receptor complex, two hydrogen bonds are located between residue D75 at ECL1 of the CB1R and residue R6 at the N-terminus of the OTR (**Figure 83**), and two hydrogen bonds are located between residue K149 at ECL2 of the CB1R and residues A269 and A271 at ECL2 of the OTR (**Figure 84**). One more hydrogen bond between residue K83 at TMH3 of the CB1R and residue E12 at TMH1 of the OTR was found to be located a little more towards the transmembrane region of the interface (**Figure 85**). At the intracellular side, residue R116 at the ICL2 of the CB1R and residue R239 at TMH6 of the OTR (**Figure 86**) form one hydrogen bond, and two more hydrogen bonds could be found between residue R194 at ICL3 of the CB1R and residue D218 at ICL3 of the OTR (**Figure 87**).

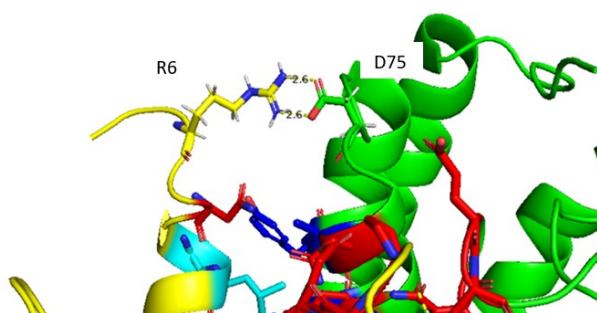


Figure 83. Hydrogen bonds between D75 at ECL1 of the CB1R and residue R6 at the N-terminus of the OTR.

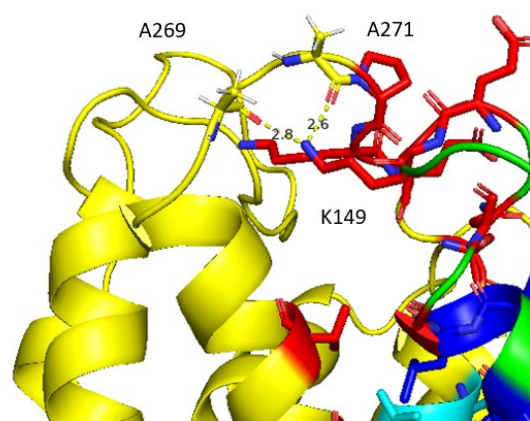


Figure 84. Hydrogen bonds between residues K149 at ECL2 of the CB1R and A269 and A271 at ECL2 of the OTR.

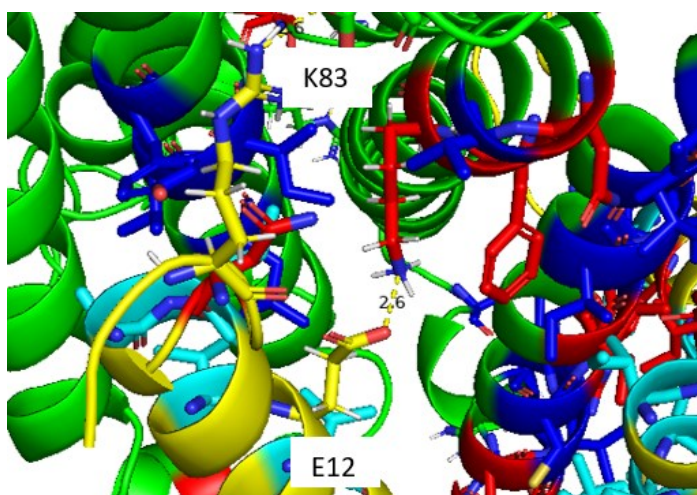


Figure 85. Hydrogen bond between residue K83 at TMH3 of the CB1R and residue E12 at TMH1 of the OTR.

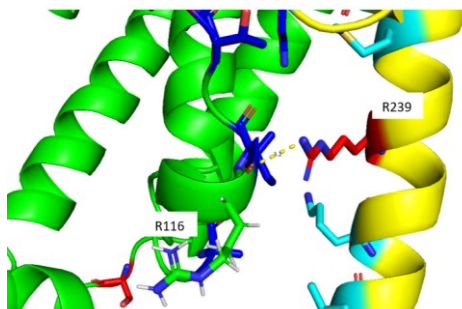


Figure 86. Hydrogen bond between residue R116 at ICL2 of the CB1R and residue R239 at TMH6 of the OTR.

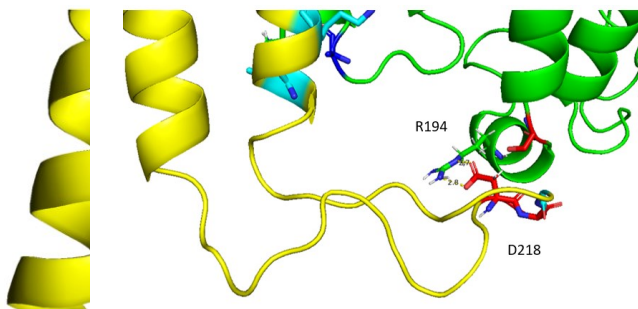


Figure 87. Hydrogen bond between residue R194 at ICL3 of the CB1R and residue D218 at ICL3 of the OTR.

Interface 8:

At interface 8 a total of 61 residues were found to be important for interactions. 29 important residues at TMH1/2/3/4 and ICL2 of the CB1R, and 32 important residues at TMH1/6/7, N-terminus, C-terminus, and H8 of the OTR were found.

Regarding the extracellular loops only N5 at the N-terminus of the OTR was found to be important. At the intracellular loops of both receptors and the C-terminus, and H8 of the OTR important residues were found. At the intracellular loops, four important residues were found by the alanine scan. These residues are residue T119 at ICL2 of the CB1R, residues G301 and F309 at the C-terminus of the OTR, and residue V306 at H8 of the OTR.

The interactions between TMHs of the receptors were found to be between TMH2 of the CB1R and TMH1 of the OTR, TMH3 of the CB1R, and TMH7 of the OTR and between TMH4 of the CB1R and TMH6/7 of the OTR. A characteristic of this interface is that residue C43 at TMH1 of the CB1R in part of the interface as it was shown to interact with TMH1 of the OTR.

In **Table 19**, the residues are allocated to their localization at the receptors by visually inspecting the dimeric receptor complex.

Table 19. Residues identified by the alanine scan at the receptor.

Receptor	Position	Residues
CB1R	TMH1	C43
	TMH2	V54, L58, V61, I62, Y65, S66
	TMH3	N78, V79, F82, K83, G86
	ICL2	T119
	TMH4	R120, P121, K122, V124, V125, C128, L129, W131, T132, I133, I135, V136, V139, L140, L142, L143
OTR	N-terminus	N5
	TMH1	A7, L8, V11, E12, V15, L18,
	TMH6	246, L249, A250, V253, C254, P257, F260, V261
	TMH7	S276, A277, I280, V281, L283, L284, L287, N288, C290, C291, W294, I295, M297, L298
	C-terminus	G301, F309
	H8	V306

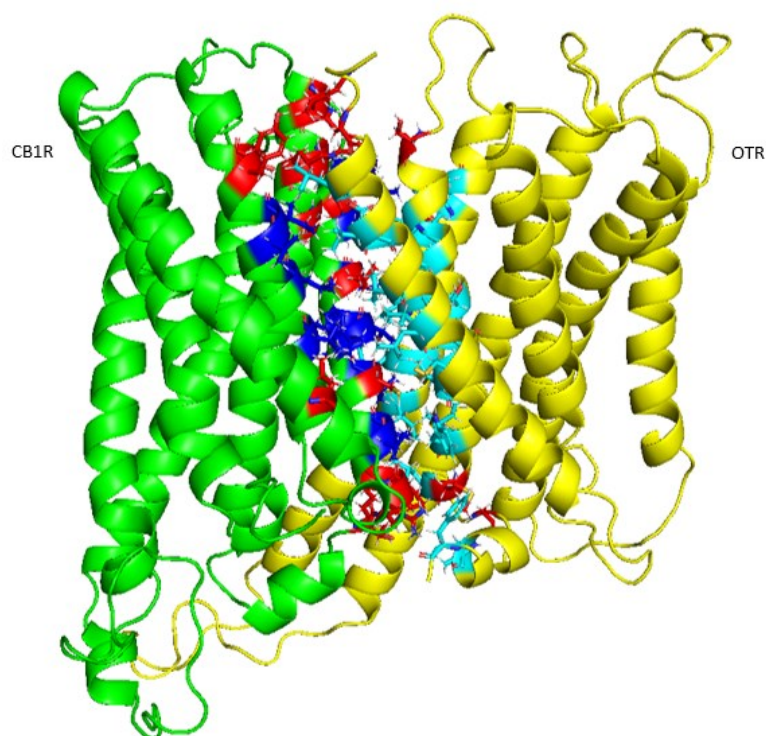


Figure 88. The view of the interface of CB1R (green) and OTR (yellow) after MD simulation.

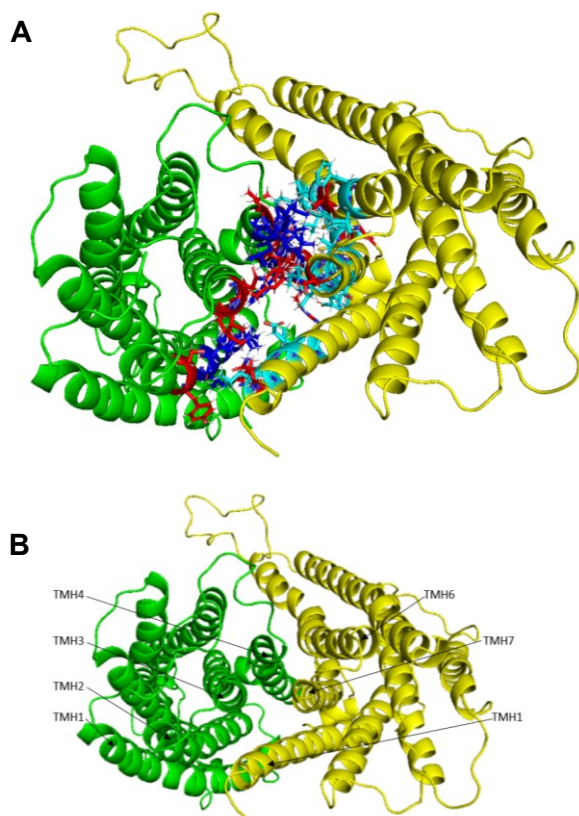


Figure 89. The top-down view of the interface of CB1R (green) and OTR (yellow) after MD simulation. **A:** Interface with highlighted residues **B:** Overview of the TMHs at the interface.

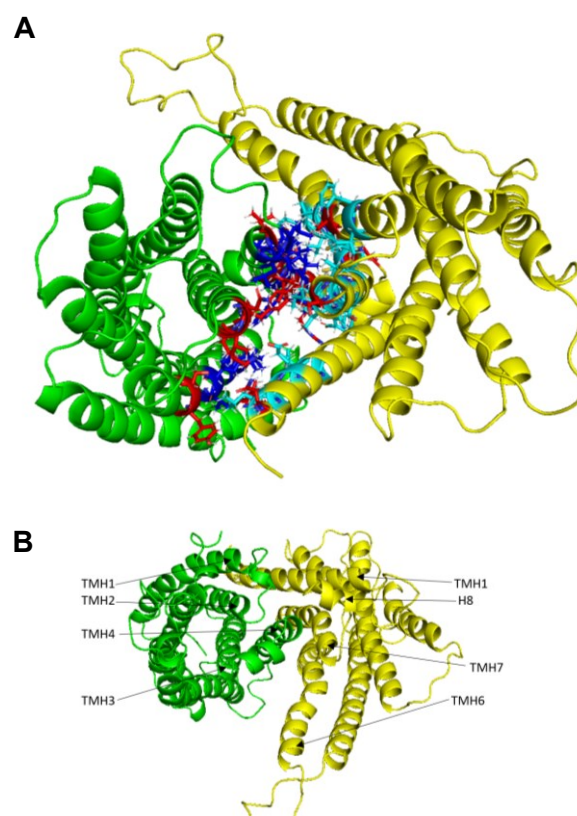


Figure 90. The bottom-up view of the interface of CB1R (green) and OTR (yellow) after MD simulation. **A:** Interface with highlighted residues **B:** Overview of the TMHs at the interface.

Only two hydrogen bonds were found between the CB1R and OTR. One at the extracellular side of the dimeric complex and one at the interface between TMHs. The first one was found to be more towards the extracellular side of the receptor complex, between residue K74 at ECL1 of the CB1R and residue L8 at the N-terminus of the OTR receptor (**Figure 91**). The second one is located at the transmembrane region of the dimeric complex, between residue T132 at TMH4 of the CB1R and residue L249 at TMH6 of the OTR (**Figure 92**).

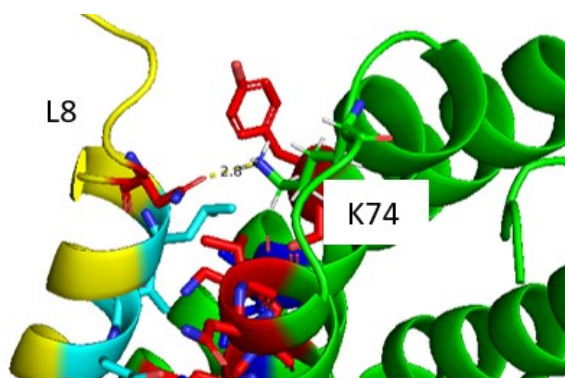


Figure 91. Hydrogen bond between residue K74 at ECL1 of the CB1R and residue L8 at the N-terminus of the OTR.

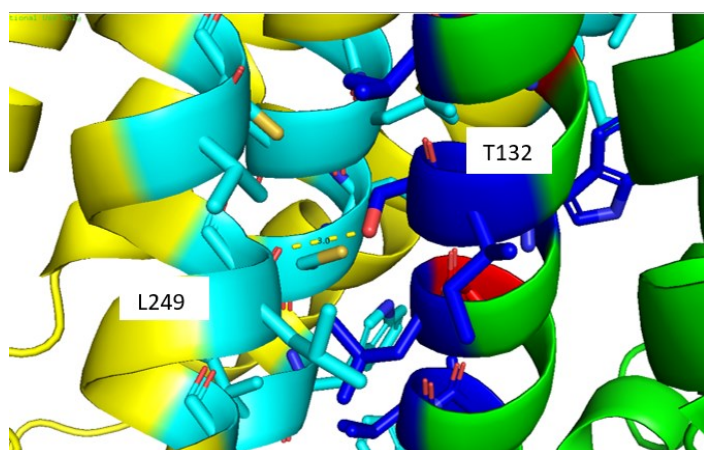


Figure 92. Hydrogen bond between residue T132 at TMH4 of the CB1R and residue L249 at TMH6 of the OTR.

Interface 9:

At this interface, 73 residues were found to be important for interactions. 35 of them were located at TMH2/3/4, ICL1, ICL2, ECL1, and ECL2 of the CB1R, and 38 residues were located at TMH1/6/7, N-terminus, ECL3, C-terminus, and H8 of the OTR.

Important residues at the extracellular loops and intracellular loops of both receptors and at the N-terminus, C-terminus, and H8 of the OTR were found. Regarding the extracellular loops of the CB1R receptor, residues F72 and S76 at ECL1, and E148 at ECL2 were shown to be important and at the extracellular loops of the OTR residues P1, P2, A7, and L8 at the N-terminus and residues P272 and E274 at ECL3 were found to be important. At the intracellular loops, residues R39 and C43 at ICL1, as well as residues T119 and R120 at ICL2 of the CB1R were identified to be important by the alanine scan and at the OTR's intracellular part, residues G301 and L310 at the C-terminus, and residues L305 and V306 at H8 are important for interactions.

The interactions between TMHs of the receptors were found to be as usually between TMH2 of the CB1R and TMH1 of the OTR, TMH3 of the CB1R, and TMH7 of the OTR and between TMH4 of the CB1R and TMH6/7 of the OTR.

In **Table 20**, the residues are allocated to their localization at the receptors by visually inspecting the dimeric receptor complex.

Table 20. Residues identified by the alanine scan at the receptor.

Receptor	Position	Residues
CB1R	ICL1	R39, C43
	TMH2	V54, L58, V61, I62, Y65, I68, D69
	ECL1	F72, S76
	TMH3	R77, N78, L81, F82, K83
	ICL2	T119, R120
	TMH4	P121, K122, V124, V125, C128, L129, W131, T132, I133, I135, V136, V139, L140, L142, L143, G144
	ECL2	E148
OTR	N-terminus	P1, P2, A7, L8
	TMH1	V11, V15, L18, L22
	TMH6	I246, L249, A250, V253, C254, P257, F260, V261, W264
	ECL3	P272, E274
	TMH7	A275, S276, A277, I280, V281, L283, L284, L287, N288, C290, C291, W294, I295, M297, L298
	C-terminus	G301, L310
	H8	L305, V306

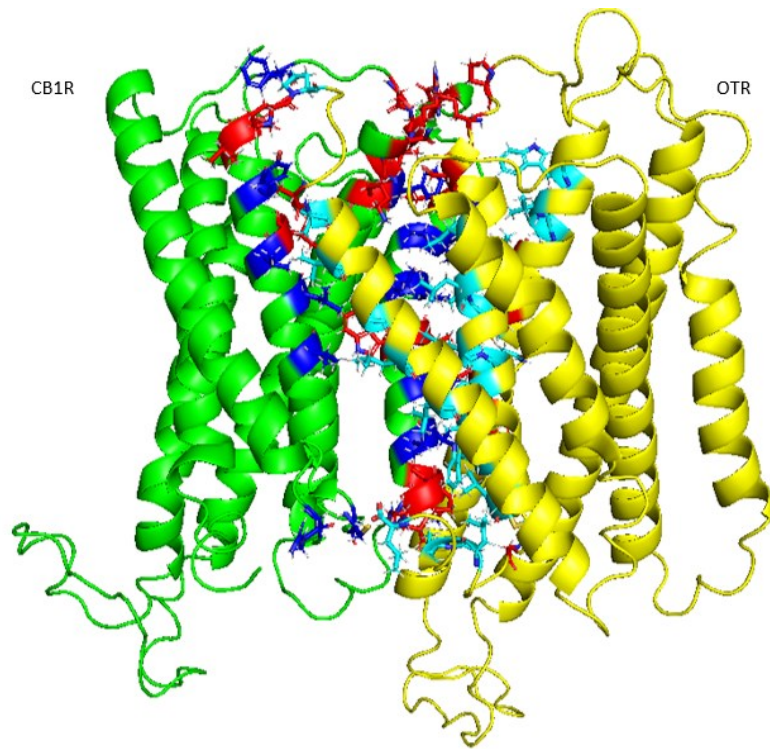


Figure 93. The view of the interface of CB1R (green) and OTR (yellow) after MD simulation.

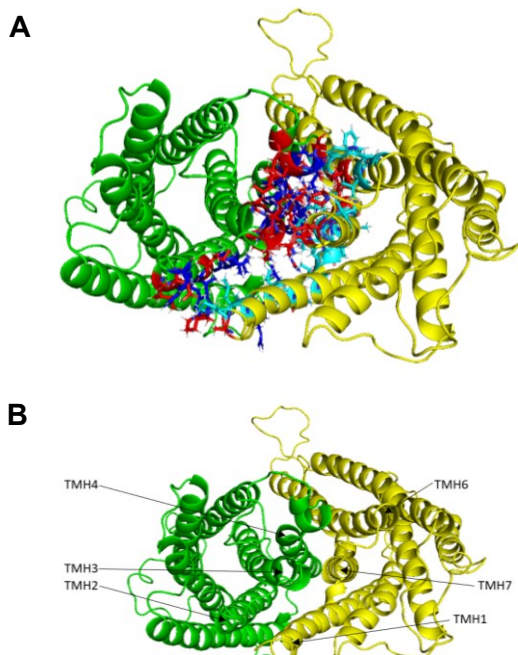


Figure 94. The top-down view of the interface of CB1R (green) and OTR (yellow) after MD simulation. **A:** Interface with highlighted residues **B:** Overview of the TMHs at the interface.

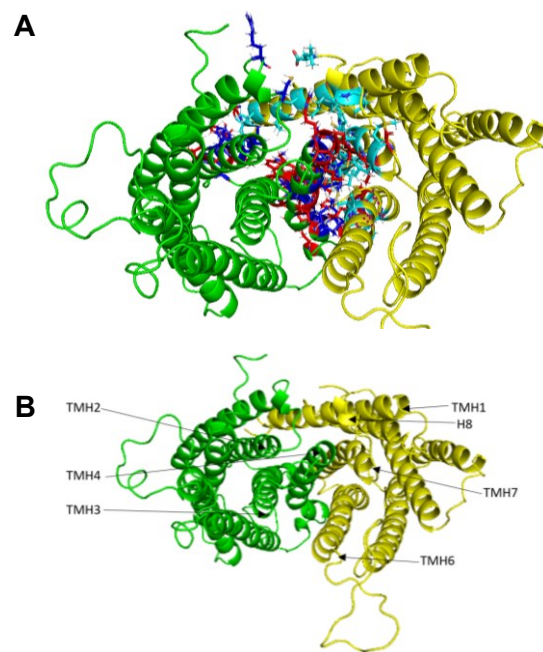


Figure 95. The bottom-up view of the interface of CB1R (green) and OTR (yellow) after MD simulation. **A:** Interface with highlighted residues **B:** Overview of the TMHs at the interface.

All in all, eleven hydrogen bonds were found between the CB1R and OTR. Nine of them are at the extracellular side and two are at the intracellular side of the dimeric complex. By inspecting the extracellular side, two hydrogen bonds between residue R77 at TMH3 of the CB1R and residue E274 at ECL3 of the OTR, one hydrogen bond between the neighboured residue S76 at ECL2 of the CB1R and the same residue E274 at ECL3 of the OTR, and two hydrogen bonds between residue N78 at TMH3 of the CB1R and residue S276 at TMH7 of the OTR were found (**Figure 96**). Further, two hydrogen bonds were found at the extracellular side between residue D69 at TMH2 of the CB1R and residue P1 at the N-terminus of the OTR and two more hydrogen bonds were found extracellularly between K83 at TMH3 of the CB1R and E12 at TMH1 of the OTR (**Figure 97**).

The two hydrogen bonds located at the intracellular side of the dimeric complex formed between residue R41 at ICL1 of the CB1R and residue L310 at the C-terminus of the OTR. (**Figure 98**).

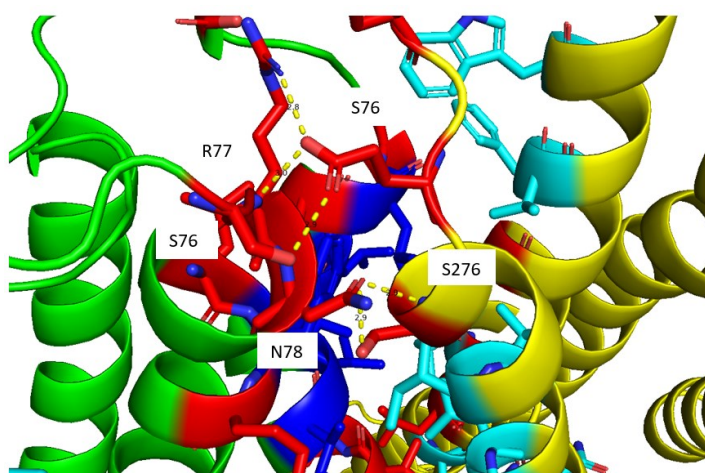


Figure 96. Hydrogen bonds between residue R77 at TMH3 of the CB1R and residue E274 at ECL3 of the OTR, between residue S76 at ECL2 of the CB1R, residue E274 at ECL3 of the OTR and between residue N78 at TMH3 of the CB1R and residue S276 at TMH7 of the OTR.

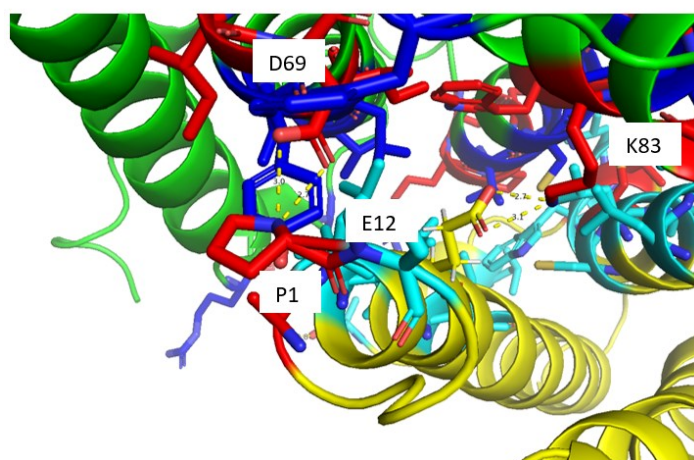


Figure 97. Hydrogen bonds between residue D69 at TMH2 of the CB1R and residue P1 at the N-terminus of the OTR and between residue K83 at TMH3 of the CB1R and residue E12 at TMH1 of the OTR.

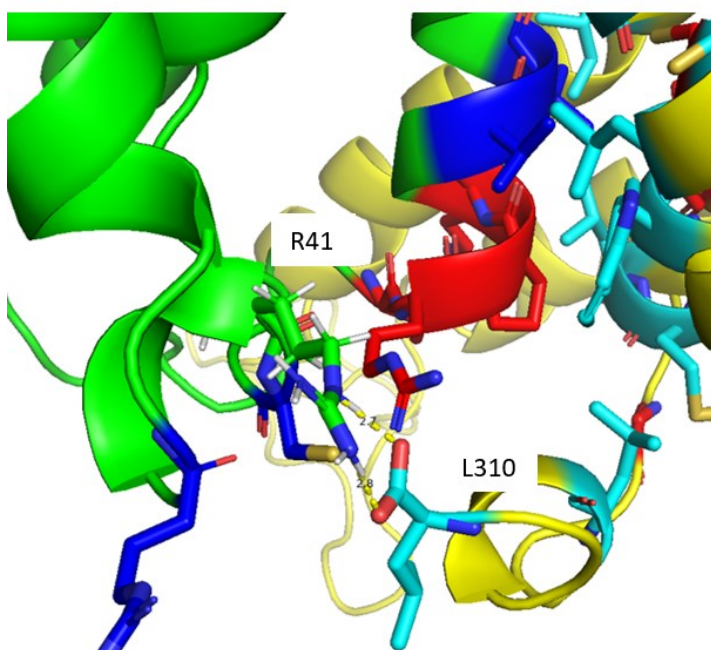


Figure 98. Hydrogen bonds between residue R41 at ICL1 of the CB1R and residue L310 at the C-terminus of the OTR.

Interface 10:

At interface 10, 78 residues were found to be important for interactions. 39 of them are located at TMH2/3/4 and ICL1, ICL2, ECL1, and ECL2 of the CB1R, and 39 residues are located at TMH1/6/7, N-terminus, ECL3, C-terminus, and H8 of the OTR.

Important residues at the extracellular loops and intracellular loops of both receptors and at the N-terminus, C-terminus, and H8 of the OTR were found. At the CB1R, twelve residues and at the OTR ten residues were found to be important. By elucidating the extracellular loops first, regarding the CB1R, residues R73 and F82 at ECL1 and residues L143, G144, N146, C147, E148, and K149 at ECL2 are marked as important and regarding the OTR, residues P2, R3, and N5 at the N-terminus as well as residues N270, A271, P272, and S276 at ECL3 are important. At the intracellular loops, residues R42 and C43 at ICL1, residues L112 and T119 at ICL2 are important residues at the CB1R and by examining the OTR receptor, residues F303 and Q307 at H8 and L310 at the C-terminus are important.

Interactions between TMHs of the receptors were found to be as usually between TMH2 of the CB1R and TMH1 of the OTR, TMH3 of the CB1R, and TMH7 of the OTR and between TMH4 of the CB1R and TMH6/7 of the OTR.

In the following **Table 21**, the residues are allocated to their localization at the receptors by visually inspecting the dimeric receptor complex.

Table 21. Residues identified by the alanine scan at the receptor.

Receptor	Position	Residues
CB1R	ICL1	R42, C43
	TMH2	L58, V61, I62, Y65, S66, I68, D69, F72
	ECL1	R73, F82
	TMH3	K83, G85, G86, A89
	ICL2	L112, T119
	TMH4	P121, K122, V124, V125, A126, C128, L129, W131, T132, I133, I135, V136, A138, V139, L142
	ECL2	L143, G144, N146, C147, E148, K149
OTR	N-terminus	P2, R3, N5
	TMH1	A7, L8, V11, E12, V15
	TMH6	K235, K242, M243, I246, I247, A250, V253, C254, P257, V261, D268
	ECL3	N270, A271, P272, S276
	TMH7	A277, I280, V281, L283, L284, L287, N288, C290, C291, W294, I295, M297, L298
	C-terminus	L310
	H8	F303, Q307

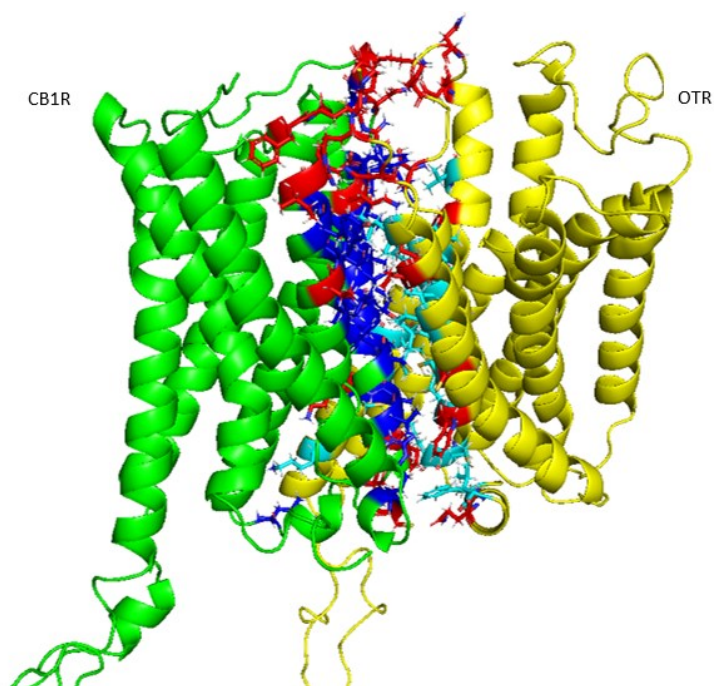


Figure 99. The view of the interface of CB1R (green) and OTR (yellow) after MD simulation.

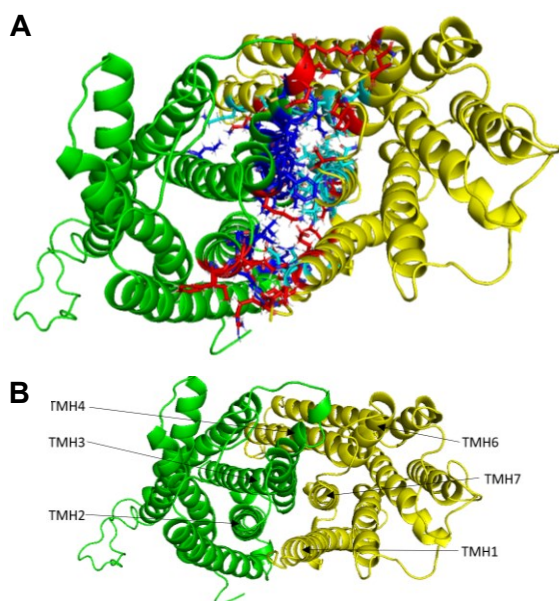


Figure 100. The top-down view of the interface of CB1R (green) and OTR (yellow) after MD simulation. **A:** Interface with highlighted residues **B:** Overview of the TMHs at the interface.

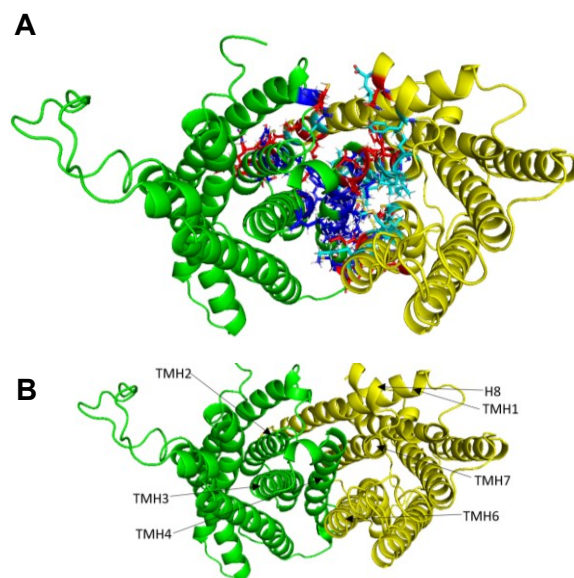


Figure 101. The bottom-up view of the interface of CB1R (green) and OTR (yellow) after MD simulation. **A:** Interface with highlighted residues **B:** Overview of the TMHs at the interface.

A total of nine hydrogen bonds were found between the CB1R and OTR. Seven of them are located exclusively at the intracellular side of the dimeric complex and two hydrogen bonds are located more towards the transmembrane region of the receptor.

Interestingly, the five hydrogen bonds depicted in **Figure 102** formed between four residues locate at ECL2 of the CB1R and ECL3/TMH6 at the OTR. One hydrogen bond between residues K149 at ECL2 of the CB1R and A269 at ECL3 of the OTR and two between the residues K149 at ECL2 of the CB1R and D268 at TMH6 of the OTR. Further, one between residues N146 at ECL2 of the CB1R and D268 at TMH6 of the OTR and one between N146 at ECL2 of the CB1R and A271 at ECL3 of the OTR. One more hydrogen bond at the intercellular side was found between residue R73 at the ECL1 of the CB1R and residue N6 at the N-terminus of the OTR and one between the neighbouring residue D69 at ECL1 and again residue N6 at the N-terminus of the OTR. More towards the transmembrane region of the interface, two hydrogen bonds between residue K83 at TMH3 of the CB1R and residue E12 at TMH1 of the OTR were observed (**Figure 103**).

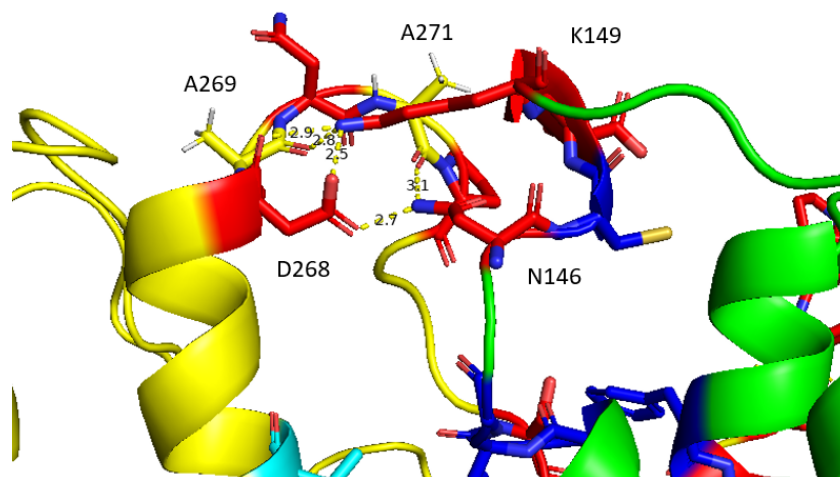


Figure 102. Hydrogen bonds between residue K149 at ECL2 of the CB1R and residue A269 at ECL3 of the OTR, residue K149 at ECL2 of the CB1R and residue D268 at TMH6 of the OTR, residue N146 at ECL2 of the CB1R and residue D268 at TMH6 of the OTR and between residue N146 at ECL2 of the CB1R and residue A271 at ECL3 of the OTR.

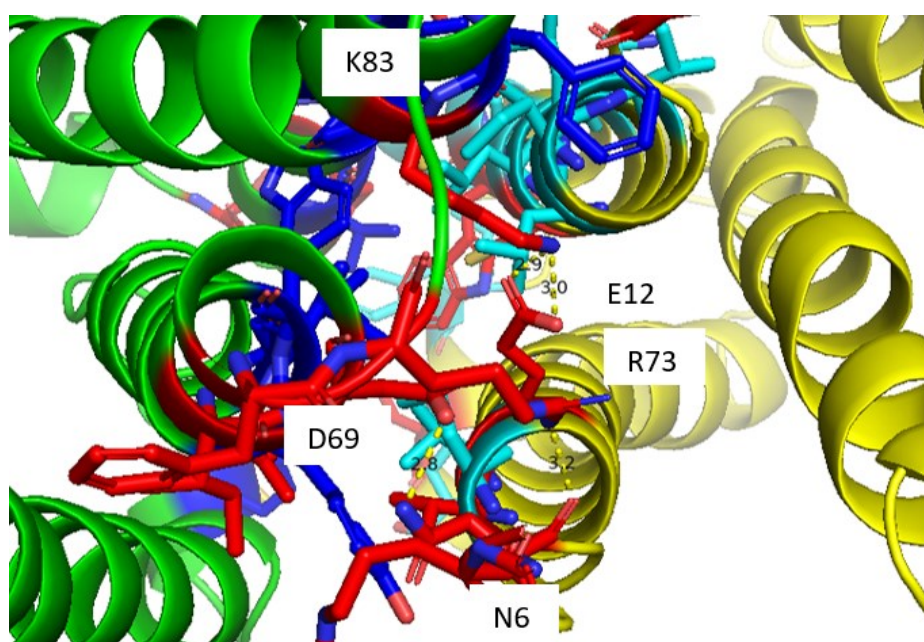


Figure 103. Hydrogen bonds between residue R73 at ECL1 of the CB1R and residue N6 at the N-terminus of the OTR and residue D69 at ECL1 and residue N6 at the N-terminus of the OTR and between residue K83 at TMH3 of the CB1R and residue E12 at TMH1 of the OTR.

Interface 11:

At this interface, 64 residues were found to be important by the alanine scan. 29 of them are located at TMH2/3/4, ICL1, ECL1, and ECL2 of the CB1R, and 35 residues are located at TMH1/6/7, N-terminus, C-terminus, and H8 of the OTR.

Important residues at the extracellular loops and intracellular loops of both receptors and at the N-terminus, C-terminus, and H8 of the OTR were found. Of those, five important residues at the CB1R and three important residues at the OTR were found to be located at extracellular loops and two important residues of the CB1R and five important residues at the OTR are located at intracellular loops. The eight residues located at the extracellular loops are residues R73, K74, N78, and V79 at ECL1 of the CB1R and G144 at ECL2 of the CB1R as well as residues P2, R3, and N5 at the N-terminus of the OTR. The seven important residues at the intracellular loops are residues C43 and S46 at ICL1 of the CB1R and residues G301, F309, and L310 at C-terminus, and residues L305 and V306 at H8 of the OTR.

Interactions between TMHs of the receptors were found to be between TMH2 of the CB1R and TMH1 of the OTR, TMH3 of the CB1R, and TMH7 of the OTR and between TMH4 of the CB1R and TMH6/7 of the OTR.

In **Table 22**, the residues are allocated to their localization at the receptors by visually inspecting the dimeric receptor complex.

Table 22. Residues identified by the alanine scan allocated at the receptor.

Receptor	Position	Residues
CB1R	ICL1	C43, S46
	TMH2	L58, V61, I62, Y65, D69
	ECL1	R73, K74, N78, V79
	TMH3	F82, K83
	TMH4	R120, P121, K122, V124, V125, C128, L129, W131, T132, I133, I135, V136, V139, L142, L143
	ECL2	G144
OTR	N-terminus	P2, R3, N5
	TMH1	A7, L8, V11, E12, V15
	TMH6	I246, L249, A250, V253, C254, P257, F260, V261, W264
	TMH7	S276, A277, I280, L283, L284, L287, N288, C290, C291, W294, I295, M297, L298
	C-terminus	G301, F309, L310
	H8	L305, V306

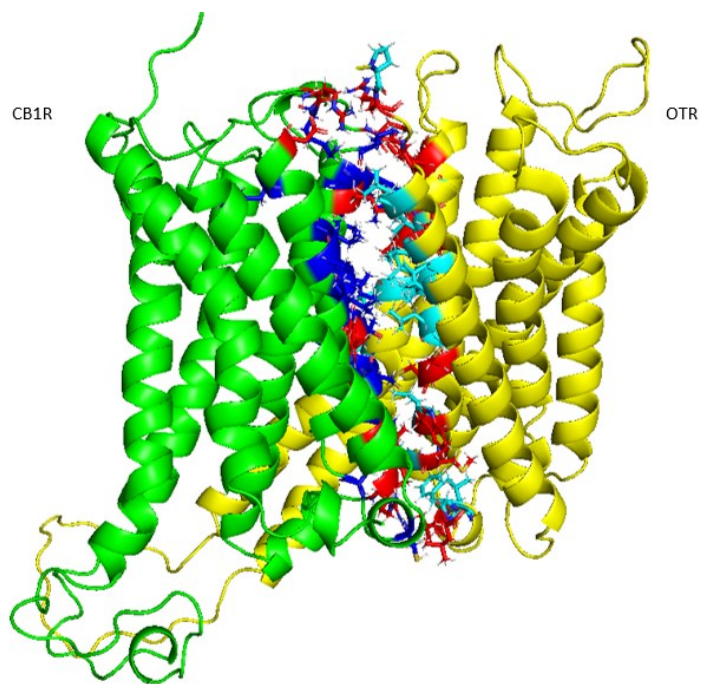


Figure 104. The view of the interface of CB1R (green) and OTR (yellow) after MD simulation.

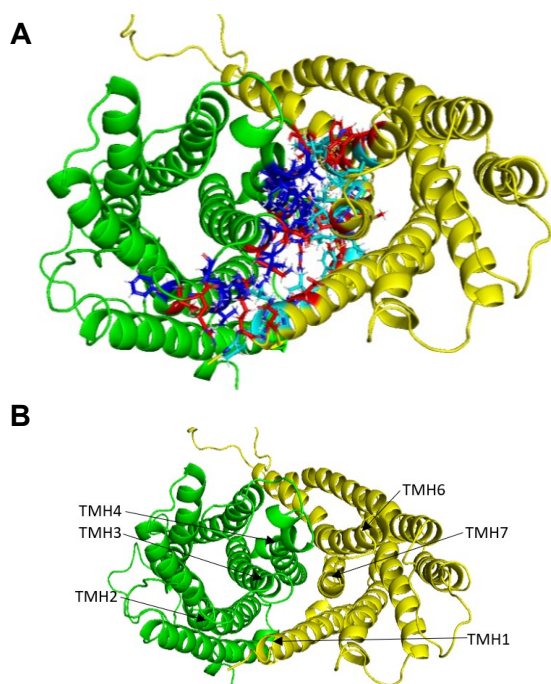


Figure 105. The top-down view of the interface of CB1R (green) and OTR (yellow) after MD simulation. **A:** Interface with highlighted residues **B:** Overview of the TMHs at the interface.

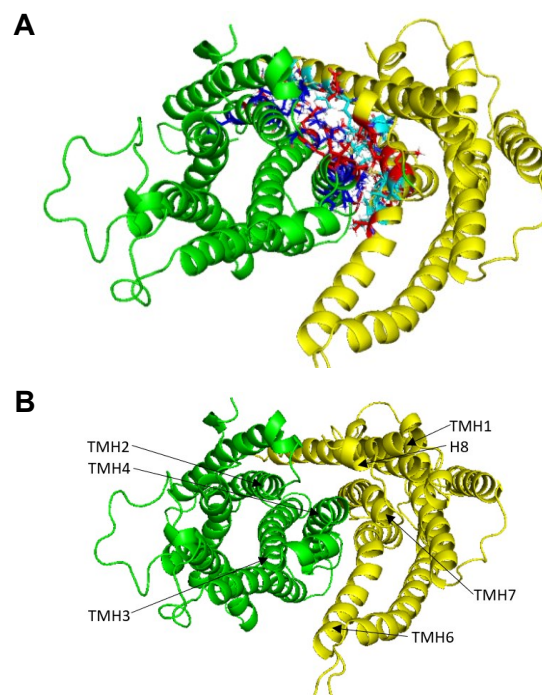


Figure 106. The bottom-up view of the interface of CB1R (green) and OTR (yellow) after MD simulation. **A:** Interface with highlighted residues **B:** Overview of the TMHs at the interface.

Five hydrogen bonds were found between the CB1R and OTR. Three of them are located at the extracellular side and one hydrogen bond is located at the intracellular side of the protein complex. Further, one hydrogen bond is located more towards the transmembrane region of the dimeric complex.

Regarding the hydrogen bonds located at the extracellular side of the complex, one is located between residue R73 at ECL1 of the CB1R and residue R3 at the N-terminus of the OTR and one between R73 at ECL1 of the CB1R and R1 at the N-terminus of the OTR (**Figure 107**).

The hydrogen bond located more towards the transmembrane region of the interface is between residue V79 at ECL1 of the CB1R and residue E12 at TMH1 of the OTR (**Figure 108**) and the hydrogen bond located at the intracellular side formed between residue R42 at ICL1 of the CB1R and residue L310 at the C-terminus of the OTR (**Figure 109**).

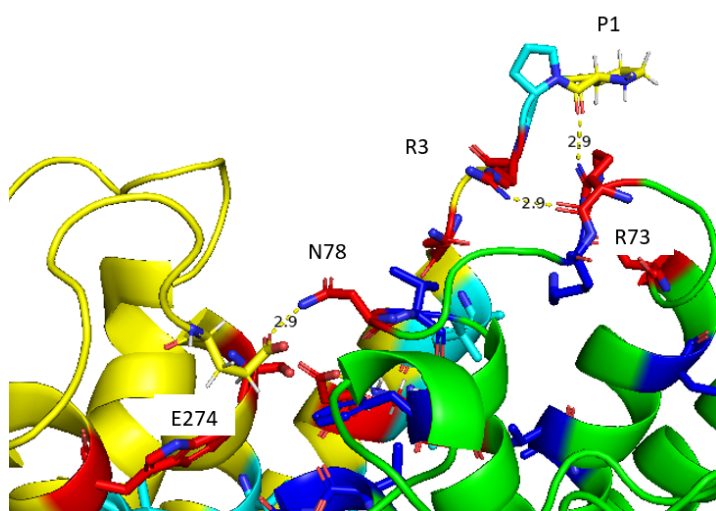


Figure 107. Hydrogen bonds between residue N78 at ECL1 of the CB1R and E274 at TMH3 of the OTR, residue R73 at ECL1 of the CB1R and residue R3 at the N-terminus of the OTR and residue R73 at ECL1 of the CB1R and residue R1 at the N-terminus of the OTR.

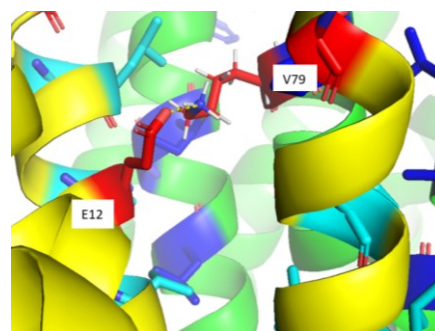


Figure 108. Hydrogen bond between residue V79 at ECL1 of the CB1R and residue E12 at TMH1 of the OTR.

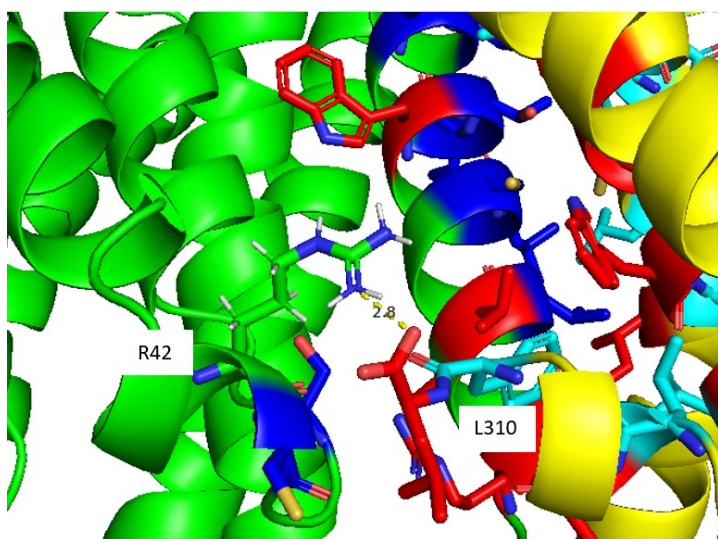


Figure 109. Hydrogen bond between residue R42 at ICL1 of the CB1R and residue L310 at the C-terminus of the OTR.

Interface 12:

At interface 12, 78 residues were found to be important for interactions. 38 of them are located at TMH2/3/4, ICL1, ICL2 and ECL2 of the CB1R, and 40 residues are located at TMH1/6/7, N-terminus, ECL3, C-terminus, and H8 of the OTR.

Important residues at the extracellular loops and intracellular loops of both receptors and at the N-terminus, C-terminus, and H8 of the OTR were found. Seven of them were found at the CB1R and eleven at the OTR. At the extracellular side, the four residues W145, N146, E148, and K149 were found to be located at ECL2 of the CB1R and the eight residues at the extracellular loops and N-terminus of the OTR are residues R4 and N5 at the N-terminus and residues N270, A271, P272, K273, E274, and S276 at ECL3. Regarding the intracellular loops of the CB1R, two residues R39 and C43 are located at ICL1 and residue T119 at ICL2 and at the intracellular loops of the OTR, residue V306 is located at H8 and residues F309 and L310 are located at the C-terminus.

Interactions between TMHs of the receptors were found to be as usually between TMH2 of the CB1R and TMH1 of the OTR, TMH3 of the CB1R, and TMH7 of the OTR and between TMH4 of the CB1R and TMH6/7 of the OTR.

In the following **Table 23**, the residues are allocated to their localization at the receptors by visually inspecting the dimeric receptor complex.

Table 23. Residues identified by the alanine scan at the receptor.

Receptor	Position	Residues
CB1R	ICL1	R39, C43
	TMH2	V54, L57, L58, V61, I62, V64, Y65, D69, R73
	TMH3	F82, K83, G85
	ICL2	T119
	TMH4	R120, P121, K122, V124, V125, C128, L129, W131, T132, I133, I135, V136, A138, V139, L140, P141, L142, L143, G144
	ECL2	W145, N146, E148, K149
OTR	N-terminus	R4, N5
	TMH1	A7, L8, V11, E12, V15, L18, I19, L22
	TMH6	I246, L249, A250, V253, C254, P257, V261, W264
	ECL3	N270, A271, P272, K273, E274, S276
	TMH7	A277, F278, I280, V281, L283, L284, L287, C290, C291, W294, I295, M297, L298
	C-terminus	F309, L310
	H8	V306

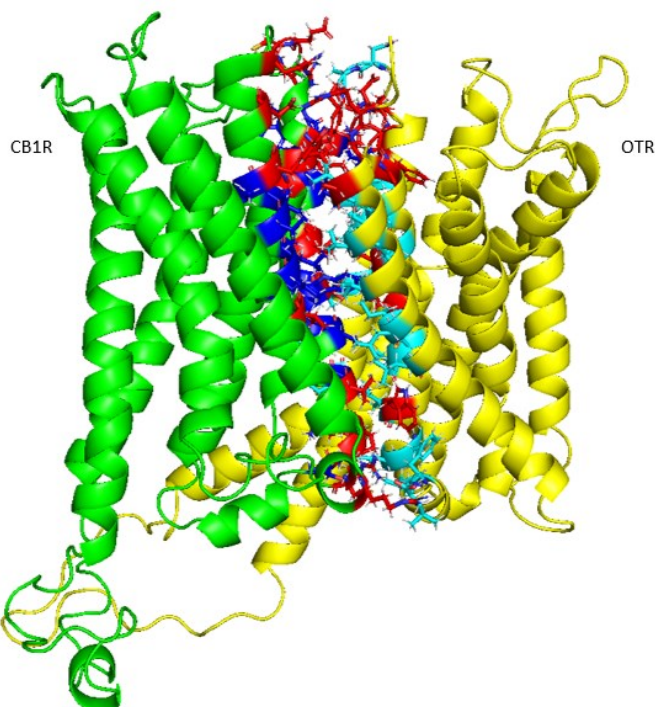


Figure 110. The view of the interface of CB1R (green) and OTR (yellow) after MD simulation.

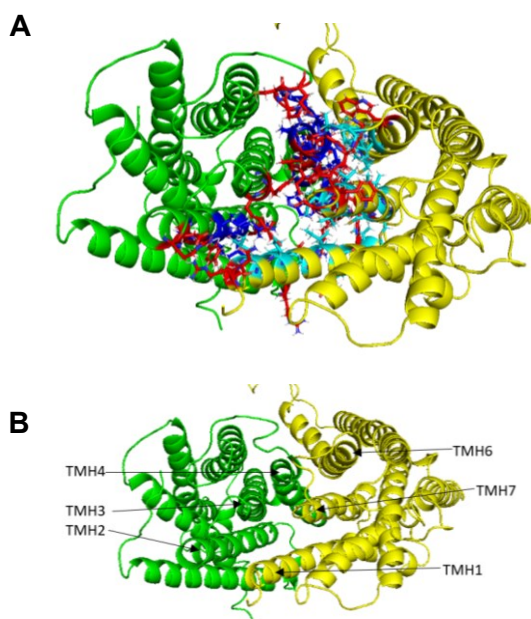


Figure 111. The top-down view of the interface of CB1R (green) and OTR (yellow) after MD simulation. **A:** Interface with highlighted residues **B:** Overview of the TMHs at the interface.

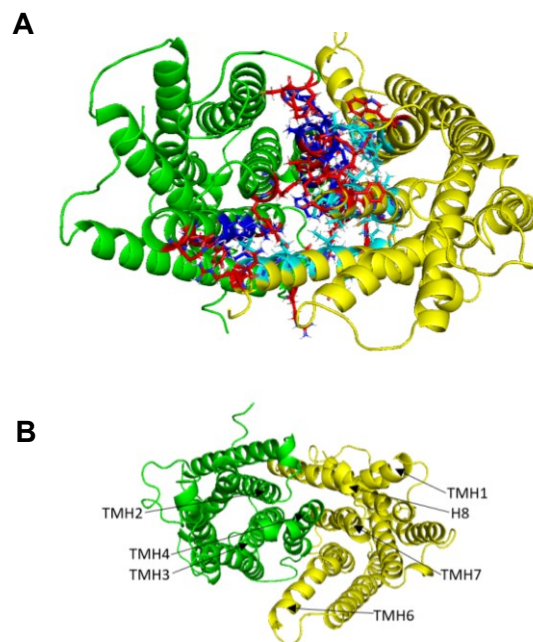


Figure 112. The bottom-up view of the interface of CB1R (green) and OTR (yellow) after MD simulation. **A:** Interface with highlighted residues **B:** Overview of the TMHs at the interface.

Seven hydrogen bonds were found between the CB1R and OTR. Four of them are located at the extracellular side of the dimeric receptor complex and three hydrogen bonds are located at the intracellular side.

At the extracellular side, one hydrogen bond is located between residue D69 at TMH2 of the CB1R and residue R4 at the C-terminus of the OTR, one between nearby residues Y65 at TMH2 of the CB1R and N5 at the C-terminus of the OTR and one hydrogen bond is located between residue K83 at TMH3 of the CB1R and residue E12 at TMH1 of the OTR (**Figure 113**). One more hydrogen bond at the extracellular side was found between residue K149 at ECL2 of the CB1R and residue D269 at ECL3 of the OTR (**Figure 114**).

At the intracellular side, one hydrogen bond was found between residue R120 at TMH4 of the CB1R and residue F309 at the C-terminus of the OTR, and two hydrogen bonds are located between residue R42 at ICL1 of the CB1R and residue L310 at the C-terminus of the OTR (**Figure 115**).

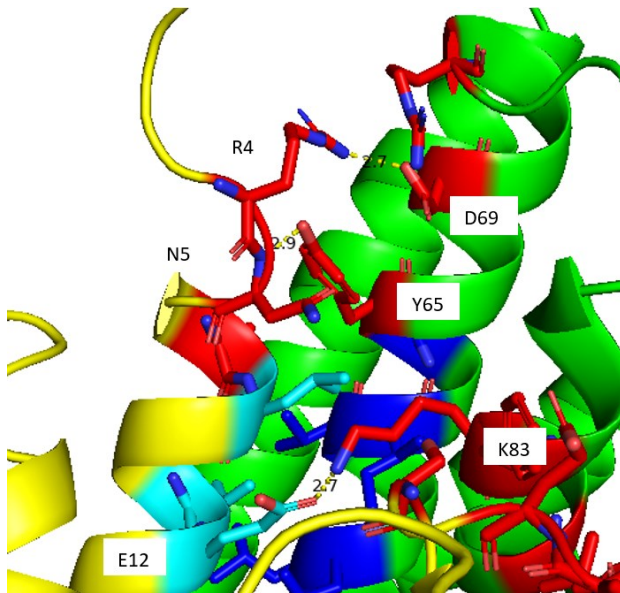


Figure 113. Hydrogen bond between residue D69 at TMH2 of the CB1R and residue R4 at the C-terminus of the OTR, residues Y65 at TMH2 of the CB1R and residue N5 at the C-terminus of the OTR, and between residue K83 at TMH3 of the CB1R and residue E12 at TMH1 of the OTR.

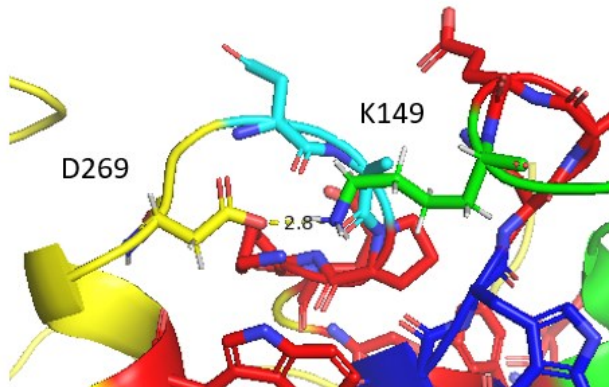


Figure 114. Hydrogen bond between K149 at ECL2 of the CB1R and residue D269 at ECL3 of the OTR.

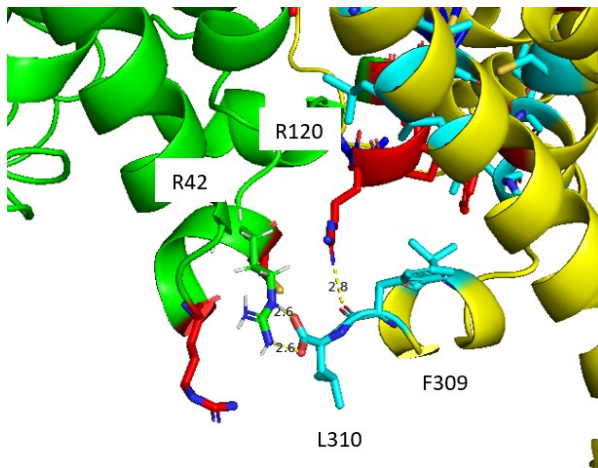


Figure 115. Hydrogen bond between residue R120 at TMH4 of the CB1R and residue F309 at the C-terminus of the OTR and between residue R42 at ICL1 of the CB1R and residue L310 at the C-terminus of the OTR.

4.4.3.2 Energy scores

The result of each alanine scan shows the important amino acid for interactions at the receptor complexes' interfaces (interface 1 to interface 12) and the respective energy scores (**Chart 13 – Chart 24**).

The energy scores demonstrate the shift of the binding free energy due to the mutation of the wildtype amino acids to alanine. A shift of the energy levels of the amino acids towards a higher value led to a higher binding free energy of the receptor complexes resulting in a destabilization of the complex. A shift to lower energy levels, therefore lead to higher stability of the complex.

In the charts, blue and cyan bars show a shift to a higher binding free energy, whereas red shows a shift to a lower binding free energy upon mutation to alanine. The detailed position of each residue at the receptor is shown in the previous chapter 4.4.3.1 in **Tables 12 to 23**.

First, residues with a negative shift of the binding free energy, leading to higher stability of the receptor complex, are located mainly at the upper or lower part of the TMHs and at the ECL, ICL, N-terminus, and C-terminus of each receptor. Only a few of these residues are located inside the core region of the interfaces, where dominantly residues with a positive shift of the binding free energy leading to less stability of the receptor complex, are located. Residues with shifts dominantly to a lower energy level are located at the TMH3, intracellular side of TMH4 and ECL2 of the CB1R and at TMH6, the extracellular side of TMH7 and ECL3 of the OTR.

The energy scores shown in chart 5.4.3.2a to chart 5.4.3.2l identified residues at TMH4 of the CB1R and TMH7 of the OTR with the highest changes in their energy value. This underlines the fact that TMH4 and MH7 are, as part of the interfaces' core domain, very important for the interactions between CB1R and OTR.

Further, at the core of the interfaces, between TMH4 of the CB1R and TMH7 of the OTR, it could be seen that predominantly residues with a shift to a higher energy value are located there, leading to less stability of the receptor complex. This leads to the assumption that a high shape complementarity regarding the wildtype residues is given between the CB1R and OTR.

Interface 1:

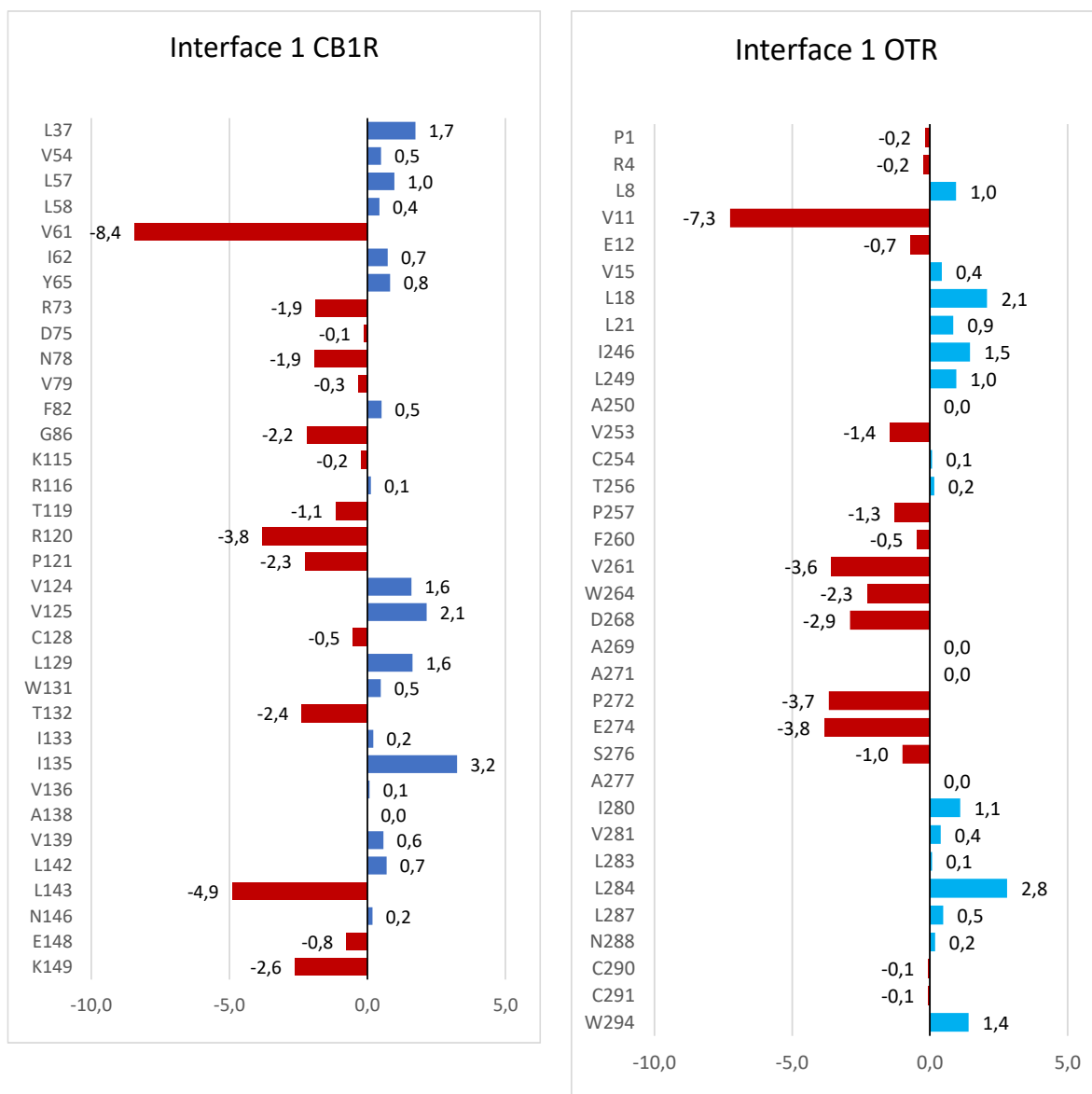


Chart 13. At this interface residue V61 at TMH2 of the CB1R and residue V11 at TMH1 of the OTR showed a high shift of the energy score to a lower value upon mutation to alanine. The other residues were inconspicuous by comparison.

Interface 2:

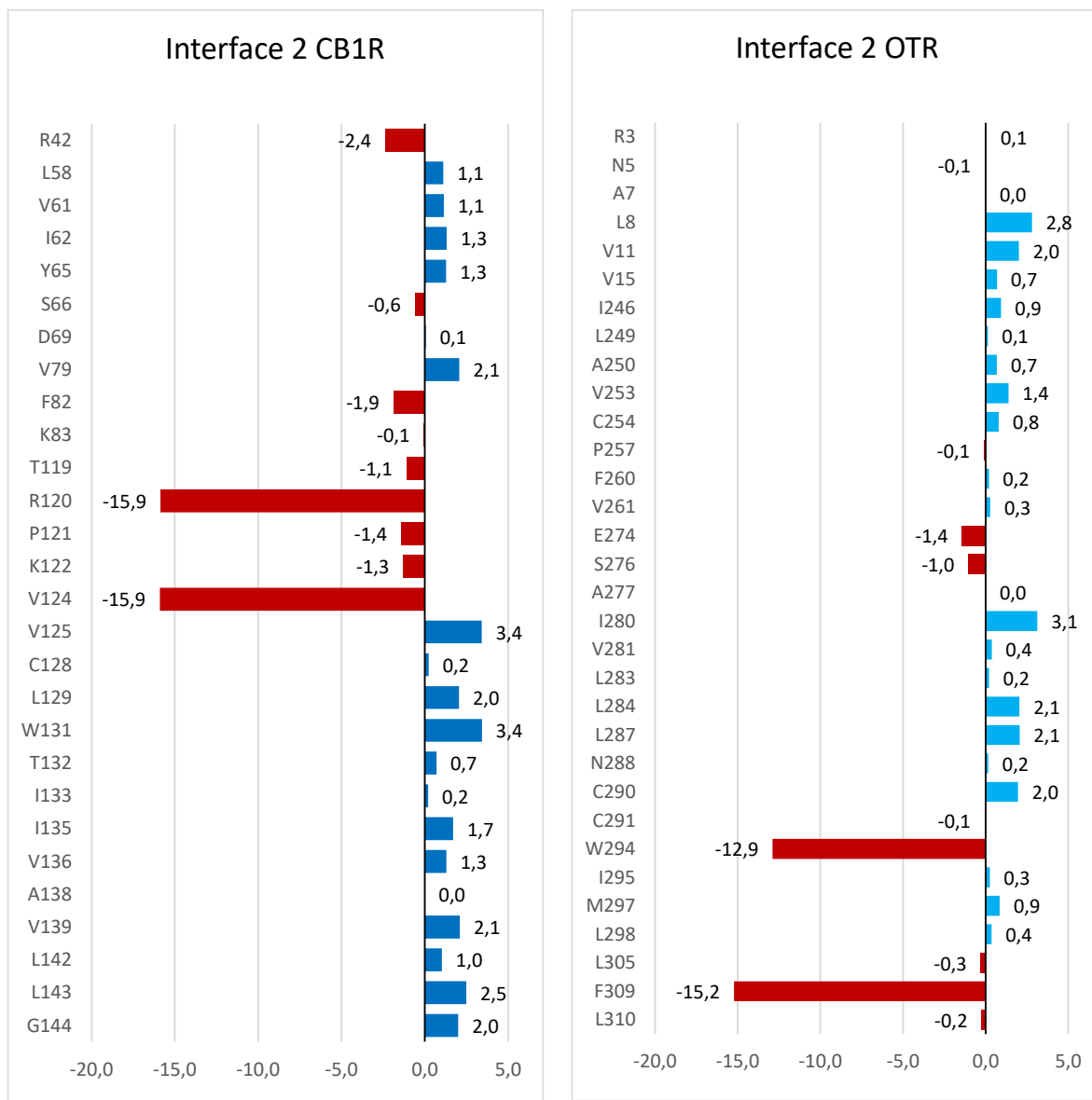


Chart 14. Here it is shown that the mutation of the two residues R120 at ICL2 and V124 at TMH4 of the CB1R and the two residues W294 at TMH7 and L210 at the C-terminus of the OTR resulted in a lower binding free energy. A remarkable shift of any residue towards a higher level was not obvious.

Interface 3:

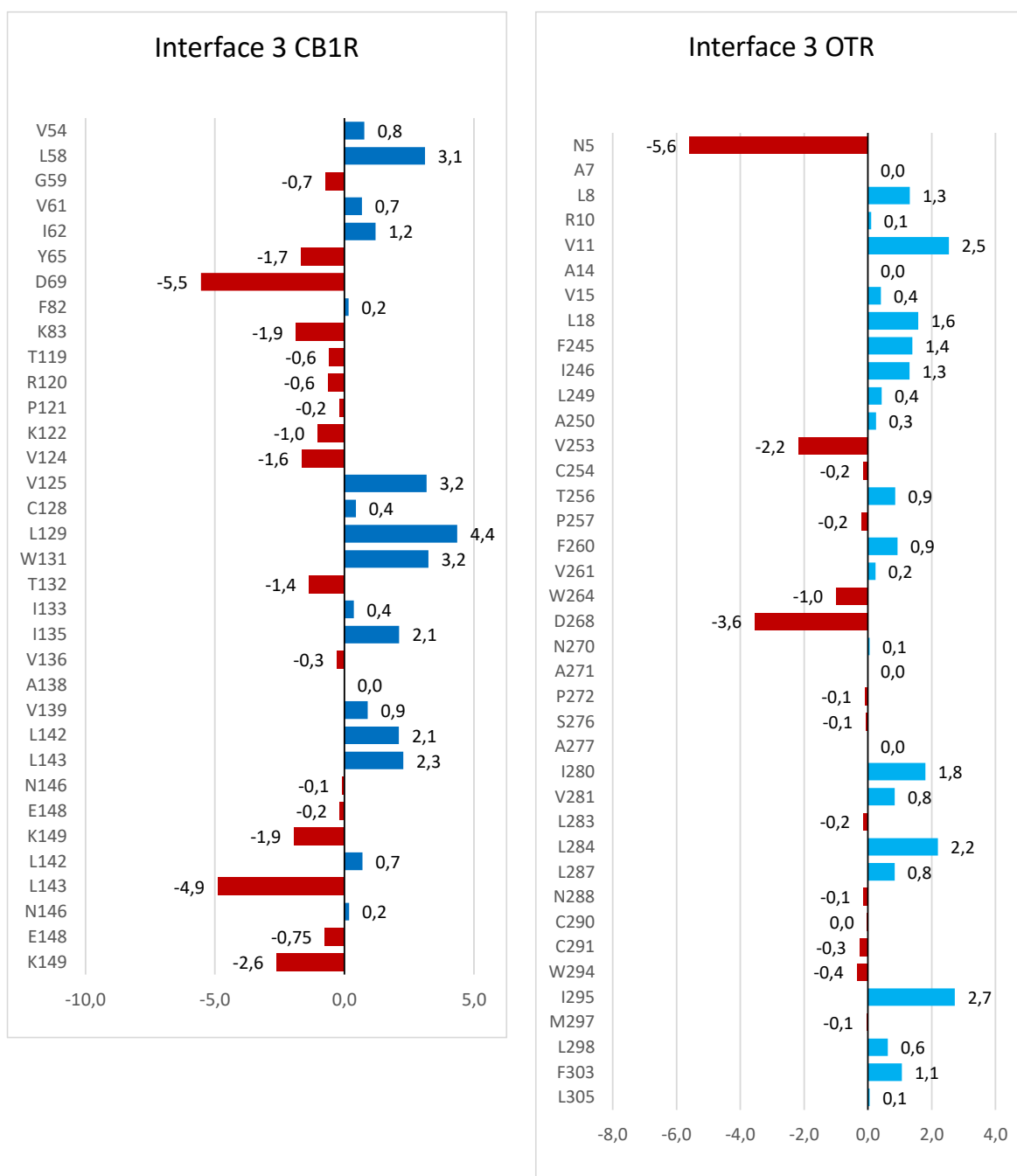


Chart 15. Residues D69 at TMH2 and L143 at TMH4 of the CB1R, as well as residue N5 at the N-terminus of the OTR showed a noteworthy energy shift to a lower energy level, even though the shifts were not too high.

Interface 4:

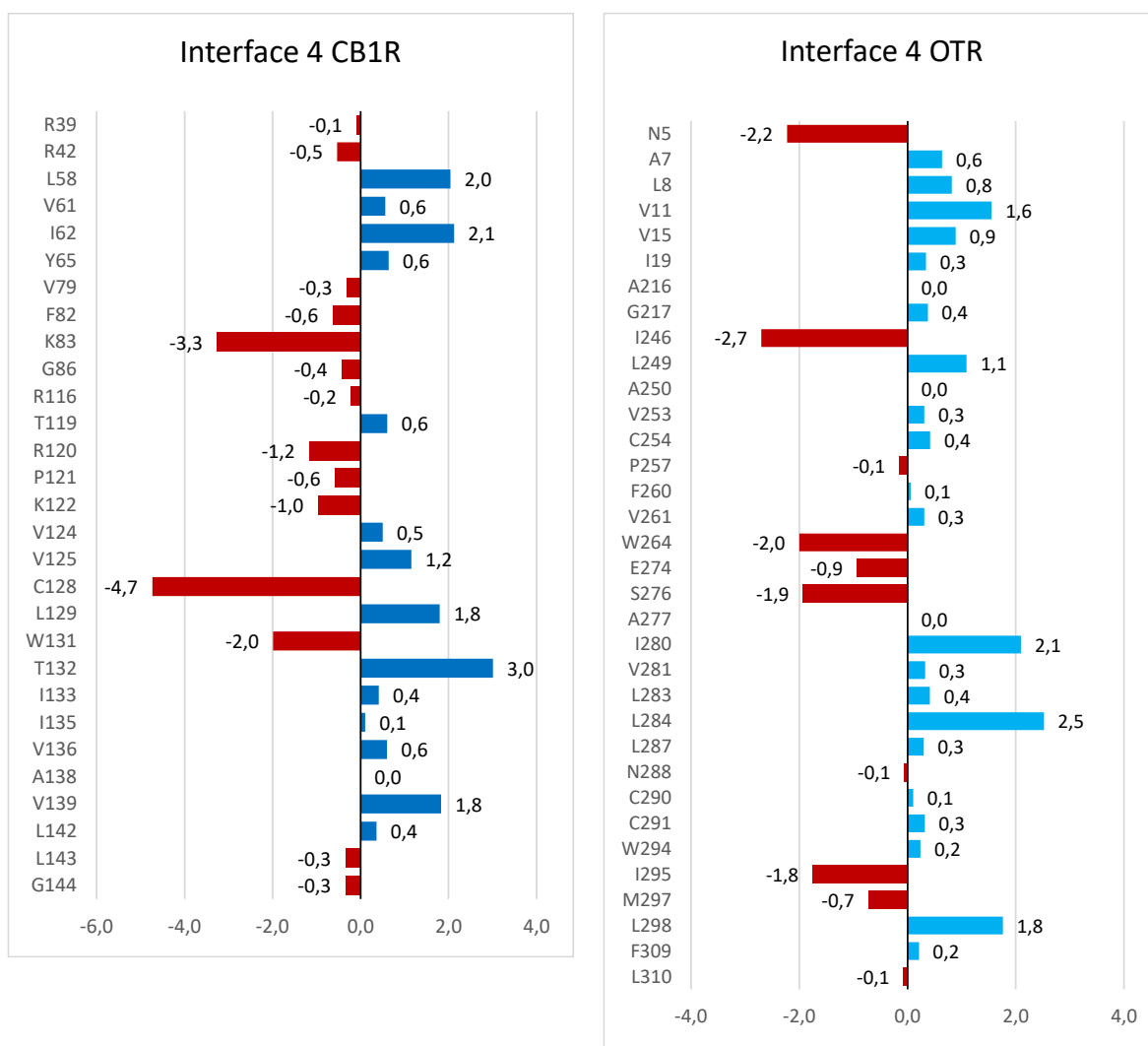


Chart 16. At this interface, no outstanding shifts of energy levels were noticed. The residues with the highest energy shifts in this interface were residue C128 at TMH4 of the CB1R, with a shift to a lower energy value, and concerning the OTR, a shift of the energy level to a lower value was identified concerning residue I246 at TMH6.

Interface 5:

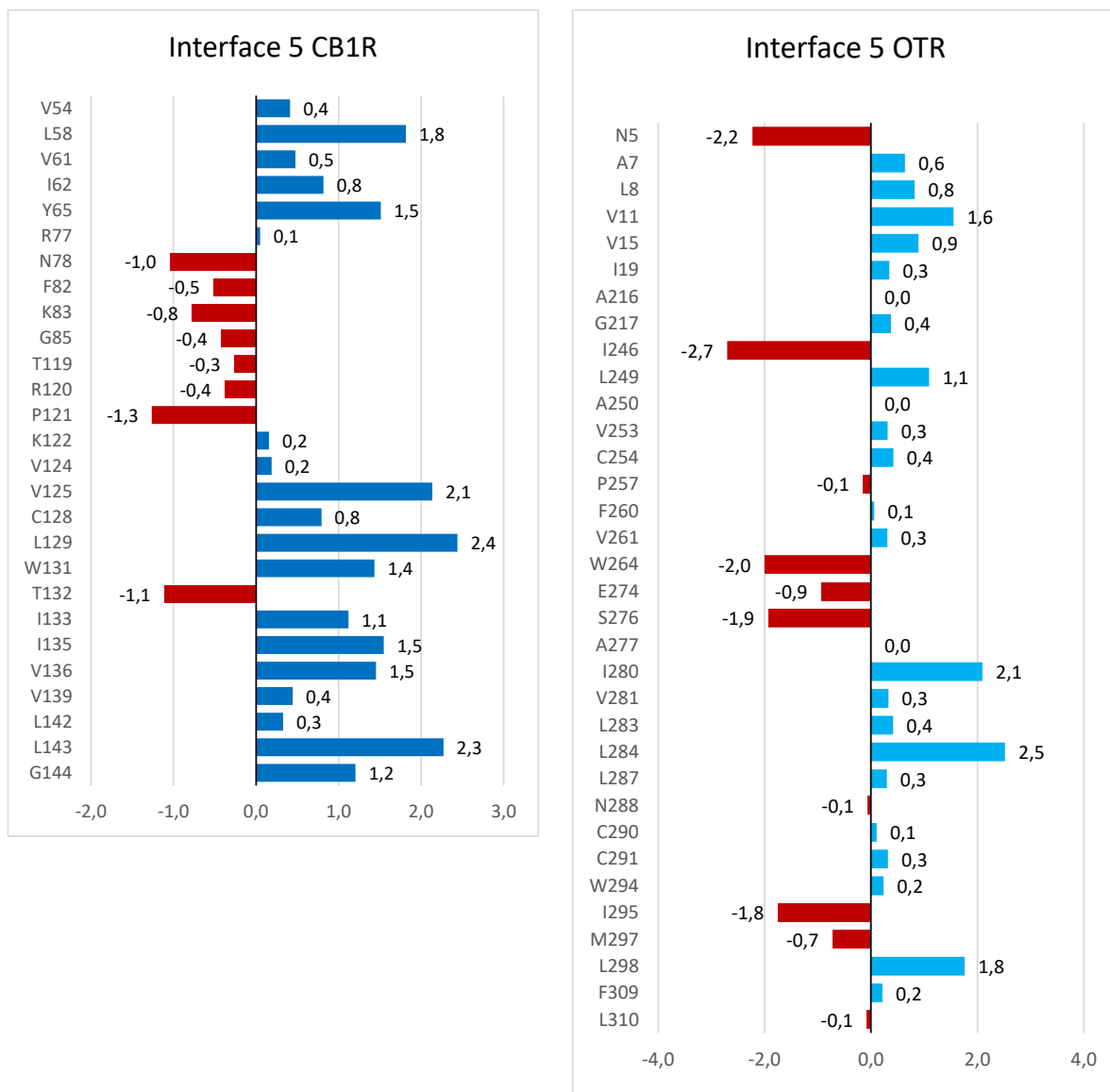


Chart 17. At this interface, residues N78 – P121 at the extracellularly part of TMH3/TMH4 and at LCI2 of the CB1R show a typical shift to a lower level. This is representative for all interfaces and here it is demonstrated well.

The energy shifts of the residues at this interface were not very high. The highest energy shifts were towards a higher level and took place at residue L129 at TMH4 of the CB1R and at residue L284 at TMH7 of the OTR.

Interface 6:

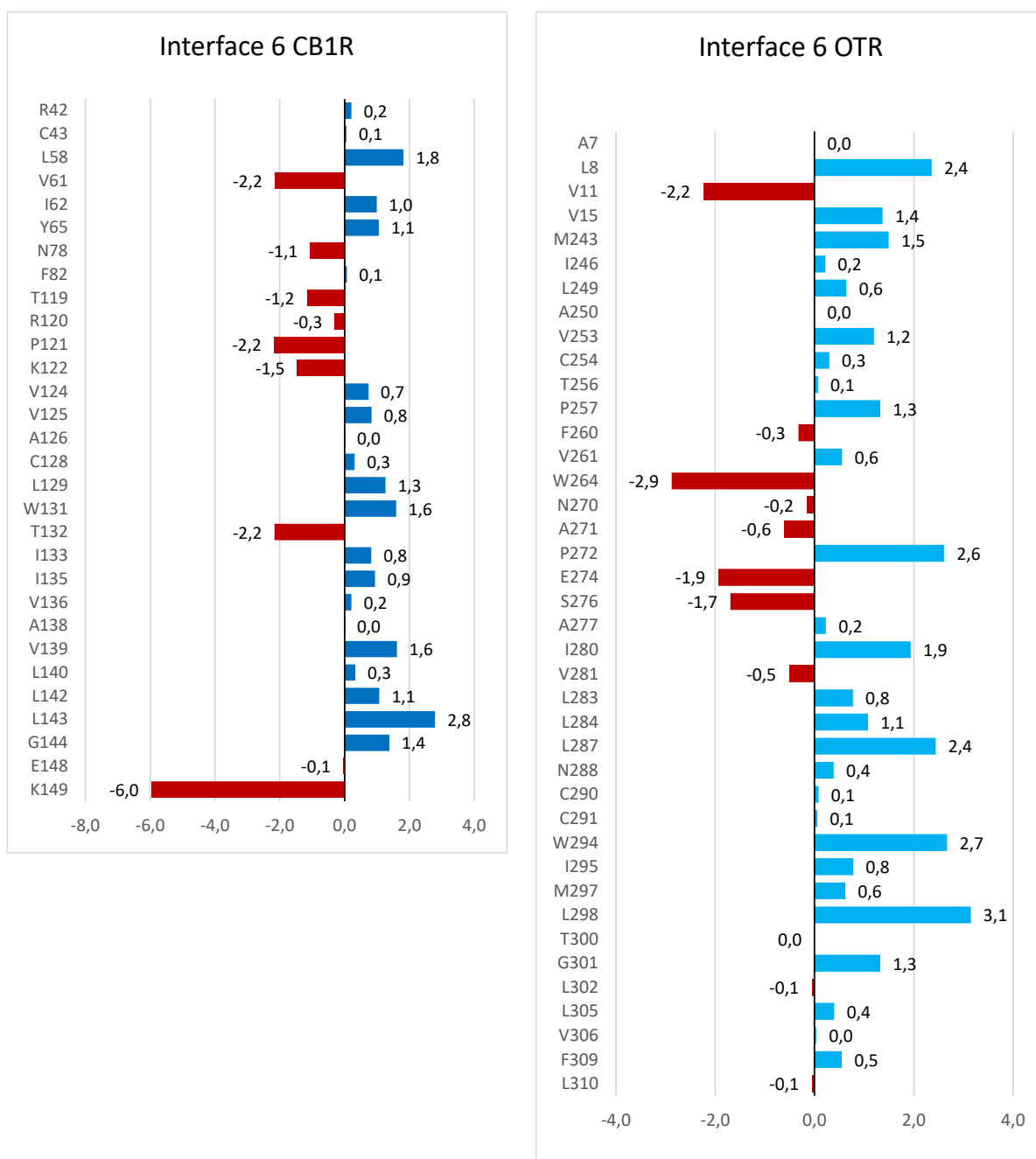


Chart 18. At interface 6, the only notable residue with a high shift of the energy score towards a lower energy value was residue K149 at ECL2 of the CB1R. All the other energy shifts were very small. The highest energy shift at the OTR was noticed at residue L298 at TMH7 with a shift to a higher energy value.

Interface 7:

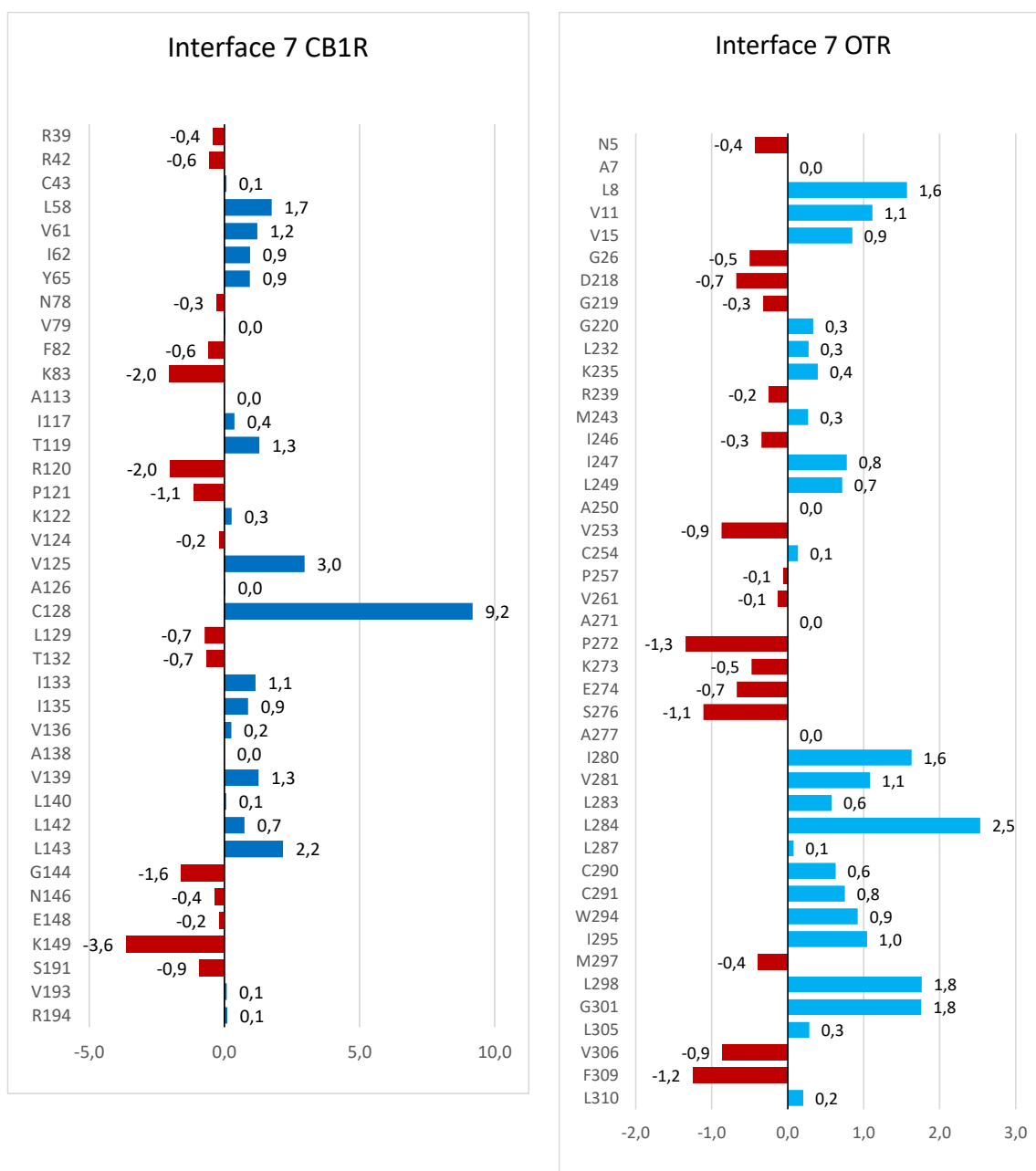


Chart 19. At interface 7, residue C128 at TMH4 of the CB1R marked the highest energy shift to a higher value. At the OTR, residue L284 at TMH7 was the one with the highest energy shift, also towards a higher value.

Interface 8:

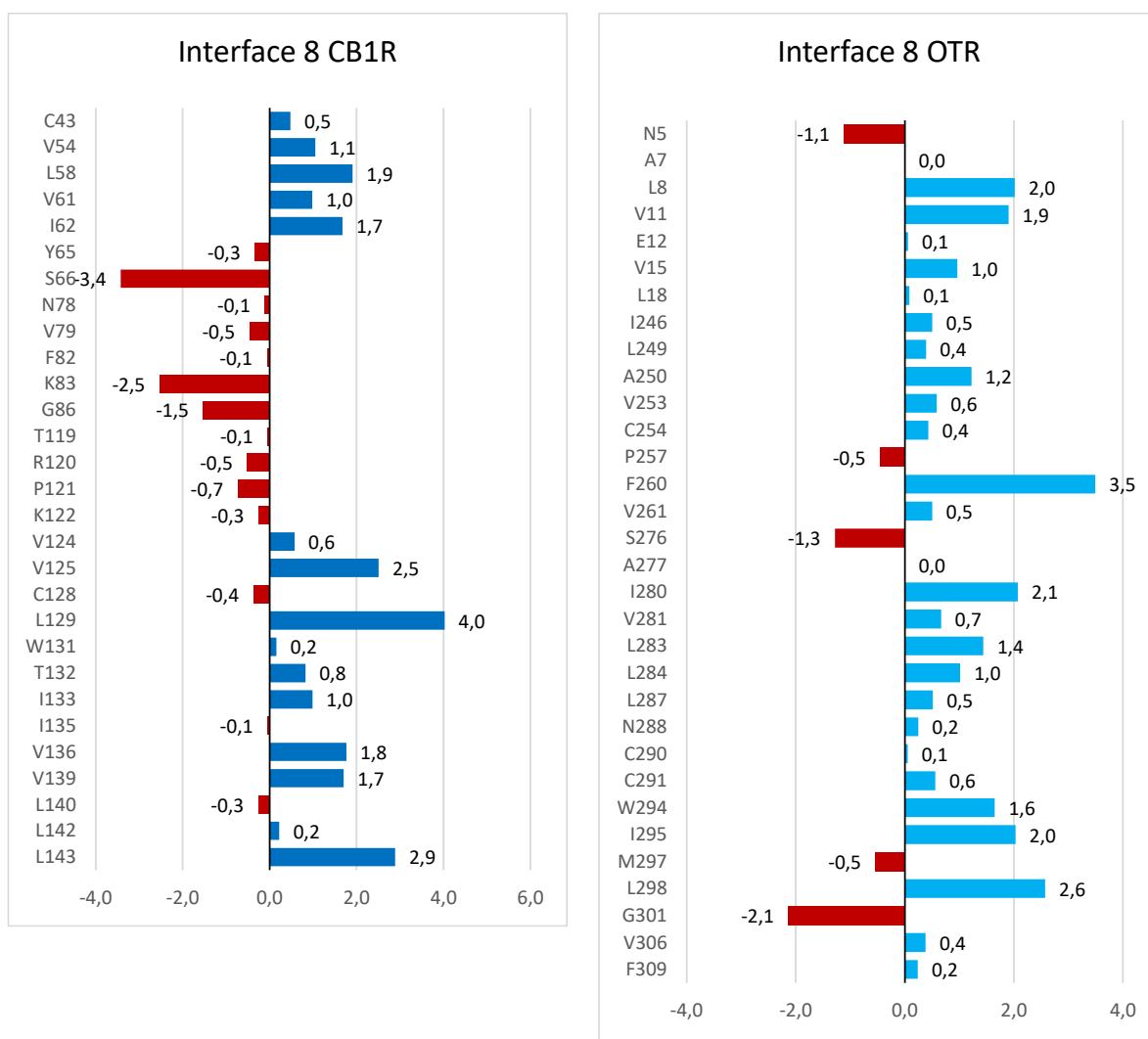


Chart 20. At interface 8, the energy shifts were marginal with a leader at the CB1R, residue L129 at TMH4. At the OTR, residue F260 at TMH6 showed the highest energy shift and both energy shifts were towards a higher value.

Interface 9:

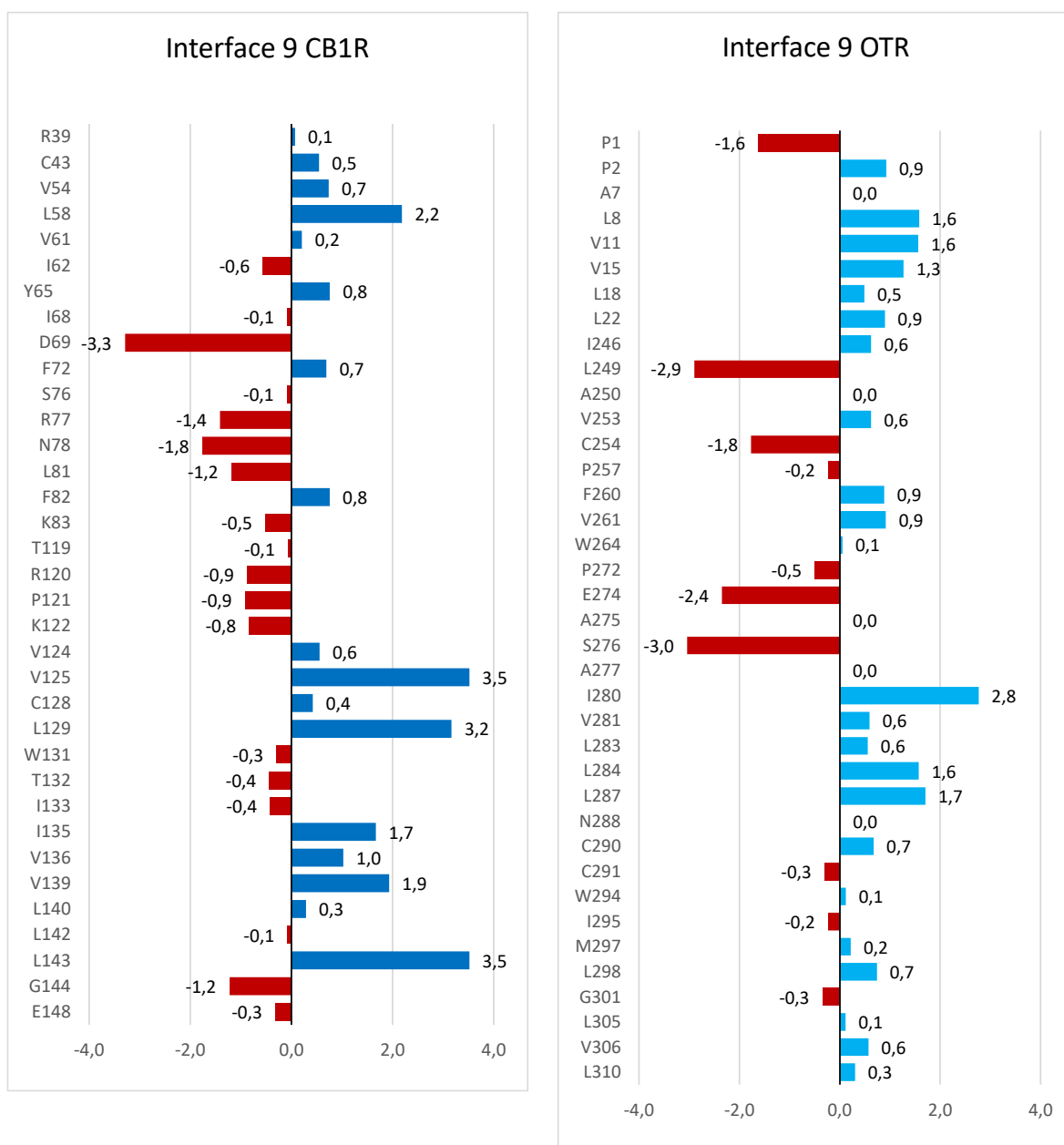


Chart 21. Here, no residues showed markable changes in their energy level. The highest changes at the CB1R were concerning residue V125 and residue L143 at TMH4, each characterized by a shift towards a higher level. At the OTR, the highest change in the binding free energy was at residue S276 at TMH7.

Interface 10:

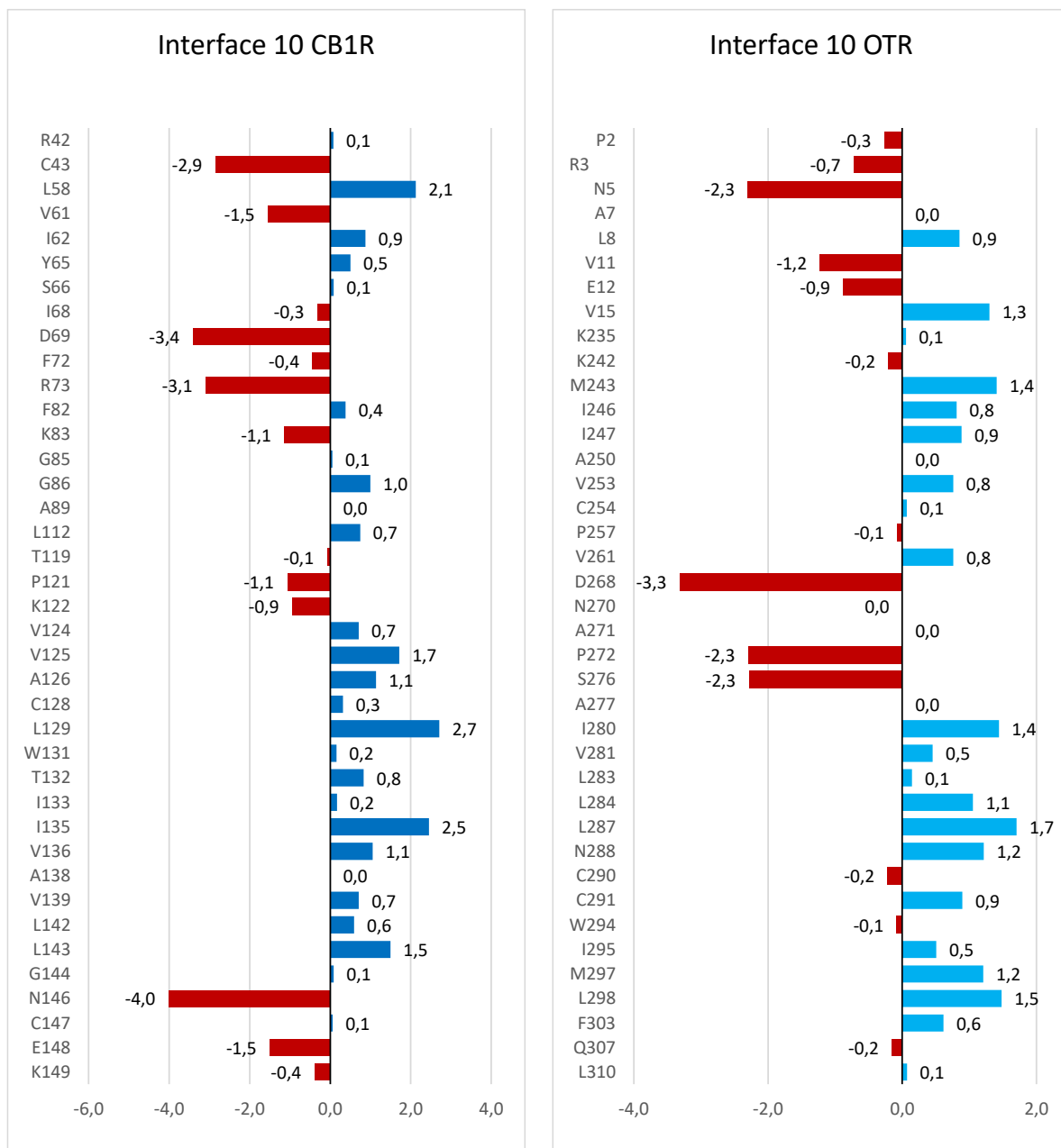


Chart 22. At this interface, the changes of the binding free energy concerning to alanine scan were not too high. Noticeable were the highest energy shift towards a lower value of residue N146 at ECL2 of the CB1R and residue D268 at TMH6 of the OTR.

Interface 11:

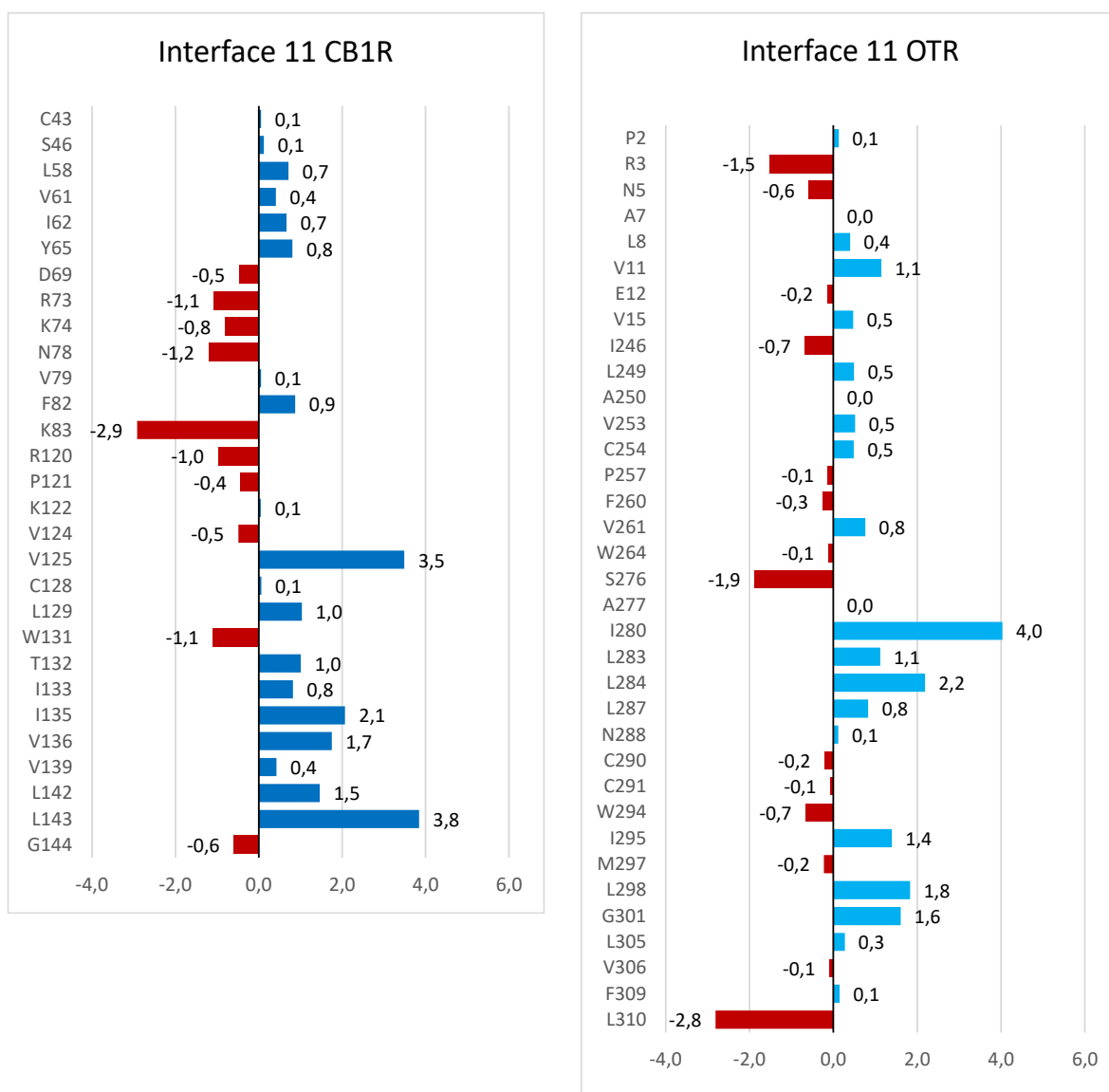


Chart 23. Interface 11 was also characterized by no notable energy changes of the residues. Residue V125 at TMH4 of the CB1R and residue I280 at TMH7 of the OTR showed the highest energy shift towards a higher energy level.

Interface 12:

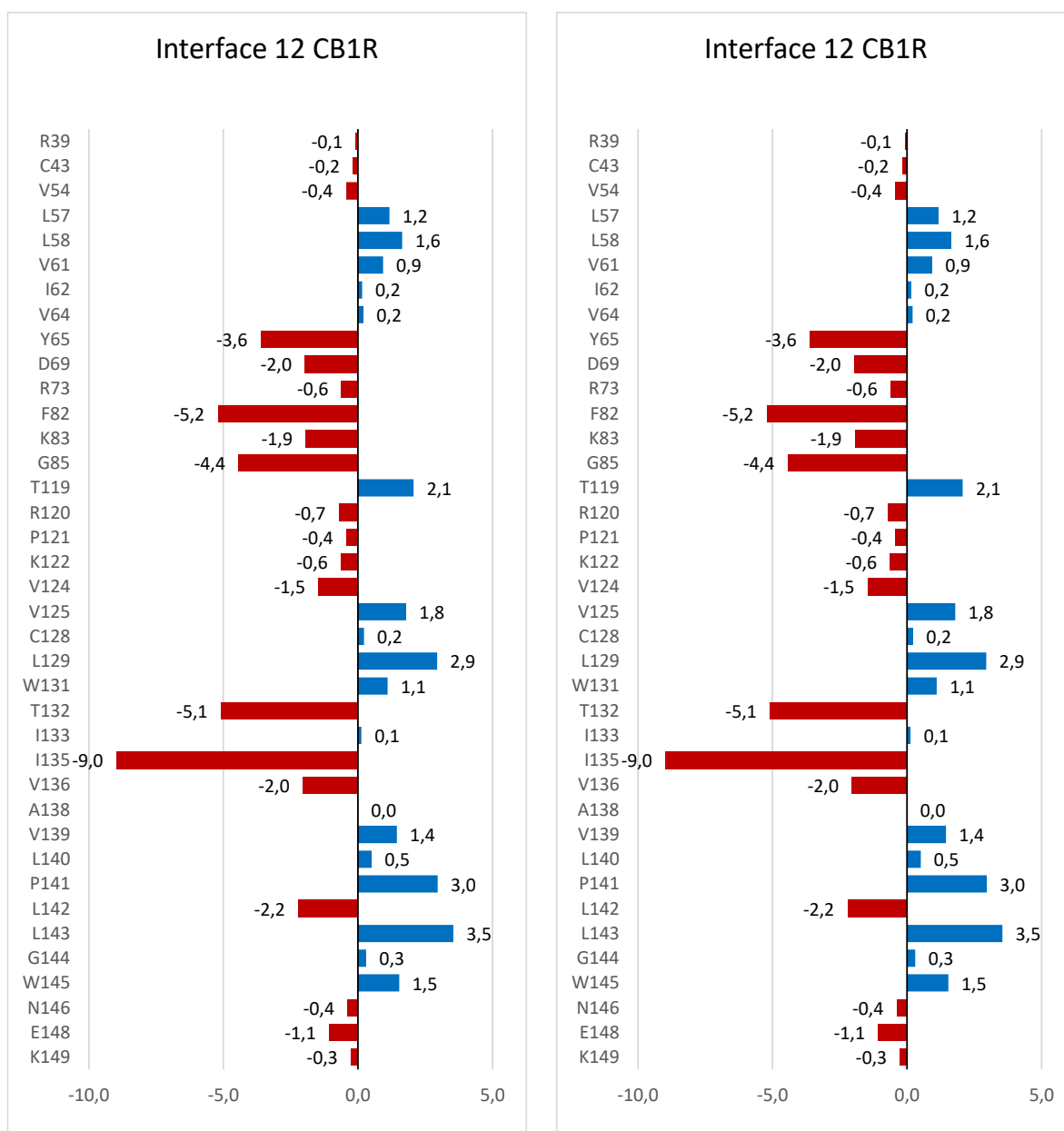


Chart 24. At interface 12, higher energy shifts were noticed. At residue I135 at TMH4 of the CB1R and at L284 at TMH7 of the OTR, these higher shifts towards a lower binding free energy level were detected.

5 Conclusion and outlook

The Memdock server, used for docking the CB1R and OTR, revealed one preferred docking pose with an asymmetrical interface involving TMH1/2/3/4 of the CB1R and TMH1/6/7 of the OTR.

When the five chosen ligands (compound **20-24**) were docked to the respective orthosteric binding pockets of the OTR or CB1R the ligands' attachment sites pointed toward the outside of the binding pocket so the attachment of linkers to design heterobivalent ligands is possible without steric collision in the next steps. When examining the polyethylene glycol linkers COOH-PEG5-NH-Fmoc, COOH-PEG10-NH-Fmoc, and COOH-PEG15-NH-Fmoc, the shortest linker COOH-PEG5-NH-Fmoc was discarded since its average length of 20Å was too short for linking the ligands in their respective binding pocket with an average distance of 40Å and 60Å. Therefore, the linkers COOH-PEG10-NH-Fmoc with a length of 40Å and COOH-PEG15-NH-Fmoc with a length of 60Å were considered to be suitable for the design of heterobivalent ligands for the CB1R-OTR protein complex. Hence, they were chosen as starting point for twelve heterobivalent ligands at the CB1R-OTR complex.

After integrating the resulting complexes into a membrane, molecular dynamics simulations were carried out. Apart from the similarities between complexes 1 to 12, the analyses of the MD simulations' results identified differences. The average RMSDs of the protein backbones revealed high stability of the receptor complexes as well as their heterobivalent ligands at the binding pockets. Nevertheless, three complexes showed less stability. At complexes 3 and 12, the instability was caused, by the compound **24** moiety of the heterobivalent ligand because it did not bind sufficiently to the binding pocket of the OTR. Regarding complex 10, the instability was assumed to be caused by high structural changes of the receptor complex that could be seen by the high fluctuation of the RMSD values. The higher variability of the RMSD values of the OTR compared to the CB1R lead to the assumption that the OTR might not be as stable as the CB1R. For further investigations of the stability of the protein complexes a simulation time longer than 10 ns would be recommended.

When investigating the changes of the BSA and ASA_{bound} of all twelve complexes during MD simulation, increased and reduced surface areas were discovered. Further, the changes of the average BSA and ASA_{bound} of complex 1 to 12 upon MD simulation revealed slightly reduced BSAs and slightly increased $ASAs_{\text{bound}}$. The high standard deviations especially after the MD simulation were caused by the short simulation time of 10ns. It was assumed that a simulation time longer than 10ns would lead to a smaller deviation from the mean value.

Performing the alanine scan on complex 1 to complex 12 the corresponding interfaces showed a maximum of 81 residues (interface 7) and a minimum of 59 residues (interface 5) to be

important for the protein interactions. Further, the interfaces showed interactions between TMH2 of the CB1R and TMH1 of the OTR, TMH3 of the CB1R and TMH7 of the OTR as well as TMH4 of the CB1R and TMH6 of the OTR. In two of the examined interfaces, interface 1 and interface 8, TMH1 of the CB1R showed interactions with TMH1 of the OTR. Further, residues at ECL1/2, ICL1/2/3, and H8 of the CB1R and the N-terminus, ICL3, ECL3, H8, and C-terminus of the OTR were noticed to be important for the complex's stability. Here primarily shifts toward lower values of the binding free energy upon mutation of the wildtype residues were seen, resulting in a stabilization of the complex. However, a majority of the residues showed shifts toward higher energy values upon mutation to alanine especially at the core domain of the interface between TMH4 and TMH7. This suggests a destabilization of the receptor complexes when the residues are mutated to alanine and underlines the high shape complementarity of the wildtype residues at the core domain. Moreover, high changes of the binding free energy regarding amino acids at this core domain are highlighting the importance of this domain for the complexes' stability.

Hydrogen bonds found at the interfaces between the OTR and CB1R are primarily located at the extracellular and intracellular sides of the receptor complexes. At the transmembrane region of the interfaces, only a few hydrogen bonds were located, since fewer amino acids with hydrophobic side-chains are placed there, compared to the extracellular and intracellular domains of the receptors.

The outcomes are meant to ease further research in the field of *in vitro* studies concerning bivalent ligands of the CB1R-OTR complex. Further, *in vitro* mutational experiments would be interesting to prove the real-life impact of mutating certain residues, identified to be important by the alanine scan, in cells or tissues. As shown in the study by Busnelli et al., 2016, BRET assays with OTR, CB1R, and fragments of the helices that are meant to be at the interface, would be interesting to show, whether the fragments disturb the complex formation of the receptors. If they do so, their importance at the formation of the interface is given. Moreover, computational experiments regarding the CB1R-OTR complex, using other protein-protein docking programs such as Rosetta MPDock, would be interesting, thus the results could be compared to the Memdock results to gain more information about the interface and stability of the receptor complex. One fundamental question, which remains unanswered, is whether OTR and CB1R form dimeric complexes. Therefore, FRET or BRET assays would be the methods of choice for *in vitro* experiments on cells that are expressing these heterodimers.

6 References

- Agnati, L. F., Fuxe, K., Zoli, M., Rondanini, C., & Ogren, S. O. (1982). New vistas on synaptic plasticity: the receptor mosaic hypothesis of the engram. *Medical biology*, 60(4), 183-190. PMID:6128444.
- Åkerlund, M., Bossmar, T., Brouard, R., Kostrzevska, A., Laudanski, T., Lemancewicz, A., ... & Steinwall, M. (1999). Receptor binding of oxytocin and vasopressin antagonists and inhibitory effects on isolated myometrium from preterm and term pregnant women. *BJOG: An International Journal of Obstetrics & Gynaecology*, 106(10), 1047-1053. doi:10.1111/j.1471-0528.1999.tb08112.x.
- Al-Zoubi, R., Morales, P., & Reggio, P. H. (2019). Structural insights into CB1 receptor biased signaling. *International journal of molecular sciences*, 20(8), 1837. doi:10.3390/ijms20081837.
- Angers, S., Salahpour, A., Joly, E., Hilaiet, S., Chelsky, D., Dennis, M., & Bouvier, M. (2000). Detection of β 2-adrenergic receptor dimerization in living cells using bioluminescence resonance energy transfer (BRET). *Proceedings of the National Academy of Sciences*, 97(7), 3684-3689. doi:10.1073/pnas.97.7.3684
- Bauer, M., Chicca, A., Tamborrini, M., Eisen, D., Lerner, R., Lutz, B., ... & Gertsch, J. (2012). Identification and quantification of a new family of peptide endocannabinoids (Pepcans) showing negative allosteric modulation at CB1 receptors. *Journal of biological chemistry*, 287(44), 36944-36967. doi:10.1074/jbc.M112.382481.
- Basith, S., Cui, M., Macalino, S. J., Park, J., Clavio, N. A., Kang, S., & Choi, S. (2018). Exploring G protein-coupled receptors (GPCRs) ligand space via cheminformatics approaches: impact on rational drug design. *Frontiers in pharmacology*, 9, 128. doi:10.3389/fphar.2018.00128.
- Bonifacino, J. S., Dell'Angelica, E. C., & Springer, T. A. (1999). Immunoprecipitation. *Current protocols in molecular biology*, 48(1), 10-16. doi:10.1002/0471142727.mb1016s48.
- Bonger, K. M., van den Berg, R. J., Heitman, L. H., IJzerman, A. P., Oosterom, J., Timmers, C. M., ... & van der Marel, G. A. (2007). Synthesis and evaluation of homo-bivalent GnRHR ligands. *Bioorganic & medicinal chemistry*, 15(14), 4841-4856. doi:10.1016/j.bmc.2007.04.065.
- Bosier, B., Muccioli, G. G., Hermans, E., & Lambert, D. M. (2010). Functionally selective cannabinoid receptor signalling: therapeutic implications and opportunities. *Biochemical pharmacology*, 80(1), 1-12. doi:10.1016/j.bcp.2010.02.013.

- Brooijmans, N., & Kuntz, I. D. (2003). Molecular recognition and docking algorithms. *Annual review of biophysics and biomolecular structure*, 32(1), 335-373. doi:10.1146/annurev.biophys.32.110601.142532.
- Brooks, B. R., Brooks III, C. L., Mackerell Jr, A. D., Nilsson, L., Petrella, R. J., Roux, B., ... & Karplus, M. (2009). CHARMM: the biomolecular simulation program. *Journal of computational chemistry*, 30(10), 1545-1614. doi:10.1002/jcc.21287.
- Brooks, B. R., Bruccoleri, R. E., Olafson, B. D., States, D. J., Swaminathan, S. A., & Karplus, M. (1983). CHARMM: a program for macromolecular energy, minimization, and dynamics calculations. *Journal of computational chemistry*, 4(2), 187-217. doi:10.1002/jcc.540040211.
- Busnelli, M., & Chini, B. (2017). Molecular basis of oxytocin receptor signalling in the brain: what we know and what we need to know. *Behavioral Pharmacology of Neuropeptides: Oxytocin*, 3-29. doi:10.1007/7854_2017_6.
- Busnelli, M., Kleinau, G., Muttenthaler, M., Stoev, S., Manning, M., Bibic, L., ... & Chini, B. (2016). Design and characterization of superpotent bivalent ligands targeting oxytocin receptor dimers via a channel-like structure. *Journal of medicinal chemistry*, 59(15), 7152-7166. doi:10.1021/acs.jmedchem.6b00564.
- Callén, L., Moreno, E., Barroso-Chinea, P., Moreno-Delgado, D., Cortés, A., Mallol, J., ... & McCormick, P. J. (2012). Cannabinoid receptors CB1 and CB2 form functional heteromers in brain. *Journal of Biological Chemistry*, 287(25), 20851-20865. doi:10.1074/jbc.M111.335273.
- Chan, W. C. W. P. D., & White, P. (Eds.). (1999). Fmoc solid phase peptide synthesis: a practical approach (Vol. 222). *OUP Oxford*. doi:10.1002/psc.2836.
- Canti, C., Page, K. M., Stephens, G. J., & Dolphin, A. C. (1999). Identification of residues in the N terminus of $\alpha 1B$ critical for inhibition of the voltage-dependent calcium channel by $G\beta\gamma$. *Journal of Neuroscience*, 19(16), 6855-6864. doi:10.1523/JNEUROSCI.19-16-06855.1999.
- Chaudhury, S., Lyskov, S., & Gray, J. J. (2010). PyRosetta: a script-based interface for implementing molecular modeling algorithms using Rosetta. *Bioinformatics*, 26(5), 689-691. doi:10.1093/bioinformatics/btq007.
- Carriba, P., Navarro, G., Ciruela, F., Ferré, S., Casadó, V., Agnati, L., ... & Franco, R. (2008). Detection of heteromerization of more than two proteins by sequential BRET-FRET. *Nature methods*, 5(8), 727-733. doi:10.1038/nmeth.1229.
- Chothia, C., & Janin, J. (1975). Principles of protein-protein recognition. *Nature*, 256(5520), 705-708. doi:10.1038/256705a0.

- Chuang, G. Y., Kozakov, D., Brenke, R., Comeau, S. R., & Vajda, S. (2008). DARS (Decoys As the Reference State) potentials for protein-protein docking. *Biophysical journal*, 95(9), 4217-4227. doi:10.1529/biophysj.108.135814.
- Congreve, M., de Graaf, C., Swain, N. A., & Tate, C. G. (2020). Impact of GPCR structures on drug discovery. *Cell*, 181(1), 81-91. doi:10.1016/j.cell.2020.03.003.
- Cooper, D. M. (2003). Regulation and organization of adenylyl cyclases and cAMP. *Biochemical Journal*, 375(3), 517-529. doi:10.1042/bj20031061.
- Cottet, M., Faklaris, O., Maurel, D., Scholler, P., Doumazane, E., Trinquet, E., ... & Durroux, T. (2012). BRET and time-resolved FRET strategy to study GPCR oligomerization: from cell lines toward native tissues. *Frontiers in endocrinology*, 3, 92. doi:10.3389/fendo.2012.00092.
- Daub, H., Weiss, F. U., Wallasch, C., & Ullrich, A. (1996). Role of transactivation of the EGF receptor in signalling by G-protein-coupled receptors. *Nature*, 379(6565), 557-560. doi:10.1038/379557a0.
- Dekan, Z., Kremsmayr, T., Keov, P., Godin, M., Teakle, N., Dürbauer, L., ... & Muttenthaler, M. (2021). Nature-inspired dimerization as a strategy to modulate neuropeptide pharmacology exemplified with vasopressin and oxytocin. *Chemical Science*, 12(11), 4057-4062. doi:10.1039/D0SC05501H.
- Devane, W. A., Hanus, L., Breuer, A., Pertwee, R. G., Stevenson, L. A., Griffin, G., ... & Mechoulam, R. (1992). Isolation and structure of a brain constituent that binds to the cannabinoid receptor. *Science*, 258(5090), 1946-1949. doi:10.1126/science.1470919.
- Devost, D., Wrzal, P., & Zingg, H. H. (2008). Oxytocin receptor signalling. *Progress in brain research*, 170, 167-176. doi:10.1016/S0079-6123(08)00415-9.
- Donaldson, Z. R., & Young, L. J. (2008). Oxytocin, vasopressin, and the neurogenetics of sociality. *Science*, 322(5903), 900-904. doi:10.1126/science.1158668.
- Eastman, P., Swails, J., Chodera, J. D., McGibbon, R. T., Zhao, Y., Beauchamp, K. A., ... & Pande, V. S. (2017). OpenMM 7: Rapid development of high performance algorithms for molecular dynamics. *PLoS computational biology*, 13(7), e1005659. doi:10.1371/journal.pcbi.1005659.
- Eldridge, M. D., Murray, C. W., Auton, T. R., Paolini, G. V., & Mee, R. P. (1997). Empirical scoring functions: I. The development of a fast empirical scoring function to estimate the binding affinity of ligands in receptor complexes. *Journal of computer-aided molecular design*, 11(5), 425-445. doi:10.1023/A:1007996124545.

Ferreira, L. G., Dos Santos, R. N., Oliva, G., & Andricopulo, A. D. (2015). Molecular docking and structure-based drug design strategies. *Molecules*, 20(7), 13384-13421. doi:10.3390/molecules200713384.

Filizola, M., & Weinstein, H. (2005). The study of G-protein coupled receptor oligomerization with computational modeling and bioinformatics. *The FEBS journal*, 272(12), 2926-2938. doi:10.1111/j.1742-4658.2005.04730.x.

Frantz, M. C., Rodrigo, J., Boudier, L., Durroux, T., Mouillac, B., & Hibert, M. (2010). Subtlety of the Structure– Affinity and Structure– Efficacy Relationships around a Nonpeptide Oxytocin Receptor Agonist. *Journal of medicinal chemistry*, 53(4), 1546-1562. doi:10.1021/jm901084f.

George, S. R., Fan, T., Xie, Z., Tse, R., Tam, V., Varghese, G., & O'Dowd, B. F. (2000). Oligomerization of μ - and δ -opioid receptors: generation of novel functional properties. *Journal of Biological Chemistry*, 275(34), 26128-26135. doi:10.1074/jbc.M000345200.

Gesty-Palmer, D., Chen, M., Reiter, E., Ahn, S., Nelson, C. D., Wang, S., ... & Lefkowitz, R. J. (2006). Distinct β -arrestin- and G protein-dependent pathways for parathyroid hormone receptor-stimulated ERK1/2 activation. *Journal of Biological Chemistry*, 281(16), 10856-10864. doi:10.1074/jbc.M513380200.

Gimpl, G., Reitz, J., Brauer, S., & Trossen, C. (2008). Oxytocin receptors: ligand binding, signalling and cholesterol dependence. *Progress in brain research*, 170, 193-204. doi:10.1016/S0079-6123(08)00417-2.

Gimpl, G., & Fahrenholz, F. (2001). The oxytocin receptor system: structure, function, and regulation. *Physiological reviews*, 81(2), 629-683. doi:10.1152/physrev.2001.81.2.629.

Glass, M., & Felder, C. C. (1997). Concurrent stimulation of cannabinoid CB1 and dopamine D2 receptors augments cAMP accumulation in striatal neurons: evidence for a Gs linkage to the CB1 receptor. *Journal of Neuroscience*, 17(14), 5327-5333. doi:10.1523/JNEUROSCI.17-14-05327.1997.

Gouldson, P. R., Higgs, C., Smith, R. E., Dean, M. K., Gkoutos, G. V., & Reynolds, C. A. (2000). Dimerization and domain swapping in G-protein-coupled receptors: a computational study. *Neuropsychopharmacology*, 23(4), S60-S77. doi:10.1016/S0893-133X(00)00153-6.

Gong, K., Li, Z., Xu, M., Du, J., Lv, Z., & Zhang, Y. (2008). A Novel Protein Kinase A-independent, β -Arrestin-1-dependent Signaling Pathway for p38 Mitogen-activated Protein Kinase Activation by β 2-Adrenergic Receptors*. *Journal of Biological Chemistry*, 283(43), 29028-29036. doi:10.1074/jbc.M801313200.

Goodson, J. L. (2013). Deconstructing sociality, social evolution and relevant nonapeptide functions. *Psychoneuroendocrinology*, 38(4), 465-478. doi:10.1016/j.psyneuen.2012.12.005. doi:10.1016/j.psyneuen.2012.12.005.

Grant, P. S., Kahlcke, N., Govindpani, K., Hunter, M., MacDonald, C., Brimble, M. A., ... & Furkert, D. P. (2019). Divalent cannabinoid-1 receptor ligands: A linker attachment point survey of SR141716A for development of high-affinity CB1R molecular probes. *Bioorganic & medicinal chemistry letters*, 29(21), 126644. doi:10.1016/j.bmcl.2019.126644.

Gray, J. J., Moughon, S., Wang, C., Schueler-Furman, O., Kuhlman, B., Rohl, C. A., & Baker, D. (2003). Protein–protein docking with simultaneous optimization of rigid-body displacement and side-chain conformations. *Journal of molecular biology*, 331(1), 281-299. doi:10.1016/S0022-2836(03)00670-3

Gromiha, M. M., Yugandhar, K. A., & Jemimah, S. (2017). Protein–protein interactions: scoring schemes and binding affinity. *Current opinion in structural biology*, 44, 31-38. doi:10.1016/j.sbi.2016.10.016.

Guedes, I. A., de Magalhães, C. S., & Dardenne, L. E. (2014). Receptor–ligand molecular docking. *Biophysical reviews*, 6(1), 75-87. doi:10.1007/s12551-013-0130-2.

Guo, W., Shi, L., Filizola, M., Weinstein, H., & Javitch, J. A. (2005). Crosstalk in G protein-coupled receptors: changes at the transmembrane homodimer interface determine activation. *Proceedings of the National Academy of Sciences*, 102(48), 17495-17500. doi:10.1073/pnas.0508950102.

Gurevich, V. V., & Gurevich, E. V. (2008). How and why do GPCRs dimerize?. *Trends in pharmacological sciences*, 29(5), 234-240. doi:10.1016/j.tips.2008.02.004.

Guvench, O., Hatcher, E., Venable, R. M., Pastor, R. W., & MacKerell Jr, A. D. (2009). CHARMM additive all-atom force field for glycosidic linkages between hexopyranoses. *Journal of chemical theory and computation*, 5(9), 2353-2370. doi:10.1021/ct900242e.

Hadi, T., Barrichon, M., Mourtialon, P., Wendremaire, M., Garrido, C., Sagot, P., ... & Lirussi, F. (2013). Biphasic Erk1/2 activation sequentially involving Gs and Gi signaling is required in beta3-adrenergic receptor-induced primary smooth muscle cell proliferation. *Biochimica et Biophysica Acta (BBA)-Molecular Cell Research*, 1833(5), 1041-1051. doi:10.1016/j.bbamcr.2013.01.019.

Halperin, I., Ma, B., Wolfson, H., & Nussinov, R. (2002). Principles of docking: An overview of search algorithms and a guide to scoring functions. *Proteins: Structure, Function, and Bioinformatics*, 47(4), 409-443. doi:10.1002/prot.10115.

- Hammock, E. A. (2015). Developmental perspectives on oxytocin and vasopressin. *Neuropsychopharmacology*, 40(1), 24-42. doi:10.1038/npp.2014.120.
- Harrison, R. L. (2010, January). Introduction to monte carlo simulation. In AIP conference proceedings (Vol. 1204, No. 1, pp. 17-21). *American Institute of Physics*. doi:10.1063/1.3295638.
- Haspula, D., & Clark, M. A. (2020). Cannabinoid receptors: An update on cell signaling, pathophysiological roles and therapeutic opportunities in neurological, cardiovascular, and inflammatory diseases. *International journal of molecular sciences*, 21(20), 7693. doi:10.3390/ijms21207693.
- Herkenham, M. A. B. L., Lynn, A. B., Little, M. D., Johnson, M. R., Melvin, L. S., De Costa, B. R., & Rice, K. C. (1990). Cannabinoid receptor localization in brain. *Proceedings of the national Academy of sciences*, 87(5), 1932-1936. doi:10.1073/pnas.87.5.1932.
- Hilger, D., Masureel, M., & Kobilka, B. K. (2018). Structure and dynamics of GPCR signaling complexes. *Nature structural & molecular biology*, 25(1), 4-12. doi:10.1038/s41594-017-0011-7.
- Hollingsworth, S. A., & Dror, R. O. (2018). Molecular dynamics simulation for all. *Neuron*, 99(6), 1129-1143. doi:10.1016/j.neuron.2018.08.011.
- Horn, F., Bettler, E., Oliveira, L., Campagne, F., Cohen, F. E., & Vriend, G. (2003). GPCRDB information system for G protein-coupled receptors. *Nucleic acids research*, 31(1), 294-297. doi:10.1093/nar/gkg103.
- Hurley, J. H. (1999). Structure, mechanism, and regulation of mammalian adenylyl cyclase. *Journal of Biological Chemistry*, 274(12), 7599-7602. doi:10.1074/jbc.274.12.7599.
- Hsin, J., Arkhipov, A., Yin, Y., Stone, J. E., & Schulten, K. (2008). Using VMD: an introductory tutorial. *Current protocols in bioinformatics*, 24(1), 5-7. doi:10.1002/0471250953.bi0507s24.
- Hua, T., Li, X., Wu, L., Iliopoulos-Tsoutsouvas, C., Wang, Y., Wu, M., ... & Liu, Z. J. (2020). Activation and signaling mechanism revealed by cannabinoid receptor-Gi complex structures. *Cell*, 180(4), 655-665. doi:10.1016/j.cell.2020.01.008.
- Hua, T., Vemuri, K., Pu, M., Qu, L., Han, G. W., Wu, Y., ... & Liu, Z. J. (2016). Crystal structure of the human cannabinoid receptor CB1. *Cell*, 167(3), 750-762. doi:10.1016/j.cell.2016.10.004.
- Huang, N., Shoichet, B. K., & Irwin, J. J. (2006). Benchmarking sets for molecular docking. *Journal of medicinal chemistry*, 49(23), 6789-6801. doi:10.1021/jm0608356.

- Huang, S. Y. (2015). Exploring the potential of global protein–protein docking: an overview and critical assessment of current programs for automatic ab initio docking. *Drug Discovery Today*, 20(8), 969-977. doi:10.1016/j.drudis.2015.03.007.
- Humphrey, W., Dalke, A., & Schulten, K. (1996). VMD: visual molecular dynamics. *Journal of molecular graphics*, 14(1), 33-38. doi:10.1016/0263-7855(96)00018-5.
- Hurwitz, N., Schneidman-Duhovny, D., & Wolfson, H. J. (2016). Memdock: an α -helical membrane protein docking algorithm. *Bioinformatics*, 32(16), 2444-2450. doi:10.1093/bioinformatics/btw184.
- Hwang, H., Vreven, T., Janin, J., & Weng, Z. (2010). Protein–protein docking benchmark version 4.0. *Proteins: Structure, Function, and Bioinformatics*, 78(15), 3111-3114. doi:10.1002/prot.22830.
- Irwin, J. J. (2008). Community benchmarks for virtual screening. *Journal of computer-aided molecular design*, 22(3), 193-199. doi:10.1007/s10822-008-9189-4.
- Jacoby, E., Bouhelal, R., Gerspacher, M., & Seuwen, K. (2006). The 7 TM G-protein-coupled receptor target family. *ChemMedChem: Chemistry Enabling Drug Discovery*, 1(8), 760-782. doi:10.1002/cmdc.200600134.
- Jaghoori, M. M., Bleijlevens, B., & Olabarriaga, S. D. (2016). 1001 Ways to run AutoDock Vina for virtual screening. *Journal of computer-aided molecular design*, 30(3), 237-249. doi:10.1007/s10822-016-9900-9.
- Janin, J., Henrick, K., Moult, J., Eyck, L. T., Sternberg, M. J., Vajda, S., ... & Wodak, S. J. (2003). CAPRI: a critical assessment of predicted interactions. *Proteins: Structure, Function, and Bioinformatics*, 52(1), 2-9. doi:10.1002/prot.10381.
- Jo, S., Cheng, X., Islam, S. M., Huang, L., Rui, H., Zhu, A., ... & Im, W. (2014). CHARMM-GUI PDB manipulator for advanced modeling and simulations of proteins containing nonstandard residues. *Advances in protein chemistry and structural biology*, 96, 235-265. doi:10.1016/bs.apcsb.2014.06.002.
- Jo, S., Cheng, X., Lee, J., Kim, S., Park, S. J., Patel, D. S., ... & Im, W. (2017). CHARMM-GUI 10 years for biomolecular modeling and simulation. *Journal of computational chemistry*, 38(15), 1114-1124. doi:10.1002/jcc.24660.
- Jo, S., Kim, T., Iyer, V. G., & Im, W. (2008). CHARMM-GUI: a web-based graphical user interface for CHARMM. *Journal of computational chemistry*, 29(11), 1859-1865. doi:10.1002/jcc.20945.

- Kaczor, A. A., Bartuzi, D., Stępniewski, T. M., Matosiuk, D., & Selent, J. (2018). Protein–protein docking in drug design and discovery. *In Computational Drug Discovery and Design* (pp. 285-305). Humana Press, New York, NY. doi:10.1007/978-1-4939-7756-7_15.
- Katsidoni, V., Kastellakis, A., & Panagis, G. (2013). Biphasic effects of Δ^9 -tetrahydrocannabinol on brain stimulation reward and motor activity. *International journal of neuropsychopharmacology*, 16(10), 2273-2284. doi:10.1017/S1461145713000709.
- Kirchmair, J., Markt, P., Distinto, S., Wolber, G., & Langer, T. (2008). Evaluation of the performance of 3D virtual screening protocols: RMSD comparisons, enrichment assessments, and decoy selection—what can we learn from earlier mistakes?. *Journal of computer-aided molecular design*, 22(3), 213-228. doi:10.1007/s10822-007-9163-6.
- Kitchen, D. B., Decornez, H., Furr, J. R., & Bajorath, J. (2004). Docking and scoring in virtual screening for drug discovery: methods and applications. *Nature reviews Drug discovery*, 3(11), 935-949. doi:10.1038/nrd1549.
- Kooistra, A. J., Mordalski, S., Pándy-Szekeres, G., Esguerra, M., Mamyrbekov, A., Munk, C., ... & Gloriam, D. E. (2021). GPCRRdb in 2021: integrating GPCR sequence, structure and function. *Nucleic Acids Research*, 49(D1), D335-D343. doi:10.1093/nar/gkaa1080.
- Kortemme, T., & Baker, D. (2002). A simple physical model for binding energy hot spots in protein–protein complexes. *Proceedings of the National Academy of Sciences*, 99(22), 14116-14121. doi:10.1073/pnas.202485799.
- Kozakov, D., Hall, D. R., Xia, B., Porter, K. A., Padhorny, D., Yueh, C., ... & Vajda, S. (2017). The ClusPro web server for protein–protein docking. *Nature protocols*, 12(2), 255-278. doi:10.1038/nprot.2016.169.
- Kroese, D. P., & Rubinstein, R. Y. (2012). Monte carlo methods. *Wiley Interdisciplinary Reviews: Computational Statistics*, 4(1), 48-58. doi:10.1002/wics.194.
- Lauckner, J. E., Hille, B., & Mackie, K. (2005). The cannabinoid agonist WIN55, 212-2 increases intracellular calcium via CB1 receptor coupling to Gq/11 G proteins. *Proceedings of the National Academy of Sciences*, 102(52), 19144-19149. doi:10.1073/pnas.0509588102.
- Lee, J., Cheng, X., Swails, J. M., Yeom, M. S., Eastman, P. K., Lemkul, J. A., ... & Im, W. (2016). CHARMM-GUI input generator for NAMD, GROMACS, AMBER, OpenMM, and CHARMM/OpenMM simulations using the CHARMM36 additive force field. *Journal of chemical theory and computation*, 12(1), 405-413. doi:10.1021/acs.jctc.5b00935.

- Lee, J., Patel, D. S., Stähle, J., Park, S. J., Kern, N. R., Kim, S., ... & Im, W. (2018). CHARMM-GUI membrane builder for complex biological membrane simulations with glycolipids and lipoglycans. *Journal of chemical theory and computation*, 15(1), 775-786. doi:10.1021/acs.jctc.8b01066.
- Leggett, J. D., Aspley, S., Beckett, S. R. G., D'antona, A. M., Kendall, D. A., & Kendall, D. A. (2004). Oleamide is a selective endogenous agonist of rat and human CB1 cannabinoid receptors. *British journal of pharmacology*, 141(2), 253-262. doi:10.1038/sj.bjp.0705607.
- Li, J., Fu, A., & Zhang, L. (2019). An overview of scoring functions used for protein–ligand interactions in molecular docking. *Interdisciplinary Sciences: Computational Life Sciences*, 11(2), 320-328. doi:10.1007/s12539-019-00327-w.
- Li, X., Hua, T., Vemuri, K., Ho, J. H., Wu, Y., Wu, L., ... & Liu, Z. J. (2019). Crystal structure of the human cannabinoid receptor CB2. *Cell*, 176(3), 459-467. doi:10.1016/j.cell.2018.12.011.
- Liang, Y. L., Khoshouei, M., Radjainia, M., Zhang, Y., Glukhova, A., Tarrasch, J., ... & Sexton, P. M. (2017). Phase-plate cryo-EM structure of a class B GPCR–G-protein complex. *Nature*, 546(7656), 118-123. doi:10.1038/nature22327.
- Liu, H., Gruber, C. W., Alewood, P. F., Möller, A., & Muttenthaler, M. (2020). The oxytocin receptor signalling system and breast cancer: A critical review. *Oncogene*, 39(37), 5917-5932. doi:10.1038/s41388-020-01415-8.
- Liu, S., & Vakser, I. A. (2011). DECK: Distance and environment-dependent, coarse-grained, knowledge-based potentials for protein-protein docking. *BMC bioinformatics*, 12(1), 1-7. doi:10.1186/1471-2105-12-280.
- LigandScout, Version 4.3, Release built 20181012 [i1_10], Inte:Ligand GmbH, Vienna, Austria
- Lomize, M. A., Pogozheva, I. D., Joo, H., Mosberg, H. I., & Lomize, A. L. (2012). OPM database and PPM web server: resources for positioning of proteins in membranes. *Nucleic acids research*, 40(D1), D370-D376. doi:10.1093/nar/gkr703.
- Lyskov, S., & Gray, J. J. (2008). The RosettaDock server for local protein–protein docking. *Nucleic acids research*, 36(suppl_2), W233-W238. doi:10.1093/nar/gkn216.
- Mallipeddi, S., Kreimer, S., Zvonok, N., Vemuri, K., Karger, B. L., Ivanov, A. R., & Makriyannis, A. (2017). Binding site characterization of AM1336, a novel covalent inverse agonist at human cannabinoid 2 receptor, using mass spectrometric analysis. *Journal of proteome research*, 16(7), 2419-2428. doi:10.1021/acs.jproteome.7b00023.

- Manning, M., Miteva, K., Pancheva, S., Stoev, S., Wo, N. C., & Chan, W. Y. (1995). Design and synthesis of highly selective in vitro and in vivo uterine receptor antagonists of oxytocin: comparisons with Atosiban. *International journal of peptide and protein research*, 46(3-4), 244-252. doi:10.1111/j.1399-3011.1995.tb00596.x.
- Margolskee, R. F. (2002). Molecular mechanisms of bitter and sweet taste transduction. *Journal of Biological Chemistry*, 277(1), 1-4. doi:10.1074/jbc.R100054200.
- Masuh, I., Martemyanov, K. A., & Lambert, N. A. (2015). Monitoring G protein activation in cells with BRET. In *G Protein-Coupled Receptors in Drug Discovery* (pp. 107-113). Humana Press, New York, NY. doi:10.1007/978-1-4939-2914-6_8.
- McCudden, C. R., Hains, M. D., Kimple, R. J., Siderovski, D. P., & Willard, F. S. (2005). G-protein signaling: back to the future. *Cellular and molecular life sciences*, 62(5), 551-577. doi:10.1007/s00018-004-4462-3.
- Mechoulam, R., Ben-Shabat, S., Hanus, L., Ligumsky, M., Kaminski, N. E., Schatz, A. R., ... & Vogel, Z. V. I. (1995). Identification of an endogenous 2-monoglyceride, present in canine gut, that binds to cannabinoid receptors. *Biochemical pharmacology*, 50(1), 83-90. doi:10.1016/0006-2952(95)00109-D.
- Meng, X. Y., Mezei, M., & Cui, M. (2014). Computational approaches for modeling GPCR dimerization. *Current pharmaceutical biotechnology*, 15(10), 996-1006. doi:10.2174/1389201015666141013102515.
- Mills, N. (2006). ChemDraw Ultra 10.0 CambridgeSoft, 100 CambridgePark Drive, Cambridge, MA 02140. www.cambridgesoft.com. Commercial Price: 1910fordownload, 2150 for CD-ROM; Academic Price: 710fordownload, 800 for CD-ROM. doi:10.1021/ja0697875.
- Mitre, M., Minder, J., Morina, E. X., Chao, M. V., & Froemke, R. C. (2017). Oxytocin modulation of neural circuits. *Behavioral Pharmacology of Neuropeptides: Oxytocin*, 31-53. doi:10.1007/7854_2017_7.
- Morales, P., & Reggio, P. H. (2017). An update on non-CB1, non-CB2 cannabinoid related G-protein-coupled receptors. *Cannabis and cannabinoid research*, 2(1), 265-273. doi:10.1089/can.2017.0036.
- Morris, G. M., & Lim-Wilby, M. (2008). Molecular docking. In *Molecular modeling of proteins* (pp. 365-382). Humana Press. doi:10.1007/978-1-59745-177-2_19.
- Muller, C., Morales, P., & Reggio, P. H. (2019). Cannabinoid ligands targeting TRP channels. *Frontiers in molecular neuroscience*, 11, 487. doi:10.3389/fnmol.2018.00487.

- Neves, S. R., Ram, P. T., & Iyengar, R. (2002). G protein pathways. *Science*, 296(5573), 1636-1639. doi:10.1126/science.1071550.
- Nilsson, L., Reinheimer, T., Steinwall, M., & Åkerlund, M. (2003). FE 200 440: a selective oxytocin antagonist on the term-pregnant human uterus. *BJOG: an international journal of obstetrics and gynaecology*, 110(11), 1025-1028. doi:10.1016/S1470-0328(03)20540-1.
- Oldham, W. M., & Hamm, H. E. (2008). Heterotrimeric G protein activation by G-protein-coupled receptors. *Nature reviews Molecular cell biology*, 9(1), 60-71. doi:10.1038/nrm2299.
- Pamplona, F. A., Ferreira, J., de Lima, O. M., Duarte, F. S., Bento, A. F., Forner, S., ... & Takahashi, R. N. (2012). Anti-inflammatory lipoxin A4 is an endogenous allosteric enhancer of CB1 cannabinoid receptor. *Proceedings of the National Academy of Sciences*, 109(51), 21134-21139. doi:10.1073/pnas.1202906109.
- Parmentier, M. (2015). Heterodimer-specific signaling. *Nature chemical biology*, 11(4), 244-245. doi:10.1038/nchembio.1772.
- Pierzynski, P., Lemancewicz, A., Reinheimer, T., Akerlund, M., & Laudanski, T. (2004). Inhibitory effect of barusiban and atosiban on oxytocin-induced contractions of myometrium from preterm and term pregnant women. *The Journal of the Society for Gynecologic Investigation: JSGI*, 11(6), 384-387. doi:10.1016/j.jsgi.2004.02.008.
- Pinzi, L., & Rastelli, G. (2019). Molecular docking: shifting paradigms in drug discovery. *International journal of molecular sciences*, 20(18), 4331. doi:10.3390/ijms20184331.
- Porter, A. C., Sauer, J. M., Knierman, M. D., Becker, G. W., Berna, M. J., Bao, J., ... & Felder, C. C. (2002). Characterization of a novel endocannabinoid, virodhamine, with antagonist activity at the CB1 receptor. *Journal of Pharmacology and Experimental Therapeutics*, 301(3), 1020-1024. doi:10.1124/jpet.301.3.1020.
- Porter, K. A., Desta, I., Kozakov, D., & Vajda, S. (2019). What method to use for protein-protein docking?. *Current opinion in structural biology*, 55, 1-7. doi:10.1016/j.sbi.2018.12.010.
- Portoghese, P. S. (2001). From models to molecules: opioid receptor dimers, bivalent ligands, and selective opioid receptor probes. doi:10.1021/jm010158+.
- Rajeswaran, W. G., Cao, Y., Huang, X. P., Wroblewski, M. E., Colclough, T., Lee, S., ... & Messer, W. S. (2001). Design, synthesis, and biological characterization of bivalent 1-methyl-1, 2, 5, 6-tetrahydropyridyl-1, 2, 5-thiadiazole derivatives as selective muscarinic agonists. *Journal of medicinal chemistry*, 44(26), 4563-4576. doi:10.1021/jm0102405.

- Ribas, C., Penela, P., Murga, C., Salcedo, A., García-Hoz, C., Jurado-Pueyo, M., ... & Mayor Jr, F. (2007). The G protein-coupled receptor kinase (GRK) interactome: role of GRKs in GPCR regulation and signaling. *Biochimica et Biophysica Acta (BBA)-Biomembranes*, 1768(4), 913-922. doi:10.1016/j.bbamem.2006.09.019.
- Richard, P. H. I. L. I. P. P. E., Moos, F. R. A. N. C. O. I. S. E., & Freund-Mercier, M. J. (1991). Central effects of oxytocin. *Physiological Reviews*, 71(2), 331-370. doi:10.1152/physrev.1991.71.2.331.
- Ritter, S. L., & Hall, R. A. (2009). Fine-tuning of GPCR activity by receptor-interacting proteins. *Nature reviews Molecular cell biology*, 10(12), 819-830. doi:10.1038/nrm2803.
- Rios, C. D., Jordan, B. A., Gomes, I., & Devi, L. A. (2001). G-protein-coupled receptor dimerization: modulation of receptor function. *Pharmacology & therapeutics*, 92(2-3), 71-87. doi:10.1016/S0163-7258(01)00160-7.
- Romero-Fernandez, W., Borroto-Escuela, D. O., Agnati, L. F., & Fuxe, K. (2013). Evidence for the existence of dopamine d2-oxytocin receptor heteromers in the ventral and dorsal striatum with facilitatory receptor-receptor interactions. *Molecular psychiatry*, 18(8), 849-850. doi:10.1038/mp.2012.103.
- Rozenfeld, R., Bushlin, I., Gomes, I., Tzavaras, N., Gupta, A., Neves, S., ... & Devi, L. A. (2012). Receptor heteromerization expands the repertoire of cannabinoid signaling in rodent neurons. *PLoS One*, 7(1), e29239. doi:10.1371/journal.pone.0029239.
- Salon, J. A., Lodowski, D. T., & Palczewski, K. (2011). The significance of G protein-coupled receptor crystallography for drug discovery. *Pharmacological reviews*, 63(4), 901-937. doi:10.1124/pr.110.003350.
- Sarfaraz, S., Afaq, F., Adhami, V. M., & Mukhtar, H. (2005). Cannabinoid receptor as a novel target for the treatment of prostate cancer. *Cancer research*, 65(5), 1635-1641. doi:10.1158/0008-5472.
- Schneidman-Duhovny, D., Inbar, Y., Nussinov, R., & Wolfson, H. J. (2005). PatchDock and SymmDock: servers for rigid and symmetric docking. *Nucleic acids research*, 33(suppl_2), W363-W367. doi:10.1093/nar/gki481.
- Seeliger, D., & de Groot, B. L. (2010). Ligand docking and binding site analysis with PyMOL and Autodock/Vina. *Journal of computer-aided molecular design*, 24(5), 417-422. doi:10.1007/s10822-010-9352-6.

- Shah, U. H., Toneatti, R., Gaitonde, S. A., Shin, J. M., & González-Maeso, J. (2020). Site-specific incorporation of genetically encoded photo-crosslinkers locates the heteromeric interface of a GPCR complex in living cells. *Cell Chemical Biology*, 27(10), 1308-1317. doi:10.1016/j.chembiol.2020.07.006.
- Shao, Z., Yin, J., Chapman, K., Grzemska, M., Clark, L., Wang, J., & Rosenbaum, D. M. (2016). High-resolution crystal structure of the human CB1 cannabinoid receptor. *Nature*, 540(7634), 602-606. doi:10.1038/nature20613.
- Shonberg, J., Scammells, P. J., & Capuano, B. (2011). Design strategies for bivalent ligands targeting GPCRs. *ChemMedChem*, 6(6), 963-974. doi:10.1002/cmdc.201100101.
- Smith, J. S., Lefkowitz, R. J., & Rajagopal, S. (2018). Biased signalling: from simple switches to allosteric microprocessors. *Nature reviews Drug discovery*, 17(4), 243-260. doi:10.1038/nrd.2017.229.
- Smrcka, A. V. (2008). G protein $\beta\gamma$ subunits: central mediators of G protein-coupled receptor signaling. *Cellular and molecular life sciences*, 65(14), 2191-2214. doi:10.1007/s00018-008-8006-5.
- Sugiura, T., Kondo, S., Sukagawa, A., Nakane, S., Shinoda, A., Itoh, K., ... & Waku, K. (1995). 2-Arachidonoylglycerol: a possible endogenous cannabinoid receptor ligand in brain. *Biochemical and biophysical research communications*, 215(1), 89-97. doi:10.1006/bbrc.1995.2437.
- Suzuki, N., Hajicek, N., & Kozasa, T. (2009). Regulation and physiological functions of G12/13-mediated signaling pathways. *Neurosignals*, 17(1), 55-70. doi:10.1159/000186690. doi:10.1042/bj20031061.
- Terrillon, S., & Bouvier, M. (2004). Roles of G-protein-coupled receptor dimerization: From ontogeny to signalling regulation. *EMBO reports*, 5(1), 30-34. doi:10.1038/sj.embor.7400052.
- Torres, P. H., Sodero, A. C., Jofily, P., & Silva-Jr, F. P. (2019). Key topics in molecular docking for drug design. *International journal of molecular sciences*, 20(18), 4574. doi:10.3390/ijms20184574.
- Trott, O., & Olson, A. J. (2010). AutoDock Vina: improving the speed and accuracy of docking with a new scoring function, efficient optimization, and multithreading. *Journal of computational chemistry*, 31(2), 455-461. doi:10.1002/jcc.21334.
- Vajda, S., & Kozakov, D. (2009). Convergence and combination of methods in protein-protein docking. *Current opinion in structural biology*, 19(2), 164-170. doi:10.1016/j.sbi.2009.02.008.

- Vakser, I. A. (2014). Protein-protein docking: From interaction to interactome. *Biophysical journal*, 107(8), 1785-1793. doi:10.1016/j.bpj.2014.08.033.
- Veenema, A. H., & Neumann, I. D. (2008). Central vasopressin and oxytocin release: regulation of complex social behaviours. *Progress in brain research*, 170, 261-276. doi:10.1016/S0079-6123(08)00422-6.
- Venkatakrishnan, A. J., Deupi, X., Lebon, G., Tate, C. G., Schertler, G. F., & Babu, M. M. (2013). Molecular signatures of G-protein-coupled receptors. *Nature*, 494(7436), 185-194. doi:10.1038/nature11896.
- Wacker, D., Stevens, R. C., & Roth, B. L. (2017). How ligands illuminate GPCR molecular pharmacology. *Cell*, 170(3), 414-427. doi:10.1016/j.cell.2017.07.009.
- Waldhoer, M., Fong, J., Jones, R. M., Lunzer, M. M., Sharma, S. K., Kostenis, E., ... & Whistler, J. L. (2005). A heterodimer-selective agonist shows in vivo relevance of G protein-coupled receptor dimers. *Proceedings of the National Academy of Sciences*, 102(25), 9050-9055. doi:10.1073/pnas.0501112102.
- Waltenspühl, Y., Schöppe, J., Ehrenmann, J., Kummer, L., & Plückthun, A. (2020). Crystal structure of the human oxytocin receptor. *Science advances*, 6(29), eabb5419. doi:10.1126/sciadv.abb5419.
- Wang, R., Fang, X., Lu, Y., & Wang, S. (2004). The PDBbind database: Collection of binding affinities for protein–ligand complexes with known three-dimensional structures. *Journal of medicinal chemistry*, 47(12), 2977-2980. doi:10.1021/jm030580l.
- Wang, W., Qiao, Y., & Li, Z. (2018). New insights into modes of GPCR activation. *Trends in pharmacological sciences*, 39(4), 367-386. doi:10.1016/j.tips.2018.01.001.
- Wei, D., Lee, D., Cox, C. D., Karsten, C. A., Peñagarikano, O., Geschwind, D. H., ... & Piomelli, D. (2015). Endocannabinoid signaling mediates oxytocin-driven social reward. *Proceedings of the National Academy of Sciences*, 112(45), 14084-14089. doi:10.1073/pnas.1509795112.
- Wolber, G., & Langer, T. (2005). LigandScout: 3-D pharmacophores derived from protein-bound ligands and their use as virtual screening filters. *Journal of chemical information and modeling*, 45(1), 160-169. doi:10.1021/ci049885e.
- Wouters, E., Walraed, J., Banister, S. D., & Stove, C. P. (2019). Insights into biased signaling at cannabinoid receptors: synthetic cannabinoid receptor agonists. *Biochemical pharmacology*, 169, 113623. doi:10.1016/j.bcp.2019.08.025.

- Wu, E. L., Cheng, X., Jo, S., Rui, H., Song, K. C., Dávila-Contreras, E. M., ... & Im, W. (2014). CHARMM-GUI membrane builder toward realistic biological membrane simulations. doi:10.1002/jcc.23702.
- Yarov-Yarovoy, V., Schonbrun, J., & Baker, D. (2006). Multipass membrane protein structure prediction using Rosetta. *Proteins: Structure, Function, and Bioinformatics*, 62(4), 1010-1025. doi:10.1002/prot.20817.
- Ye, L., Cao, Z., Wang, W., & Zhou, N. (2019). New insights in cannabinoid receptor structure and signaling. *Current molecular pharmacology*, 12(3), 239. doi:10.2174/1874467212666190215112036.
- Yuan, S., Chan, H. S., & Hu, Z. (2017). Using PyMOL as a platform for computational drug design. *Wiley Interdisciplinary Reviews: Computational Molecular Science*, 7(2), e1298. doi:10.1002/wcms.1298.
- Zhang, A., Liu, Z., & Kan, Y. (2007). Receptor dimerization-Rationale for the design of bivalent Ligands. *Current topics in medicinal chemistry*, 7(4), 343-345. doi:10.2174/156802607779941279.
- Zhang, Q., Feng, T., Xu, L., Sun, H., Pan, P., Li, Y., ... & Hou, T. (2016). Recent advances in protein-protein docking. *Current drug targets*, 17(14), 1586-1594. doi:10.2174/1389450117666160112112640.
- Zhang, Y., Gilliam, A., Maitra, R., Damaj, M. I., Tajuba, J. M., Seltzman, H. H., & Thomas, B. F. (2010). Synthesis and biological evaluation of bivalent ligands for the cannabinoid 1 receptor. *Journal of medicinal chemistry*, 53(19), 7048-7060. doi:10.1021/jm1006676.
- Zou, S., & Kumar, U. (2018). Cannabinoid receptors and the endocannabinoid system: signaling and function in the central nervous system. *International journal of molecular sciences*, 19(3), 833. doi:10.3390/ijms19030833.
- Zhu, X., Lopes, P. E., & MacKerell Jr, A. D. (2012). Recent developments and applications of the CHARMM force fields. *Wiley Interdisciplinary Reviews: Computational Molecular Science*, 2(1), 167-185. doi:10.1002/wcms.74.